HARNESSING MICROGEL SOFTNESS FOR BIOINTERFACING

A Dissertation
Presented to
The Academic Faculty

by

Grant Robert Hendrickson

In Partial Fulfillment
of the Requirements for the Degree
Doctor of Philosophy in the
School of Chemistry and Biochemistry

Georgia Institute of Technology
December 2013

HARNESSING MICROGEL SOFTNESS FOR BIOINTERFACING

Approved by:

Dr. L. Andrew Lyon, Advisor
School of Chemistry and Biochemistry
Georgia Institute of Technology

Dr. Joseph W. Perry
School of Chemistry and Biochemistry
Georgia Institute of Technology

Dr. Robert M. Dickson
School of Chemistry and Biochemistry
Georgia Institute of Technology

Dr. Roger M. Wartell
School of Biology
Georgia Institute of Technology

Dr. Jiri Janata
School of Chemistry and Biochemistry
Georgia Institute of Technology

Date Approved: July 11, 2013

In memory and honor of Dr. Randall “Papaw” Enlow

ACKNOWLEDGEMENTS

I would first and foremost like to thank my wife, Lee, for her incredible support during these last six and a half years. We will be married for six years this November and she has been a large part of making my graduate school journey possible and much more enjoyable. It is a great blessing to have dinner with someone you love most every night no matter what the surrounding hours bring.

In addition, my family played a large part in supporting me as I went through my graduate studies. I would like to thank specifically my mom, Val Hendrickson, and my dad, Rob Hendrickson, for all of their consistent support over the years. It is not to be taken for granted when you have parents who are emotionally and intellectually invested in your education, and I am blessed to have two who are. In addition, I would like to thank my grandmothers; Ruth Hendrickson (Grandma Ruth) and Betty Enlow (Nana) for all of their prayers and support. I would also like to thank my step mother, Doris Hendrickson, for her and her very large and gracious family's support. Lastly, I am grateful to have a little brother that brings a huge amount of love and comic relief to my life. I appreciate Jake Hendrickson's love and countless stories that only he could provide during stressful times.

Also, I am blessed with a fun, supportive, and loving group of in-laws. I would like to thank Craig and Tommie Evans; John, Ella, Lilly, and Lilah McAfee; Bo Evans and Danielle "soon to be Evans" Rydzewski, and Walter and Carol Evans. Trips to the farm, playing in the woods, eating good food, and chopping wood were just what I needed at times during my graduate school journey.

During graduate school, there are many people who I counted on at Georgia Tech for help outside of my lab. I would like to thank all of the current and former Georgia Tech staff, especially Kourtnie Augustin, Dione Morton, Alicia Gardener-Aben, Carmen Rivera, Kevin Brantley, Jason Robinson, Mamie Gaskin, Don Woodyard, Richard Bedell, Arian Padron, Christopher Wright, Andrew Shaw, Mike Riley, Jeff Curtiss, and Vic Summey. Their help and friendly personalities made my time at Tech and my graduate student life much more enjoyable.

One of the reasons I that I decided to come to Georgia Tech for graduate school is because of the collaborative atmosphere. My time at Tech has not disappointed; I have had the opportunity to work with, in, and around many different labs including: Prof. Rob Dickson, Prof. Joe Perry, Prof. Roger Wartell, Prof. Neils Kroger, Prof. Hang Lu, Prof. Alberto Fernandez-Nieves, and Prof. Thomas Barker. In some cases, these interactions involved just a willingness to let me borrow a piece of equipment or use an instrument. No matter what the contribution, I really appreciated the help which was vital to research progress. More specifically, I want to thank Prof. Henry White (University of Utah) and his talented student Dr. Deric Holden for their hard work and collaboration that resulted in two publications. Also, I have worked more recently with Dr. Wilbur Lam and Yumiko Sakurai on developing an antithrombotic drug delivery vehicle. I appreciate the knowledge, time, and effort that all of the collaborators have shared.

Next, I would like to thank my fellow Lyon Group lab mates. It is hard to imagine a more intelligent, hard-working, and collaborative group of people who also are extremely accommodating with their time and fun to be around. When I joined the lab as a green first year student, I had great assistance learning the ropes from Dr. Courtney

Sorrell, Dr. Ashlee St. John, Dr. Zhiyong Meng, Prof. Neetu Singh, Dr. Bart Blackburn, and Dr. Toni South. I am very grateful for their help getting me up to speed on the workings of the Lyon lab and graduate school in general. I would like to thank Dr. Toni South, Dr. Bart Blackburn, and Dr. Mike Smith for their friendship and continued support as they moved on to start their post-graduate school careers. More recently, I have enjoyed and learned from countless conversations about both science and life with, recently graduated, Dr. Jeff Gaulding. I really appreciate the professional and personal camaraderie that we shared during our graduate school lives. Lastly, I would like to thank the current lab members, Akriti Singh, Dr. Hiroaki Yoshida, Emily Herman, Shalini Saxena, Kim Clarke, Caroline Hansen, Mark Spears, Tanya Su, Haylee Bachman, Dr. Nicole Welsch, Kenny Winburn, Purva Kodlekere, Kabir Dhada, and Dr. Ashley Brown for their friendship and hard work as I have completed my studies. I especially thank Caroline Hansen for being very proactive in her efforts to learn the ropes as she will carry on my current projects. I am also very grateful for all the work that Emily Herman put in on the nanopore project. I have enjoyed getting to know all of these Lyon group lab members and hope that we can continue to keep in touch over the years.

Finally, I would like to thank Prof. Andrew Lyon, my advisor, for his patience and constant willingness to help. Prof. Lyon is always available for his students despite the many different things he has going on both personally and professionally and that is greatly appreciated. His ability to explain experiments and phenomena that can be hard to grasp by simply reading the literature has been very valuable to me. I have always appreciated that he lets his students know he is interested in their projects, yet allows his students the leeway to explore them on their own. He also has interesting prospective on

graduate school, research, teaching, careers, and life that I have appreciated over the years. I am very grateful that I have gotten to know Prof. Lyon as a creative scientist, an excellent teacher, and an insightful mentor.

TABLE OF CONTENTS

LIST OF TABLES

LIST OF FIGURES

LIST OF SCHEMES

LIST OF SYMBOLS AND ABBREVIATIONS

AAc	acrylic acid
AFA	4-acrylamidofluorescein
AFM	atomic force microscopy
AFP	alpha-fectoprotein
Ag/AgCl	silver/silver chloride electrode
APBA	3-acrylamidophenylboronic acid
APS	ammonium persulfate
APTMS	3-aminopropyltrimethoxysilane
BIS	*N,N'*-methylenebisacrylamide
BSA	bovine serum albumin
CaM	calmodulin
Con A	concanavalin A
CPZ	chlorpromazine
cryo-SEM	cryogenic scanning electron microscopy
D	diffusion coefficient
DI	deionized
DIC	differential interference contrast
DLS	dynamic light scattering
DMAEMA	2-(dimethylamino)ethyl methacrylate
DNA	deoxyribonucleic acid
dsDNA	double stranded deoxyribonucleic acid
EB	ethidium bromide
EDC	1-ethyl-3-(3-dimethylaminopropyl)carbodiimide hydrochloride

EPR	enhanced permeability and retention
evoo	extra virgin olive oil
FIB	focused ion beam
FITC	fluorescein isothiocyanate
FMOC	9H-fluoren-9-ylmethoxycarbonyl
FRET	fluorescence resonance energy transfer
HABA	4’-hydroxyazobenzene-2-carboxylic acid
HSA	human serum albumin
I.D.	inner diameter
IgG	immunoglobulin G
IPN	interpenetrating network
IS	ionic strength
k_B	Boltzmann’s constant
K_d	dissociation constant
LbL	layer-by-layer
LCST	lower critical solution temperature
MALLS	multiangle laser light scattering
MES	2-(*N*-morpholino)ethane sulfonic acid
MMA	methacrylic acid
η	viscosity
NA	numerical aperture
NHS	*N*-hydroxysuccinimide
NIPAm	*N*-isopropylacrylamide
NIPMAm	*N*-isopropylmethacrylamide
O.D.	outer diameter

OP	organophosphorous
O/W	oil-in-water
PBS	phosphate buffered saline
PCCA	polymerized crystalline colloidal array
PDMS	poly(dimethylsiloxane)
PEG	poly(ethylene glycol)
PEGA	poly(ethylene glycol)-poly(acrylamide)
PMA	polymethacrylate
pNIPAm	poly(*N*-isopropylacrylamide)
p(NIPAm -co-AAc)	poly(*N*-isopropylacrylamide-co-acrylic acid)
pNIPMAm	poly(N-isopropylmethacrylamide)
poly(GEMA)	poly(2-glucosyloxyethylmethacrylate)
PPP	platelet poor plasma
PRP	platelet rich plasma
PS	polystyrene
R_g	radius of gyration
R_h	hydrodynamic radius
SDS	sodium dodecylsulfate
SEM	scanning electron microscopy
STM	scanning tunneling microscopy
TFP	trifluoperazine
TRIM	trimethylolpropane trimethacrylate
TRITC	tetramethylrhodamine isothiocyanate
W/O	water-in-oil
WP	washed platelets

SUMMARY

Hydrogel materials have become a heavily studied as materials for interfacing with biology both for laboratory investigations and the development of devices for biomedical applications. These polymers are water swollen and can be made responsive to many different stimuli by choice of monomers, co-monomers, and cross-linkers or functionalization with pendent ligands, substrates, or charged groups. The high water content, low moduli and potential responsively of these polymers make good candidates for biomaterials. A specific type of hydrogel called a microgel or a hydrogel micro/nanoparticle has similar properties to bulk hydrogel materials with some key differences. Namely, the response kinetics to external stimuli are much faster than their bulk counterpart simply due to the decreased dimensions. Also, microgels can be utilized in dilute or concentrate suspensions for applications such as drug delivery or study of colloidal phase transitions. Furthermore, microgels have been used as building blocks for bottom-up fabrication of thin films or 3D matrices for biomedical coating, sensing, and tissue engineering applications. Many of the interesting results and utility of the microgels in these applications are due to their inherent softness of the material.

In this dissertation, the softness, flexibility, and conformability of these water swollen particles is used to create an interesting sensor platform (**Chapter 2**), studied in the context of a microgel passing through a pore (**Chapter 3** and **4**), and used as an emulsifier to create a drug delivery platform (**Appendix A** and **B**). First, however, overviews of hydrogels as biomaterials, biomaterial design, microgels, and the importance of biomaterial mechanics are given in **Chapter 1**. Then, our efforts to use

microgels deformed on a surface as individual biosensing lenses are discussed in **Chapter 2**. In **Chapter 3**, results showing the incredible flexibility of the microgels to squeeze through pores 10xs smaller than their diameter are discussed. These results are interesting considering the number of biological pores that might have to be traversed in a drug delivery application. The experiments described here involve a large number of particles passing through many pores. Next, resistive pulse analysis, as described in **Chapter 4**, was used to analyze single microgels passing through a single pore (**Chapter 5**). This technique detects disruptions in ion current passing through a pore by a particle. Resistive pulse analysis allowed for detection of passage as well as deduction of possible mechanisms of passage.

The unifying theme of this dissertation is the softness of microgels which is critical for all of these experiments. However, the study of individual microgel softness is challenging and complex, since the softness is composed of two different components. The first is that the microgel is a swollen polymer which can be deswollen by an external stimuli or force. The second is that the microgel is a volume conserving elastic colloid which can deform without deswelling under the certain conditions. Throughout, this dissertation will discuss the ramifications of the complex softness of microgels in each experimental result and potential application.

CHAPTER 1

INTRODUCTION

Adapted in part from:

Hendrickson, G.R.;Smith, M.H.;South, A.B.;Lyon, L.A. Design of Multiresponsive Hydrogel Particles and Assemblies. *Adv. Funct. Mater.* **2010**, *20*, 1697-1712

Lyon, L.A.; Hendrickson, G.R.; Meng, Z.; Iyer, A.N.S. "Exploiting the Optical Properties of Microgels as Microlenses and Photonic Crystals in Sensing Applications." Microgel Suspensions-Fundamentals and Applications. Editors: Fernandez-Nieves, A.; Wyss, H.; Mattsson, J.; Weitz, D.A. Wiley-VCH Verlag GmbH&Co., **2011**, Chapter 14.

1.1 Biointerfacing

In 1994, Peppas and Langer defined a biomaterial as "substances other than food or drugs contained in therapeutic or diagnostic systems that are in contact with tissues or biological fluids."[1] Under this definition, biomaterials include permanent implants (e.g. internal pacemakers and replacement joints), temporary or semi-permanent hospital devices (e.g. catheters or dialyzers), and consumer products used everyday (e.g. contact lenses). In other words, a biomaterial could be described as a material that is intended to biointerface. The effectiveness of the material is based on its ability to interface favorably with the intended nucleic acids, proteins, cells or organs both micro and macroscopically.

The choice of material has been as numerous as the applications. Some interesting early examples include glass eyes and wooden teeth.[2] More recently, ceramics,[3,4] metals,[5,6] carbon nanotubes,[7] gold nanoparticles,[8,9] magnetic nanoparticles,[10] silica particles,[11] quantum dots,[12] lipid particles,[13] or micelles[14] to name a few have been of interest. Biomaterials have even been formed out of

biological building blocks using self-assembly of proteins or peptides[20,21] These materials have been developed mostly for drug delivery, tissue engineering, sensing or diagnostic platforms. Another large class of materials are polymeric biomaterials which include synthetic polymers (methacrylates, acrylamides, etc.) as well as biopolymers such as chitosan,[15,16] chitin,[15] alginate,[17] and silk.[18,19] Polymeric materials have become of particular interest due to the diverse chemical and physical properties that can be controlled using different synthetic strategies. With such chemical and physical diversity, there is the opportunity to design-in responsiveness to temperature, pH, proteins, nucleic acids, or cells. The ability to respond to a particular environment is the basis of developing a good biosensor. Likewise, a responsive biomaterial should not only act as a physical biomedical stand-in, but communicate favorably with biological environments or actively biointerface.

1.2 Polymeric and Hydrogel Biomaterials

Responsive polymeric materials are becoming increasingly attractive in tissue replacement,[20-25] biological coating technologies,[26-28] drug delivery,[23,29-42] and biosensing.[23,40-42] Hydrogels in particular are of interest for these applications due to the tunability of their mechanical and chemical properties, and therefore their versatility as device components. Wichterle and Lim in 1960 published a paper in Nature suggesting that a biomaterial should have three attributes; high water content, inertness toward toxic degradation and natural organ function, and permeability to metabolites.[43] These scientists were working with a methacrylate hydrogel and spawned the interest in using these soft gel materials for biological applications. Since then many hydrogel products such as contact lenses have been marketed and commercially sold. These commercial

successes and more importantly the interesting properties of hydrogels have made hydrogel biomaterials a rich area of study.[44-51]

Hydrogel materials are cross-linked polymer networks which swell considerably in water, more specifically, they swell with 90-99% water by weight.[52] The high solvent content allows, not only for the passage of small molecule metabolites, as mentioned above, but provides real estate for therapeutic or diagnostic cargo.[53,54] The water content, distance between polymer chains, and therefore elasticity of the hydrogel can be tuned for the particular application. Response to stimuli can also be incorporated by inducing what is called a volume phase transition which occurs when the polymer collapses increasing the polymer density and expelling solvent. Stimuli that have been shown to induced volume phase transitions in hydrogels include temperature,[55,56] pH,[57] light,[58] macromolecules,[45,59,60] and electric fields.[61]

An interesting subset of hydrogel materials is hydrogel microparticles or microgels. Microgels (hydrogel micro- or nano- particles) exhibit similar utility to bulk hydrogels yet are spherical particles with diameters ranging from ~100 to ~2000 nm. The use of microgels offers particular advantages in terms of material architecture, response time, and versatility. Importantly, the tunability of the dynamics of these constructs is critical for their response, and therefore, the utility of microgels for applications such as sensing. Some inherent response can be engineered into a microgel by simply choosing monomers, co-monomers, and/or cross-linkers that change properties in response to stimuli. The most common responsive microgels either incorporate a monomer that when polymerized becomes thermo-responsive and shows a phase change at a given temperature, or a pH-responsive monomer that exhibits more or less intermolecular

Columbic repulsion as a function of the pH and salt content of the surrounding media. These two stimuli are advantageous for some applications, but to design materials for specific therapeutic or diagnostic applications, it is desirable to employ a generalizable construct that permits incorporation of a variety of response elements.[23,40-42,54,60,62,63] The synthesis and characterization of hydrogel particles is a rich area of research, due to the interesting biomedical applications as well as fundamental properties.[64]

1.3 Microgels

1.3.1 Microgel Synthesis

Microgel particles have been synthesized by a variety of polymerization strategies including emulsion polymerization, inverse mini- or micro-emulsion polymerization, cross-linking of polymer chains, and precipitation polymerization. Precipitation polymerization is advantageous, because it can be performed in water with water soluble monomers. The strategy, however, is dependent on a solubility change as the polymer chain grows. Two of the more commonly used monomers in precipitation polymerization of microgels include N-isopropyl acrylamide (NIPAm) or N-isopropyl methacrylamide (NIPMAm). In both cases, the monomer is water soluble, but above a certain temperature and chain length, the polymer expels water and prefers polymer-polymer interactions over polymer-water interactions. This temperature for a polymer is the lower critical solution temperature (LCST), and it is ~31 ºC and ~44 ºC for pNIPAm and pNIPMAm, respectively (**Figure 1.1**).[65] The microgel synthesis reaction proceeds as follows, the monomers (NIPAm or NIPMAm), co-monomers (e.g. acrylic acid (AAc)), and cross-linkers (e.g. N,N-methylenebisacrylamide (BIS)) are dissolved in solution

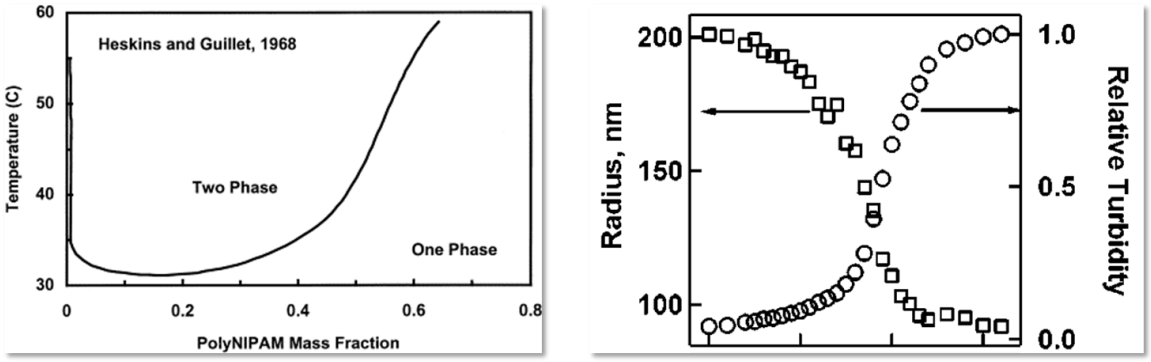

Figure 1.1. Left panel: Phase diagram illustrating the lower critical solution temperature of pNIPAm from Heskins and Guillet.[65] Right panel: Illustration of the change of radius and refractive index contrast as temperature is increased left to right of a microgel solution from Wang et al.[66]

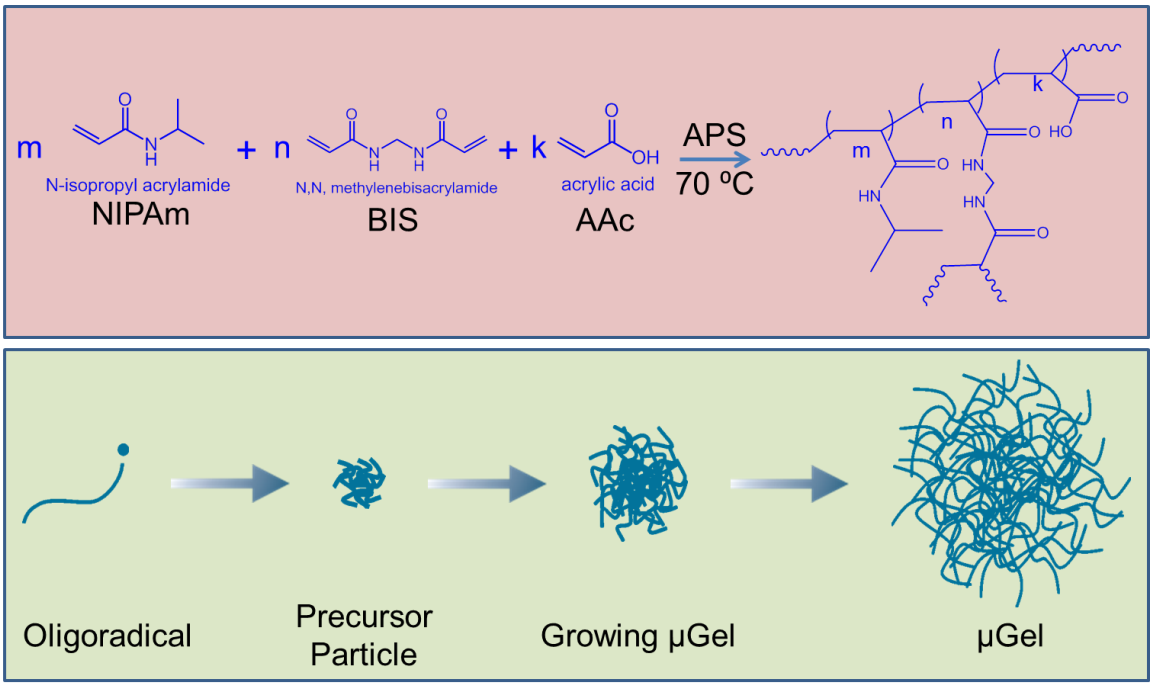

Scheme 1.1. Top panel: Common BIS cross-linked NIPAm-AAc microgel reaction Bottom panel: Scheme illustrating microgel formation during synthesis.

bubbled with nitrogen to remove oxygen radical scavengers. The solution is raised to a temperature above the LCST for the polymer and the thermal decomposition

temperature for the initiator (~70 ºC is typical) (**Scheme 1.1**).[67] Then after addition of a thermally activated initiator (e.g. ammonium persulfate (APS)), an oligo-radical is formed. Once the oligomer reaches a critical chain length, since the solution is above the LCST, it collapses on itself expelling water and creating a precursor particle. The precursor particle then grows by collection of other precursor particles and direct addition of monomer or oligomers. Since, initiation of the synthesis is relatively fast the particles all grow at approximately the same rate and a monodisperse particle population is achieved. The microgel is formed using a thermo-responsive polymer, therefore, above the LCST for the polymer, the microgel deswells due to the entropic release of water. This temperature for a microgel is called the volume phase transition temperature (VPTT) (**Figure 1.1**).[66]

There are a host of strategies to impart synthetic control over the precipitation polymerization of microgels. By varying the temperature of synthesis or incorporating a temperature ramp at initiation, microgels up to a few microns in diameter can be synthesized.[68] Also, by incorporation of surfactant and a higher initiator concentration, a high concentration of precursor particles stabilized by the surfactant is formed. The growth rate of these stabilized particles decreases by reducing aggregation of precursor particles thereby forming a stable solution of particles ~100 nm in diameter.[69] Not only can microgels from a few microns to a 100 nm in diameter be formed by precipitation polymerization, but topological control has been shown by making core/shell microgels where different monomers can be spatially separated in the particle.[70] This has led to a whole host of structures including hollow particles and core-double-shell particles as reviewed in a recent Accounts of Chemical Research article by Smith and Lyon.[71] These

are just examples of the power of simple precipitation polymerization when used to make microgels.

1.3.2 Microgel Characterization Techniques

1.3.2.1 Size

Typical size characterization of microgels is done by dynamic light scattering (DLS). Here, the hydrodynamic radius, $R_{h,}$ is determined by detecting light intensity fluctuations over time at a specific detection angle. Using the intensity fluctuations, an autocorrelation function is generated by plotting the autocorrelation value (between 1 and 2) vs. delay times, τ. The autocorrelation function, which gives an indication of the similarity or the correlation between signals over time, is then fit by one of two fitting methods. Using the fits a diffusion coefficient for the scattering species can be determined. The first method is called a cumulant fit which fits this decay curve by assuming a single exponential decay. This is the fit most often used for microgels produced by precipitation polymerization because a monodisperse size distribution is expected. The second method is called a regularization fit which will assume multiple exponential decays so this might be used if multiple populations are expected. From each exponential, a diffusion coefficient is determined. Then the diffusion coefficient, D, can be used to calculate a R_h through the Stokes-Einstein equation (**Equation 1.1**).

Equation 1.1. Stokes-Einstein Equation $R_h = \frac{kT}{6\pi\eta D}$

Here, the k, T, and η are Boltzmann‘s constant, temperature in kelvin, and viscosity of the solvent. Qualitatively, early autocorrelation decay means fast-diffusing or small particles and late decay means slow-diffusing or large particles. In our lab, two different

DLS instruments are used, a cuvette based system with 90º scattering detector and a 783 nm laser and a plate reader system with a 158º detector and an 832 nm laser. Both systems could measure particles from a few nanometers to about a micron in diameter. Often DLS measurements were carried out on microgels at different pH or temperature values in order to determine the pH and thermoresponsivity. If the approximate size of the microgels approached 1000 nm in diameter or more, they were characterized by optical microscopy and atomic force microscopy (AFM). Although not performed for the purposes of the work presented here, characterizations of radius of gyration, R_g, can be performed by multi-angle laser light scattering (MALLS) techniques. Here, the angle dependence on scattering is used to determine R_g and molecular weight.

1.3.2.2 Charge

Most commonly the surface charge of micro and nanoparticles is determined by electrophoretic mobility and is reported as a ζ-potential. This is measured using an electrophoretic light scattering instrument and different low ionic strength buffers. This instrument detects movement of particles in an electric field gradient, thereby determining the electrophoretic mobility. Then the ζ-potential is calculated from the electrophoretic mobility; however, due to the fact that the microgel particles are not smooth spheres with a well-defined surface, these numbers are not reliable when compared to ζ-potentials of other particle types. Especially when the microgels have incorporated charged monomers, there is substantial charge buried within the particle which affects the electrophoretic mobility but are not accounted for in the calculation of ζ-potential. Currently, the most accurate way to characterize microgel acidic or basic monomer is by titration.

1.3.2.3 Structure

Largely microgel topology is characterized using two microscopy techniques and a light scattering technique. The first microscopy technique is AFM. In this case, particles are deposited on a surface and then imaged using a small tip on the end of a cantilever which deflects a laser into a four quadrant detector. The deflection of the laser by the cantilever is related to a change in height and depicted in a height map of the surface. The second technique that our group has used in the past and others have used more recently is cryogenic scanning electron microscopy (cryo-SEM). Here, a better representation of the water solvated particles can be achieved. Lastly, topology can be inferred by studying the ratio of the R_g to the R_h. The radius of hydration, R_h, is representative of the particle radius with its associate hydration sphere, whereas, the radius of gyration, R_g, is representative of the center of mass of the particle. It should be noted that a sphere of uniform density has an R_g/R_h of ~0.77. Therefore, particles with a high density core and dangling chains at the periphery would have a R_g/R_h of less than < 0.77 and a particle with a high density periphery and a low density interior, such as a hollow sphere, would have a R_g/R_h of > 0.77.[72,73] These numbers are found by DLS (R_h) and MALLS (R_g).

1.4 Microgels as Biomaterials

1.4.1 Biomaterial Design Rules

Design rules for diagnostic or therapeutic material applications can be based on advantageous therapeutic effects or useful transduction mechanisms, but can often be limited by factors such as toxicity or sensitivity. These rules should help generalize the effects of both physical and chemical properties of a biomaterial, in order to achieve

maximum therapeutic or diagnostic effect with minimum long or short term toxicity to healthy cells or organs.

Design rules, in general, for biomaterials have been investigated for all kinds of systems including 2- and 3-D bulk materials for tissue scaffolds and to nanoparticulate systems for drug delivery. The design considerations include properties such as size, shape, topology, morphology, mechanics, payload entrapment, and biospecific interaction (**Scheme 1.2**). Each of these design rules can affect the performance of the material as well as its toxicity. For instance, it has been shown that the shape of polymeric nanoparticles can effect tumor penetration as well as biodistribution.[74] It is also known that effects of charge, size, and hydrophobicity can change the particle clearance mechanism, and its ability to accumulate in tumors through the enhance permeation and retention (EPR) effect.[75] These design rules along with increasing knowledge of biological processes, like the size-dependence of transdermal uptake and extravasation from the blood, emphasizes the importance of choosing the right size material for your application.[76] One of the more recent findings has been that the mechanics of the material might change the biological response to the material.

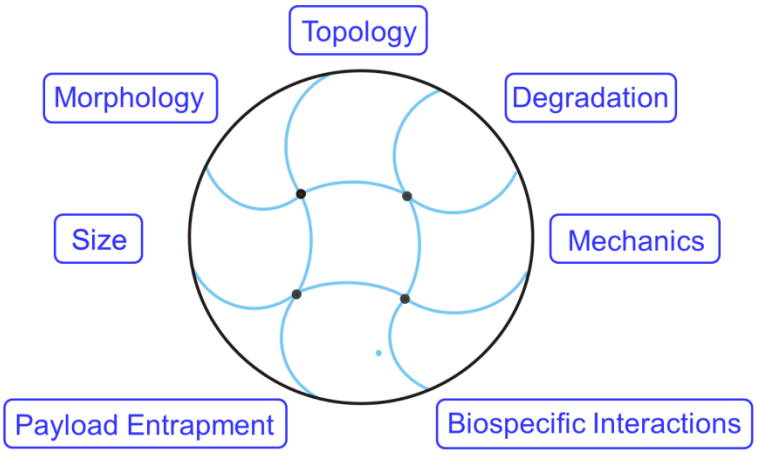

Scheme 1.2. Some biomaterial design considerations.

1.4.2 Importance of Biomaterial Mechanics

In applications utilizing synthetic biomaterials, such as drug delivery,[77-80] bioimaging,[81,82] and tissue engineering,[83-87] the material mechanical properties represent an important set of design parameters.[76] Studies of biological tissues themselves have shown a wide range of moduli for different biological tissues and cell types including cancer cells versus healthy cells.[88,89] Most studies of mechanical properties in biomaterials have focused on how cells interact with or move on surfaces of different rigidity in the context of mechanotransduction[83,86,87] and cell proliferation or differentiation.[84,85] **Figure 1.2** shows examples of substrate stiffness directed stem cell differentiation.[85] Although most studies have been based on these bulk substrates, it has been suggested, however, that the softness of nanoparticles may be relevant in processes such as phagocytosis or endocytosis.[90,91] This indicates that not only are cells affected by the mechanics of large surfaces or interfaces, but also by the rigidity of individual nanoparticles.

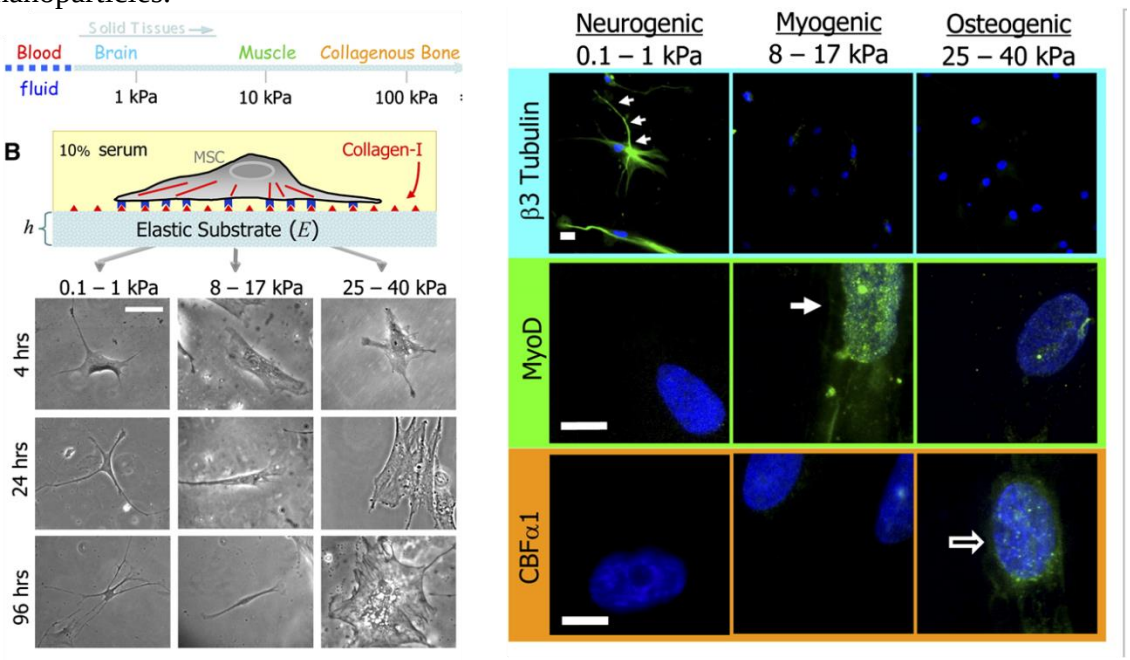

Figure 1.2. Matrix stiffness effects on stem cell differentiation from Discher and co-workers.[85]

1.4.3 Microgel Mechanical Characterization

For years, microgel suspension moduli have been studied using different rheological methods;[92,93] however, it has been more difficult to get at the moduli of single microgels. Three different methods have been developed for studying the mechanical properties of microgels; AFM measurements,[94-96] osmotic compression studies,[97-99] and capillary micromechanics.[97,100] The AFM methods use a cantilever with a particular spring constant to probe the mechanics of a surface by applying a force and measuring the materials response. The cantilevers used have had typical sharp tips used for imaging,[96] been modified with a polystyrene sphere,[94] or have been unmodified bare cantilevers.[95] These AFM methods are largely preformed on microgels >10 μm in diameter which allows for modified tips with larger surface area. When the particles are ≤1 μm in diameter, these AFM experiments become more challenging. Now, the size of the tip has to be smaller and may penetrate the particle. Similarly, in the case of the capillary micromechanics experiments, the particles have to be sufficiently large to observe under an optical microscope and to get lodged in the end of a capillary. This method forces microgel under very controlled pressures into a confined end of a pulled capillary, and by knowing the applied pressure and measuring the deformation of the particle, mechanical properties can be calculated. Lastly, the osmotic compression method is performed by placing microgels in a solution of non-interacting polymers at different concentrations which increases or decreases the osmotic pressure difference between the inside and outside of the particle. When the osmotic pressure is increased, the particle is forced to deswell. These changes in size are monitored by DLS, and after calculating the different osmotic forces, the bulk modulus of the particles can be

calculated. Although this method is promising, further development of methods to study small microgel or even nanogel mechanical properties is ongoing.

1.4.4 Microgel Softness

Microgels are viscoelastic particles that are compressible and neither shape nor volume conserving. The softness of the microgel allows it to respond to both typical polymer environmental cues such as pH, ionic strength, or temperature, but also can respond to the global lattice energy of a colloidal crystal. Because of some of these observations, in a recent review written by Lyon and Fernandez-Nieves, the microgel particles were describe as having a polymer/colloid duality especially in the context of suspensions.[101] The few examples of measurements of the classic values associated with softness, Young's, shear, and bulk moduli of individual hydrogel microparticles were shared above. To follow will be select examples of both fundamental studies illustrating the effects of microgel softness and studies utilizing the softness in application.

1.4.4.1 Fundamental Observations of Microgel Softness

Some of the most interesting observations of microgels have come from fundamental studies of microgel suspension phase behavior. Since the phase behavior of hard spheres suspensions was determine to be purely dependent on the volume fraction of particles,[102] thermoresponsive microgels seemed like an interesting candidate for these studies due to their ability to change volume fraction on an external stimulus.[103-105] Experiments first demonstrated successful formation of ordered crystals formed from microgels. Some interesting results were found using p(NIPAm-co-AAc) microgels which imparted a charge component that could be tuned by solution pH.[106] It was found that, when the particles were mostly protonated, the phase behavior was similar to hard

spheres, except the regions of crystallization extended above the appropriate volume fraction for hard spheres. This observation can be attributed to the compressibility of the microgels, which allows the particles to avoid getting trapped in a glass at these high concentrations. However, at near neutral pH, when the particles were more highly charged, the crystal region was very small or could not be observed at all. In this case, the particles cannot avoid being trapped into the glassy state potentially due to the reduced compressibility due to the charges in the microgels. In an even more dramatic example of the softness of these particles, microgel suspensions were formed with ~0.7 μm in diameter microgels with a few defect microgels of ~1.75 μm diameter.[107] In this case, the 1.75 μm particles deswelled to fit into the lattice that was created by the smaller microgels. The entropy gain from forming a crystal was greater than the loss due to deswelling the particle. This is a clear example of the softness of these particles and how they act as both a polymer and a colloid.

1.4.4.2 Microgel Softness Applied in Bioapplications

The colloidal suspension studies above can be extended to applications such as color-tunable Bragg diffraction crystals.[108] The light diffracted from the sample is based on the distance between the particles in the crystal, and the angle of the incident light. In this case, the lattice spacing could be changed by assembling the crystal at different temperatures, thereby changing the size of the pNIPAm microgels, the lattice spacing, and the resulting Bragg peak. In general, the softness of these materials allows for not only the inherit responsively due to the choice of a thermoresponsive or pH-responsive monomer, but enables the incorporation of other responsive elements due to the flexibility of the network. These are the same properties that allow for many different

sensing platforms to be developed using microgel and hydrogel materials.[44,45,52,109] In **Chapter 2**, more specific hydrogel sensing platforms will be discussed as well as our efforts to develop a microgel biosensor.

In biology there are many examples of where the softness or deformability of particles is important. One in particular is red blood cells and their ability to squeeze through vasculature. The DeSimone group has used hydrogel microparticles as a possible red blood cell mimic by loading them with hemoglobin and watching them pass through small channels, utilizing the ability of the hydrogel to deform.[110,111] Similar experiments observing the ability for microgels to deform and pass through pores will be discussed in **Chapters 3** and **Chapter 5**.

Another advantageous property of these soft materials is that they have been shown to strongly deform at interfaces creating some interesting possible applications. In our laboratory, as discussed in **Chapter 2,** the asymmetrical deformation of these particles when attached to a glass substrate has allowed for the creation of microlenses.[112,113] In other cases, these particles have been shown to deform dramatically to act as a stabilizer for oil-in-water particle-stabilized emulsions or Pickering emulsions (**Appendix A**).[114-116] It has been shown that microgels deform drastically to help lower the surface energy at the oil/water interface. This observation has been suggested as the primary reason that microgels act as good emulsifiers. Similarly, it is possible that many of the interesting observations of microgels and microgel assemblies that have been observed could be linked to the softness of the particles. In the Lyon group, it has been observed, that layer-by-layer (LbL) films formed by alternate deposition of anionic microgels and a polycation self-heal.[117,118] Here, when a film is deposited on a soft

substrate and the film is stretched in the dry state, it displays damage. Then, after wetting the film, it is repaired. These observations are under further investigation to discover the exact reasons for such an interesting result; however, one hypothesis is that due to the multi-valiancy and flexibility of the polymer it is not trapped in the high energy state that is created when damage is formed. Obviously, this is just a hypothesis that is being actively tested in the Lyon lab; however, it is just one example of a recent interesting and useful bulk property that could be a result of particle softness. In this dissertation, microgel softness is harnessed (**Chapter 2** and **Appendix A**) or studied (**Chapter 3** and **Chapter 5**) in the context of interfacing with biology.

1.5 References

[1] Peppas, N.A.; Langer, R. New Challenges in Biomaterials. *Science* **1994**, *263*, 1715-1720.

[2] Langer, R.; Tirrell, D.A. Designing Materials for Biology and Medicine. *Nature* **2004**, *428*, 487-492.

[3] Burg, K.J.L.; Porter, S.; Kellam, J.F. Biomaterial Developments for Bone Tissue Engineering. *Biomaterials* **2000**, *21*, 2347-2359.

[4] Hench, L.L. Bioceramics. *Journal of the American Ceramic Society* **1998**, *81*, 1705-1728.

[5] Long, M.; Rack, H.J. Titanium Alloys in Total Joint Replacement - a Materials Science Perspective. *Biomaterials* **1998**, *19*, 1621-1639.

[6] Staiger, M.P.; Pietak, A.M.; Huadmai, J.; Dias, G. Magnesium and Its Alloys as Orthopedic Biomaterials: A Review. *Biomaterials* **2006**, *27*, 1728-1734.

[7] Harrison, B.S.; Atala, A. Carbon Nanotube Applications for Tissue Engineering. *Biomaterials* **2007**, *28*, 344-353.

[8] Boisselier, E.; Astruc, D. Gold Nanoparticles in Nanomedicine: Preparations, Imaging, Diagnostics, Therapies and Toxicity. *Chemical Society Reviews* **2009**, *38*, 1759-1782.

[9] Ghosh, P.; Han, G.; De, M.; Kim, C.K.; Rotello, V.M. Gold Nanoparticles in Delivery Applications. *Adv. Drug Deliv. Rev.* **2008**, *60*, 1307-1315.

[10] Gao, J.H.; Gu, H.W.; Xu, B. Multifunctional Magnetic Nanoparticles: Design, Synthesis, and Biomedical Applications. *Accounts of Chemical Research* **2009**, *42*, 1097-1107.

[11] Slowing, II; Vivero-Escoto, J.L.; Wu, C.W.; Lin, V.S.Y. Mesoporous Silica Nanoparticles as Controlled Release Drug Delivery and Gene Transfection Carriers. *Adv. Drug Deliv. Rev.* **2008**, *60*, 1278-1288.

[12] Smith, A.M.; Duan, H.W.; Mohs, A.M.; Nie, S.M. Bioconjugated Quantum Dots for in Vivo Molecular and Cellular Imaging. *Adv. Drug Deliv. Rev.* **2008**, *60*, 1226-1240.

[13] Wissing, S.A.; Kayser, O.; Muller, R.H. Solid Lipid Nanoparticles for Parenteral Drug Delivery. *Adv. Drug Deliv. Rev.* **2004**, *56*, 1257-1272.

[14] O'Reilly, R.K.; Hawker, C.J.; Wooley, K.L. Cross-Linked Block Copolymer Micelles: Functional Nanostructures of Great Potential and Versatility. *Chemical Society Reviews* **2006**, *35*, 1068-1083.

[15] Rinaudo, M. Chitin and Chitosan: Properties and Applications. *Progress in Polymer Science* **2006**, *31*, 603-632.

[16] Sashiwa, H.; Aiba, S.I. Chemically Modified Chitin and Chitosan as Biomaterials. *Progress in Polymer Science* **2004**, *29*, 887-908.

[17] Augst, A.D.; Kong, H.J.; Mooney, D.J. Alginate Hydrogels as Biomaterials. *Macromolecular Bioscience* **2006**, *6*, 623-633.

[18] Vepari, C.; Kaplan, D.L. Silk as a Biomaterial. *Progress in Polymer Science* **2007**, *32*, 991-1007.

[19] Wang, Y.Z.; Kim, H.J.; Vunjak-Novakovic, G.; Kaplan, D.L. Stem Cell-Based Tissue Engineering with Silk Biomaterials. *Biomaterials* **2006**, *27*, 6064-6082.

[20] Moschou, E.A.; Madou, M.J.; Bachas, L.G.; Daunert, S. Voltage-Switchable Artificial Muscles Actuating at near Neutral Ph. *Sensors and Actuators B-Chemical* **2006**, *115*, 379-383.

[21] Moschou, E.A.; Peteu, S.F.; Bachas, L.G.; Madou, M.J.; Daunert, S. Artificial Muscle Material with Fast Electroactuation under Neutral Ph Conditions. *Chemistry of Materials* **2004**, *16*, 2499-2502.

[22] Seliktar, D.; Zisch, A.H.; Lutolf, M.P.; Wrana, J.L.; Hubbell, J.A. Mmp-2 Sensitive, Vegf-Bearing Bioactive Hydrogels for Promotion of Vascular Healing. *Journal of Biomedical Materials Research Part A* **2004**, *68A*, 704-716.

[23] Tae, G.; Kim, Y.J.; Choi, W.I.; Kim, M.; Stayton, P.S.; Hoffman, A.S. Formation of a Novel Heparin-Based Hydrogel in the Presence of Heparin-Binding Biomolecules. *Biomacromolecules* **2007**, *8*, 1979-1986.

[24] Wang, D.A.; Williams, C.G.; Yang, F.; Cher, N.; Lee, H.; Elisseeff, J.H. Bioresponsive Phosphoester Hydrogels for Bone Tissue Engineering. *Tissue Engineering* **2005**, *11*, 201-213.

[25] Yamaguchi, N.; Zhang, L.; Chae, B.S.; Palla, C.S.; Furst, E.M.; Kiick, K.L. Growth Factor Mediated Assembly of Cell Receptor-Responsive Hydrogels. *Journal of the American Chemical Society* **2007**, *129*, 3040-+.

[26] Gan, D.J.; Lyon, L.A. Synthesis and Protein Adsorption Resistance of Peg-Modified Poly(N-Isopropylacrylamide) Core/Shell Microgels. *Macromolecules* **2002**, *35*, 9634-9639.

[27] Nolan, C.M.; Reyes, C.D.; Debord, J.D.; Garcia, A.J.; Lyon, L.A. Phase Transition Behavior, Protein Adsorption, and Cell Adhesion Resistance of Poly(Ethylene Glycol) Cross-Linked Microgel Particles. *Biomacromolecules* **2005**, *6*, 2032-2039.

[28] Kim, J.; Singh, N.; Lyon, L.A. Influence of Ancillary Binding and Nonspecific Adsorption on Bioresponsive Hydrogel Microlenses. *Biomacromolecules* **2007**, *8*, 1157-1161.

[29] De Geest, B.G.; Dejugnat, C.; Sukhorukov, G.B.; Braeckmans, K.; De Smedt, S.C.; Demeester, J. Self-Rupturing Microcapsules. *Advanced Materials* **2005**, *17*, 2357-+.

[30] Deng, Y.H.; Wang, C.C.; Shen, X.Z.; Yang, W.L.; An, L.; Gao, H.; Fu, S.K. Preparation, Characterization, and Application of Multistimuli-Responsive Microspheres with Fluorescence-Labeled Magnetic Cores and Thermoresponsive Shells. *Chemistry-a European Journal* **2005**, *11*, 6006-6013.

[31] Ehrick, J.D.; Deo, S.K.; Browning, T.W.; Bachas, L.G.; Madou, M.J.; Daunert, S. Genetically Engineered Protein in Hydrogels Tailors Stimuli-Responsive Characteristics. *Nature Materials* **2005**, *4*, 298-302.

[32] Gu, J.X.; Xia, F.; Wu, Y.; Qu, X.Z.; Yang, Z.Z.; Jiang, L. Programmable Delivery of Hydrophilic Drug Using Dually Responsive Hydrogel Cages. *Journal of Controlled Release* **2007**, *117*, 396-402.

[33] Rao, K.; Naidu, B.V.K.; Subha, M.C.S.; Sairam, M.; Aminabhavi, T.M. Novel Chitosan-Based Ph-Sensitive Interpenetrating Network Microgels for the Controlled Release of Cefadroxil. *Carbohydrate Polymers* **2006**, *66*, 333-344.

[34] Soppimath, K.S.; Kulkarni, A.R.; Aminabhavi, T.M. Chemically Modified Polyacrylamide-G-Guar Gum-Based Crosslinked Anionic Microgels as Ph-Sensitive Drug Delivery Systems: Preparation and Characterization. *Journal of Controlled Release* **2001**, *75*, 331-345.

[35] Tae, G.; Scatena, M.; Stayton, P.S.; Hoffman, A.S. Peg-Cross-Linked Heparin Is an Affinity Hydrogel for Sustained Release of Vascular Endothelial Growth Factor. *Journal of Biomaterials Science-Polymer Edition* **2006**, *17*, 187-197.

[36] Thornton, P.D.; Mart, R.J.; Ulijn, R.V. Enzyme-Responsive Polymer Hydrogel Particles for Controlled Release. *Advanced Materials* **2007**, *19*, 1252-+.

[37] Wheeldon, I.R.; Barton, S.C.; Banta, S. Bioactive Proteinaceous Hydrogels from Designed Bifunctional Building Blocks. *Biomacromolecules* **2007**, *8*, 2990-2994.

[38] Wood, K.C.; Chuang, H.F.; Batten, R.D.; Lynn, D.M.; Hammond, P.T. Controlling Interlayer Diffusion to Achieve Sustained, Multiagent Delivery from Layer-by-Layer Thin Films. *Proceedings of the National Academy of Sciences of the United States of America* **2006**, *103*, 10207-10212.

[39] Zhou, J.; Wang, G.N.; Zou, L.; Tang, L.P.; Marquez, M.; Hu, Z.B. Viscoelastic Behavior and in Vivo Release Study of Microgel Dispersions with Inverse Thermoreversible Gelation. *Biomacromolecules* **2008**, *9*, 142-148.

[40] Alarcon, C.D.H.; Pennadam, S.; Alexander, C. Stimuli Responsive Polymers for Biomedical Applications. *Chemical Society Reviews* **2005**, *34*, 276-285.

[41] Galaev, I.Y.; Mattiasson, B. 'Smart' Polymers and What They Could Do in Biotechnology and Medicine. *Trends in Biotechnology* **1999**, *17*, 335-340.

[42] Mart, R.J.; Osborne, R.D.; Stevens, M.M.; Ulijn, R.V. Peptide-Based Stimuli-Responsive Biomaterials. *Soft Matter* **2006**, *2*, 822-835.

[43] Wichterle, O.; Lim, D. Hydrophilic Gels for Biological Use. *Nature* **1960**, *185*, 117-118.

[44] Buenger, D.; Topuz, F.; Groll, J. Hydrogels in Sensing Applications. *Progress in Polymer Science* **2012**, *37*, 1678-1719.

[45] Hendrickson, G.R.; Lyon, L.A. Bioresponsive Hydrogels for Sensing Applications. *Soft Matter* **2009**, *5*, 29-35.

[46] Hoffman, A.S. Hydrogels for Biomedical Applications. *Adv. Drug Deliv. Rev.* **2002**, *54*, 3-12.

[47] Jeong, B.; Gutowska, A. Lessons from Nature: Stimuli-Responsive Polymers and Their Biomedical Applications. *Trends in Biotechnology* **2002**, *20*, 305-311.

[48] Khademhosseini, A.; Langer, R.; Borenstein, J.; Vacanti, J.P. Microscale Technologies for Tissue Engineering and Biology. *Proceedings of the National Academy of Sciences of the United States of America* **2006**, *103*, 2480-2487.

[49] Kopecek, J. Hydrogels: From Soft Contact Lenses and Implants to Self-Assembled Nanomaterials. *Journal of Polymer Science Part a-Polymer Chemistry* **2009**, *47*, 5929-5946.

[50] Langer, R. Biomaterials in Drug Delivery and Tissue Engineering: One Laboratory's Experience. *Accounts of Chemical Research* **2000**, *33*, 94-101.

[51] Langer, R.; Peppas, N.A. Advances in Biomaterials, Drug Delivery, and Bionanotechnology. *Aiche Journal* **2003**, *49*, 2990-3006.

[52] Peppas, N.A.; Hilt, J.Z.; Khademhosseini, A.; Langer, R. Hydrogels in Biology and Medicine: From Molecular Principles to Bionanotechnology. *Advanced Materials* **2006**, *18*, 1345-1360.

[53] Fanger, C.; Wack, H.; Ulbricht, M. Macroporous Poly (N-Isopropylacrylamide) Hydrogels with Adjustable Size "Cut-Off" for the Efficient and Reversible Immobilization of Biomacromolecules. *Macromolecular Bioscience* **2006**, *6*, 393-402.

[54] Ulijn, R.V.; Bibi, N.; Jayawarna, V.; Thornton, P.D.; Todd, S.J.; Mart, R.J.; Smith, A.M.; Gough, J.E. Bioresponsive Hydrogels. *Materials Today* **2007**, *10*, 40-48.

[55] Liu, R.X.; Fraylich, M.; Saunders, B.R. Thermoresponsive Copolymers: From Fundamental Studies to Applications. *Colloid and Polymer Science* **2009**, *287*, 627-643.

[56] Shibayama, M.; Tanaka, T. Volume Phase-Transition and Related Phenomena of Polymer Gels. *Advances in Polymer Science* **1993**, *109*, 1-62.

[57] Hoare, T.; Pelton, R. Highly Ph and Temperature Responsive Microgels Functionalized with Vinylacetic Acid. *Macromolecules* **2004**, *37*, 2544-2550.

[58] Mamada, A.; Tanaka, T.; Kungwatchakun, D.; Irie, M. Photoinduced Phase-Transition of Gels. *Macromolecules* **1990**, *23*, 1517-1519.

[59] Hoffman, A.S. Hydrogels for Biomedical Applications. *Adv. Drug Deliv. Rev.* **2002**, *54*, 3-12.

[60] Miyata, T.; Uragami, T.; Nakamae, K. Biomolecule-Sensitive Hydrogels. *Adv. Drug Deliv. Rev.* **2002**, *54*, 79-98.

[61] Kulkarni, R.V.; Biswanath, S. Electrically Responsive Smart Hydrogels in Drug Delivery: A Review. *Journal of Applied Biomaterials & Biomechanics* **2007**, *5*, 125-139.

[62] Deo, S.; Moschou, E.; Peteu, S.; Eisenhardt, P.; Bachas, L.; Madou, M.; Daunert, S. Responsive Drug Delivery Systems. *Anal. Chem.* **2003**, *75*, 207A-213A.

[63] Kikuchi, A.; Okano, T. Pulsatile Drug Release Control Using Hydrogels. *Adv. Drug Deliv. Rev.* **2002**, *54*, 53-77.

[64] Nayak, S.; Lyon, L.A. Soft Nanotechnology with Soft Nanoparticles. *Angewandte Chemie-International Edition* **2005**, *44*, 7686-7708.

[65] Heskins, M.; Guillet, J.E. Solution Properties of Poly(N-Isopropylacrylamide). *J. Macromol. Sci. Chem.* **1968**, *A2*, 1441-1455.

[66] Wang, J.P.; Gan, D.J.; Lyon, L.A.; El-Sayed, M.A. Temperature-Jump Investigations of the Kinetics of Hydrogel Nanoparticle Volume Phase Transitions. *Journal of the American Chemical Society* **2001**, *123*, 11284-11289.

[67] Jones, C.D.; Lyon, L.A. Synthesis and Characterization of Multiresponsive Core-Shell Microgels. *Macromolecules* **2000**, *33*, 8301-8306.

[68] Meng, Z.Y.; Smith, M.H.; Lyon, L.A. Temperature-Programmed Synthesis of Micron-Sized Multi-Responsive Microgels. *Colloid and Polymer Science* **2009**, *287*, 277-285.

[69] Blackburn, W.H.; Lyon, L.A. Size-Controlled Synthesis of Monodisperse Core/Shell Nanogels. *Colloid and Polymer Science* **2008**, *286*, 563-569.

[70] Jones, C.D.; Lyon, L.A. Synthesis and Characterization of Multiresponsive Core-Shell Microgels. *Macromolecules* **2000**, *33*, 8301-8306.

[71] Smith, M.H.; Lyon, L.A. Multifunctional Nanogels for Sirna Delivery. *Accounts of Chemical Research* **2012**, *45*, 985-993.

[72] Burchard, W.; Schmidt, M.; Stockmayer, W.H. Information on Polydispersity and Branching from Combined Quasi-Elastic and Integrated Scattering. *Macromolecules* **1980**, *13*, 1265-1272.

[73] Kok, C.M.; Rudin, A. Relationship between the Hydrodynamic Radius and the Radius of Gyration of a Polymer in Solution. *Makromolekulare Chemie-Rapid Communications* **1981**, *2*, 655-659.

[74] Venkataraman, S.; Hedrick, J.L.; Ong, Z.Y.; Yang, C.; Ee, P.L.R.; Hammond, P.T.; Yang, Y.Y. The Effects of Polymeric Nanostructure Shape on Drug Delivery. *Adv. Drug Deliv. Rev.* **2011**, *63*, 1228-1246.

[75] Nel, A.E.; Madler, L.; Velegol, D.; Xia, T.; Hoek, E.M.V.; Somasundaran, P.; Klaessig, F.; Castranova, V.; Thompson, M. Understanding Biophysicochemical Interactions at the Nano-Bio Interface. *Nature Materials* **2009**, *8*, 543-557.

[76] Mitragotri, S.; Lahann, J. Physical Approaches to Biomaterial Design. *Nature Materials* **2009**, *8*, 15-23.

[77] Jain, T.K.; Reddy, M.K.; Morales, M.A.; Leslie-Pelecky, D.L.; Labhasetwar, V. Biodistribution, Clearance, and Biocompatibility of Iron Oxide Magnetic Nanoparticles in Rats. *Molecular Pharmaceutics* **2008**, *5*, 316-327.

[78] Jie, P.; Venkatraman, S.S.; Min, F.; Freddy, B.Y.C.; Huat, G.L. Micelle-Like Nanoparticles of Star-Branched Peo-Pla Copolymers as Chemotherapeutic Carrier. *Journal of Controlled Release* **2005**, *110*, 20-33.

[79] Shirota, K.; Kato, Y.; Suzuki, K.; Sugiyama, Y. Characterization of Novel Kidney-Specific Delivery System Using an Alkylglucoside Vector. *Journal of Pharmacology and Experimental Therapeutics* **2001**, *299*, 459-467.

[80] Tabata, T.; Murakami, Y.; Ikada, Y. Tumor Accumulation of Poly(Vinyl Alcohol) of Different Sizes after Intravenous Injection. *J. Controlled Release* **1998**, *50*, 123-133.

[81] He, X.X.; Nie, H.L.; Wang, K.M.; Tan, W.H.; Wu, X.; Zhang, P.F. In Vivo Study of Biodistribution and Urinary Excretion of Surface-Modified Silica Nanoparticles. *Anal. Chem.* **2008**, *80*, 9597-9603.

[82] Schipper, M.L.; Iyer, G.; Koh, A.L.; Cheng, Z.; Ebenstein, Y.; Aharoni, A.; Keren, S.; Bentolila, L.A.; Li, J.Q.; Rao, J.H.; Chen, X.Y.; Banin, U.; Wu, A.M.; Sinclair, R.; Weiss, S.; Gambhir, S.S. Particle Size, Surface Coating, and Pegylation Influence the Biodistribution of Quantum Dots in Living Mice. *Small* **2009**, *5*, 126-134.

[83] Chen, C.S.; Mrksich, M.; Huang, S.; Whitesides, G.M.; Ingber, D.E. Geometric Control of Cell Life and Death. *Science* **1997**, *276*, 1425-1428.

[84] Engler, A.J.; Griffin, M.A.; Sen, S.; Bonnetnann, C.G.; Sweeney, H.L.; Discher, D.E. Myotubes Differentiate Optimally on Substrates with Tissue-Like Stiffness:

Pathological Implications for Soft or Stiff Microenvironments. *Journal of Cell Biology* **2004**, *166*, 877-887.

[85] Engler, A.J.; Sen, S.; Sweeney, H.L.; Discher, D.E. Matrix Elasticity Directs Stem Cell Lineage Specification. *Cell* **2006**, *126*, 677-689.

[86] Shen, H.; Tan, J.; Saltzman, W.M. Surface-Mediated Gene Transfer from Nanocomposites of Controlled Texture. *Nature Materials* **2004**, *3*, 569-574.

[87] Ingber, D.E. Cellular Mechanotransduction: Putting All the Pieces Together Again. *Faseb Journal* **2006**, *20*, 811-827.

[88] Ebenstein, D.M.; Pruitt, L.A. Nanoindentation of Biological Materials. *Nano Today* **2006**, *1*, 26-33.

[89] Levental, I.; Georges, P.C.; Janmey, P.A. Soft Biological Materials and Their Impact on Cell Function. *Soft Matter* **2007**, *3*, 299-306.

[90] Beningo, K.A.; Wang, Y.L. Fc-Receptor-Mediated Phagocytosis Is Regulated by Mechanical Properties of the Target. *Journal of Cell Science* **2002**, *115*, 849-856.

[91] Banquy, X.; Suarez, F.; Argaw, A.; Rabanel, J.M.; Grutter, P.; Bouchard, J.F.; Hildgen, P.; Giasson, S. Effect of Mechanical Properties of Hydrogel Nanoparticles on Macrophage Cell Uptake. *Soft Matter* **2009**, *5*, 3984-3991.

[92] Senff, H.; Richtering, W. Temperature Sensitive Microgel Suspensions: Colloidal Phase Behavior and Rheology of Soft Spheres. *Journal of Chemical Physics* **1999**, *111*, 1705-1711.

[93] Senff, H.; Richtering, W. Influence of Cross-Link Density on Rheological Properties of Temperature-Sensitive Microgel Suspensions. *Colloid and Polymer Science* **2000**, *278*, 830-840.

[94] Hashmi, S.M.; Dufresne, E.R. Mechanical Properties of Individual Microgel Particles through the Deswelling Transition. *Soft Matter* **2009**, *5*, 3682-3688.

[95] Kumachev, A.; Tumarkin, E.; Walker, G.C.; Kumacheva, E. Characterization of the Mechanical Properties of Microgels Acting as Cellular Microenvironments. *Soft Matter* **2013**, *9*, 2959-2965.

[96] Wiedemair, J.; Serpe, M.J.; Kim, J.; Masson, J.-F.; Lyon, L.A.; Mizaikoff, B.; Kranz, C. In-Situ Afm Studies of the Phase-Transition Behavior of Single Thermoresponsive Hydrogel Particles. *Langmuir* **2007**, *23*, 130-137.

[97] Guo, M.Y.; Wyss, H.M. Micromechanics of Soft Particles. *Macromolecular Materials and Engineering* **2011**, *296*, 223-229.

[98] Sierra-Martin, B.; Frederick, J.A.; Laporte, Y.; Markou, G.; Lietor-Santos, J.J.; Fernandez-Nieves, A. Determination of the Bulk Modulus of Microgel Particles. *Colloid and Polymer Science* **2011**, *289*, 721-728.

[99] Sierra-Martin, B.; Laporte, Y.; South, A.B.; Lyon, L.A.; Fernandez-Nieves, A. Bulk Modulus of Poly(N-Isopropylacrylamide) Microgels through the Swelling Transition. *Physical Review E* **2011**, *84*.

[100] Wyss, H.M.; Franke, T.; Mele, E.; Weitz, D.A. Capillary Micromechanics: Measuring the Elasticity of Microscopic Soft Objects. *Soft Matter* **2010**, *6*, 4550-4555.

[101] Lyon, L.A.; Fernandez-Nieves, A., in *Annual Review of Physical Chemistry, Vol 63, Vol. 63* (Eds.: M. A. Johnson, T. J. Martinez), **2012**, pp. 25-43.

[102] Pusey, P.N.; Vanmegen, W. Phase-Behavior of Concentrated Suspensions of Nearly Hard Colloidal Spheres. *Nature* **1986**, *320*, 340-342.

[103] Eckert, T.; Richtering, W. Thermodynamic and Hydrodynamic Interaction in Concentrated Microgel Suspensions: Hard or Soft Sphere Behavior? *Journal of Chemical Physics* **2008**, *129*.

[104] Hellweg, T.; Dewhurst, C.D.; Bruckner, E.; Kratz, K.; Eimer, W. Colloidal Crystals Made of Poly(N-Isopropylacrylamide) Microgel Particles. *Colloid and Polymer Science* **2000**, *278*, 972-978.

[105] Stieger, M.; Pedersen, J.S.; Lindner, P.; Richtering, W. Are Thermoresponsive Microgels Model Systems for Concentrated Colloidal Suspensions? A Rheology and Small-Angle Neutron Scattering Study. *Langmuir* **2004**, *20*, 7283-7292.

[106] Meng, Z.; Cho, J.K.; Breedveld, V.; Lyon, L.A. Physical Aging and Phase Behavior of Multiresponsive Microgel Colloidal Dispersions. *Journal of Physical Chemistry B* **2009**, *113*, 4590-4599.

[107] Iyer, A.S.J.; Lyon, L.A. Self-Healing Colloidal Crystals. *Angewandte Chemie-International Edition* **2009**, *48*, 4562-4566.

[108] Debord, J.D.; Eustis, S.; Debord, S.B.; Lofye, M.T.; Lyon, L.A. Color-Tunable Colloidal Crystals from Soft Hydrogel Nanoparticles. *Advanced Materials* **2002**, *14*, 658-662.

[109] Wilson, A.N.; Guiseppi-Elie, A. Bioresponsive Hydrogels. *Advanced Healthcare Materials* **2013**, *2*, 520-532.

[110] Chen, K.; Merkel, T.J.; Pandya, A.; Napier, M.E.; Luft, J.C.; Daniel, W.; Sheiko, S.; DeSimone, J.M. Low Modulus Biomimetic Microgel Particles with High Loading of Hemoglobin. *Biomacromolecules* **2012**, *13*, 2748-2759.

[111] Merkel, T.J.; Jones, S.W.; Herlihy, K.P.; Kersey, F.R.; Shields, A.R.; Napier, M.; Luft, J.C.; Wu, H.L.; Zamboni, W.C.; Wang, A.Z.; Bear, J.E.; DeSimone, J.M. Using Mechanobiological Mimicry of Red Blood Cells to Extend Circulation Times of Hydrogel Microparticles. *Proceedings of the National Academy of Sciences of the United States of America* **2011**, *108*, 586-591.

[112] Kim, J.; Serpe, M.J.; Lyon, L.A. Hydrogel Microparticles as Dynamically Tunable Microlenses. *Journal of the American Chemical Society* **2004**, *126*, 9512-9513.

[113] Serpe, M.J.; Kim, J.; Lyon, L.A. Colloidal Hydrogel Microlenses. *Advanced Materials* **2004**, *16*, 184-+.

[114] Geisel, K.; Isa, L.; Richtering, W. Unraveling the 3d Localization and Deformation of Responsive Microgels at Oil/Water Interfaces: A Step Forward in Understanding Soft Emulsion Stabilizers. *Langmuir* **2012**, *28*, 15770-15776.

[115] Richtering, W. Responsive Emulsions Stabilized by Stimuli-Sensitive Microgels: Emulsions with Special Non-Pickering Properties. *Langmuir* **2012**, *28*, 17218-17229.

[116] Schmidt, S.; Liu, T.T.; Rutten, S.; Phan, K.H.; Moller, M.; Richtering, W. Influence of Microgel Architecture and Oil Polarity on Stabilization of Emulsions by Stimuli-Sensitive Core-Shell Poly(N-Isopropylacrylamide-Co-Methacrylic Acid) Microgels: Mickering Versus Pickering Behavior? *Langmuir*, *27*, 9801-9806.

[117] Park, C.W.; South, A.B.; Hu, X.B.; Verdes, C.; Kim, J.D.; Lyon, L.A. Gold Nanoparticles Reinforce Self-Healing Microgel Multilayers. *Colloid and Polymer Science* **2011**, *289*, 583-590.

[118] South, A.B.; Lyon, L.A. Autonomic Self-Healing of Hydrogel Thin Films. *Angewandte Chemie-International Edition* **2010**, *49*, 767-771.

CHAPTER 2

MICROGELS AS MICROLENSES

Adapted in part from:

Hendrickson, G. R.; Lyon, L. A. Bioresponsive Hydrogels for Sensing Applications. *Soft Matter* **2009**, 5, 29.

2.1 Introduction to Bioresponsive Hydrogels

Responsive materials comprise an attractive field of study due to their possible applications in tissue engineering,[1-6] biological interfaces,[7-9] drug delivery,[10-26] and biosensing.[21-24] Hydrogels in particular are interesting for these types of applications due to the flexibility of their networks in aqueous media, the degree to which their mechanical and chemical properties can be tuned, and therefore their intrinsic compatibility with biological systems. Importantly, the tunability of the dynamics of these constructs is critical for the responsiveness, and therefore the bioresponsivity, of such materials. Some inherent responsivity can be engineered into a gel based simply on the choice of monomers, co-monomers, and cross-linkers used in synthesis. The most common responsive hydrogels either incorporate a thermo-responsive polymers that shows a phase change at a given temperature, or a pH-responsive monomer that exhibits more or less intermolecular electrostatic repulsion due to the pH and salt content of the surrounding media. These two stimuli are advantageous for some applications, but for higher order responsiveness to biological stimuli, it is desirable to design responsive materials sensitive to antigen-antibody binding or enzyme-substrate interactions.[21-24,27-30] These bioresponsive materials help bridge the gap between the robustness of synthetic polymers and the functionality and specificity of

biological interactions.

In this section a more extensive introduction to hydrogels designed specifically for sensing applications will be discussed and was purposely left out of **Chapter 1**. Examples based on bulk phase transition such as sol-gel transitions[31-33] will not be discussed in great detail and the primary focus will be on swelling or deswelling responses in chemically cross-linked networks. These responsive hydrogels have been shown to give a number of different responses to analyte recognition. These include a simple expansion or contraction of the polymer network, a change in fluorescence response of fluorophore in the gel, a change in the diffracted wavelength in a colloidal assembly, or a change in the optical properties of the gel such as in the case of microlenses. Some select examples of each response will be presented.

2.1.1 Physical Expansion/Contraction Response

A physical change in the size of the gel due to a change in network density is the basis for all of the responsive hydrogel systems discussed below. This sensing modality is particularly useful given the preponderance of different physical observables that are modulated as a result of hydrogel swelling. These include, but are not limited to size, porosity, density, refractive index, and modulus. Furthermore, the extreme porosity of hydrogels permits rapid analyte diffusion into the network, thereby taking advantage of the entire three-dimensional structure. As a result of these advantages, a wide range of sensor transduction methods could, in principle, be applied to hydrogel-based bioresponsive materials. Note however, that many of the examples described below have not been specifically engineered into a sensing system or device. For many bioresponsive hydrogels, this remains a relatively

untapped area of research, with far more effort having been expended on the development of new materials than on their real-world application in sensors.

An early bioresponsive hydrogel was developed by Miyata *et al.*[34] that utilized a poly(2-glucosyloxyethyl methacrylate) (poly(GEMA)) hydrogel, which contains glucose moieties. The multivalent lectin concancavalin A (Con A) was then introduced to the polymer, which was accompanied by Con A binding to two to four glucose moieties thereby further cross-linking the poly(GEMA) hydrogel. This induced, non-covalent cross-linking was interrupted when free glucose was added into the solution, causing displacement of the polymer-pendant glucose moieties and expansion of the hydrogel network. A compression apparatus was used to detect the swelling of the gel. This construct was slightly modified in another study by covalently attaching the Con A to the hydrogel network, thereby limiting the diffusion of Con A from the gel.[35] The covalently attached Con A could then re-cross-link the network after rinsing the gel with buffer, freeing the glucose, and binding of the glucose moieties attached to the polymer network.

In a similar vein, Miyata[36,37] has published two different examples of antigen-antibody responsive gels. In one example an acrylamide-based hydrogel was synthesized using a co-monomer displaying a covalently attached "antigen" (rabbit IgG). An anti-rabbit IgG antibody was added to the material, thereby forming cross-links by binding two polymer-bound antigen equivalents. Consequently, when free rabbit IgG was present in an analyte solution, it displaced the covalently attached antigen from the bound antibody, disrupting the cross-links, and causing swelling of the gel.[36] In the other example, both the antibody and antigen were covalently linked

to co-monomers in an interpenetrating network (IPN).[37] The IPN was naturally cross-linked by the antigen-antibody interactions and upon addition of free antigen these cross-links were again disrupted and caused swelling of the gel. The advantage of a covalently attached sensing element is that it allows for reversibility of the cross-linking and therefore possibility of regeneration of the sensor after washing out the free analyte. These concepts of introducing different antibody-antigen interactions that can be used to sense either polyvalent protiens or the ligands that bind to them is an interesting for reversible/resuseable sensors and is employed by our group in the microlens construct discussed below.

Another method for introducing binding specificity into hydrogels is by molecular imprinting, which has been utilized in both bulk hydrogels and microgels (hydrogel microparticles). In a hydrogel example for recognizing the tumor specific marker glycoprotien, α-fetoprotein (AFP), the hydrogel was synthesized using both a Con A functionalized monomer and an anti-AFP functionalized monomer.[38] Free AFP was introduced to the pre-polymer solution, which bound to both the Con A and anti-AFP moieties during synthesis, creating a non-covalent cross-link. After synthesis, the AFP was washed from the system, and the hydrogel was left with specific binding sites that contained both Con A and anti-AFP recognition units, and were in theory organized appropriately for AFP binding. Therefore, when AFP was present the non-covalent cross-link was recreated and the gel collapsed. The efficacy of the imprinting process was illustrated via appropriate controls. In a microgel example, the imprinted molecules were a therapeutic drug, theophylline, and the steroid 17β-estradiol.[39] These molecules were introduced into a pre-polymer solution of methacrylic acid

(MMA) and the cross-linker trimethylolpropane trimethacrylate (TRIM). After the photo-initiated synthesis and several rounds of washing to remove the imprinted molecules, affinity and competitive binding studies were performed showing good specificity and selectivity for the target molecules. Using moleular imprinting or screening of affinity to certain biomelecular targets into hydrogels or microgels is an interesting way of designing a highly selective hydrogel network but may not be easily applied to different systems due to the variability in the network between analytes.[40,41]

Another way of introducing bio-specificity into hydrogels is by incorporating enzymes into the system.[42] Here we will focus on two specific gel transitions: sol-to-gel or gel-to-sol transitions and hydrogel swelling or deswelling. One example of a gel-to-sol transition was demonstrated in an acrylamide-based hydrogel synthesized with a tetrapeptide cross-linker.[43] In this study, two different peptide cross-linkers were used in different hydrogel synthesis: a tyrosine-lysine linkage cleavable by α-chymotrypsin and a serine-lysine linkage that could not be cleaved by the enzyme. The hydrogels were polymerized in a circular disk in a microfluidic channel, and in the presence of α-chymotrypsin, a gel-to-sol transition was observed by optical microscopy. **Figure 2.1** shows the hydrogel containing the enzyme-degradable cross-linker and the hydrogel containing the nondegradable cross-linker before and after exposure to the enzyme. This example is the only sol-to-gel transition example shared in this section mainly because these types of systems give excelent responses but are not always reversible due to the loss of material after solvating the gel.

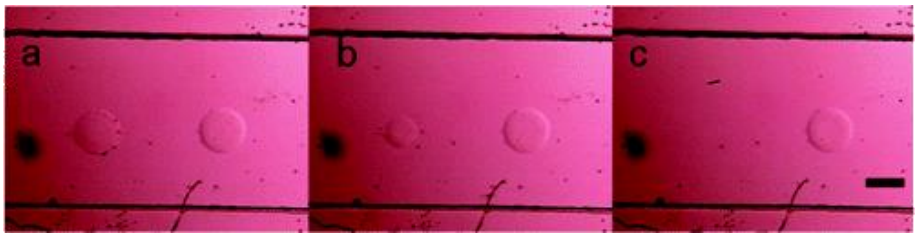

Figure 2.1. Optical micrograph of an enzyme-responsive gel with the gels containing the cleavable peptide sequence (left) and the non-cleavable sequence (right) 0 (a), 5 (b), and 20 min (c) after enzyme addition. Scale bar = 500 μm.[43]

An example of a swelling response to enzymatic activity involved the cleavage of a peptide-linker that contained both anionic and cationic residues.[17] In this case a poly(ethylene glycol)-poly(acrylamide) (PEGA) bead was synthesized with a pendent zwitterionic peptide sequence. Two different hydrogels were made with different peptide sequences, where those sequences contained the following critical components: a positively charged arginine directly attached to the hydrogel, a dialanine or diglycine linkage, a pendent aspartic acid with an 9H-fluoren-9-ylmethoxycarbonyl (FMOC) protected amine and an acid group contributing the anionic part of the polyelectrolyte. The diglycine or dialanine linkages were cleaved with various enzymes, the most effective for both being thermolysin. As these linkages were cleaved, the negative part of the polyelectrolyte was lost into solution, and the positive fragment was left attached to the gel increasing the electrostatic repulsion in the hydrogel along with an increase in internal osmotic pressure due to increased couterion ingress and causing swelling. This change could conceivably be used for enzyme responsive drug delivery, or in the screening of enzyme inhibitors, as many proteases are involved in specific disease states, including many cancers.

Physical changes in hydrogels have also been coupled to protein

conformational changes that occur during a ligand binding event.[44,45] In one example a PEG hydrogel was synthesized incorporating calmodulin (CaM) as a hydrogel cross-linker. CaM has an extended conformation in the presence of calcium ions and upon ligand binding the protein collapses into a more compact structure. Due to this dramatic change in conformation, the CaM-crosslinked hydrogel collapsed significantly upon binding of the ligand, trifluoperazine (TFP). This response is shown in **Figure 2.2**. Using a protien that has a large conformational change due to ligand binding as a cross-linker is a clever way of introducing responsivity although it may not be as widely applicable to many protiens that are eith hard to incorporate into the gel, involve time-consuming synthesis and purification techniques, or do not have such an advantageous protien structure change.

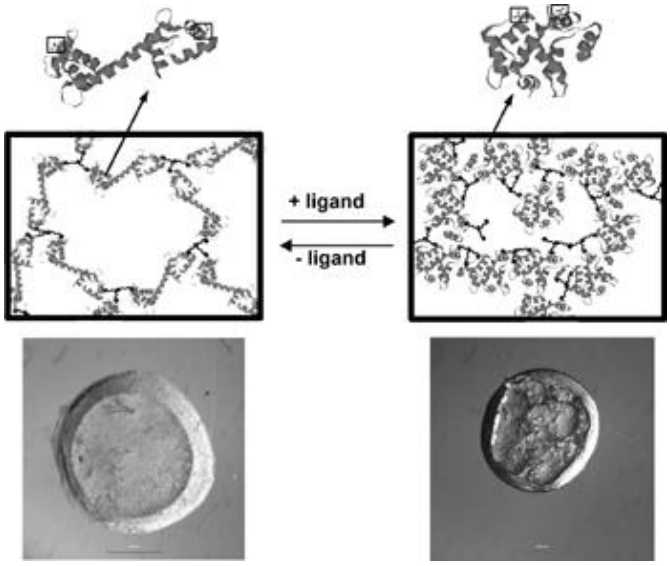

Figure 2.2. Crystal Structure, Scheme, and Optical micrograph of the CaM containing gel before (left) and after (right) ligand binding.[44]

2.1.2 Fluorescence Response

In another sensing modality, hydrogels have been integrated with fluorecenent tags to provide an easily detectable readout of a change in the hydrogel network density.[46] In one case, a glucose sensor was fabricated from an acrylamide-based hydrogel containing covalently attached rhodamine dye molecules and an amine moiety, which introduced pH sensitivity.[47] The enzymes glucose oxidase and catalase were physically entrapped in the gel by adding them into the pre-polymer solution before polymerization. The gel was cut into disks that were then affixed to the end of the optical fiber, providing a means of exciting fluorescence, and collecting the resultant emission. When the optical fiber + gel assembly was placed into a solution of glucose, the glucose was oxidized by β-D-glucose oxidase to D-gluconic acid and hydrogen peroxide. The catalase then converted the hydrogen peroxide to water and oxygen to prevent oxygen depletion within the gel. Glucose oxidation decreased the local pH, protonating the amine groups in the gel, thereby increasing the electrostatic repulsion within the network, which is accompanied by swelling of the gel. The swelling of the gel decreased the local concentration of fluorophore, and consequently the fluorescent response was strongly dependent on the solution glucose concentration. In this application the response was not linear in the physiolocical glucose concentration range and may not be the easily transitioned to in-home diagnostics.

Another glucose sensing construct was designed such that fluorescence was increased due to the presence of glucose.[48] In this case, a PEG-based hydrogel was synthesized with a covalently attached, fluorescently-labeled Con A and physically

entrapped fluorescien isothiocyanate (FITC) labeled dextran. The fluorophore attached to Con A was tetramethylrhodamine isothiocyanate (TRITC) which undergoes fluorescence resonance energy transfer (FRET) with fluorescein at short distances due to their strong spectral overlap. Therefore when the dextran binds Con A, the two chromophores undergo FRET and a decreased amount of fluorescien fluorescence is observed. However, introduction of glucose displaces the dextran from the Con A and increases the fluorescein fluorescent signal as shown in **Figure 2.3**.

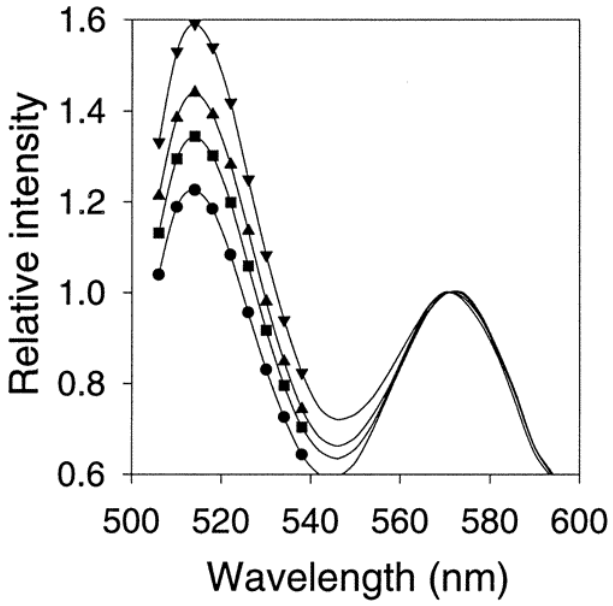

Figure 2.3. Fluorecence spectra showing the FITC-dextran signal (left) and FRET signal (right) with 0 (●), 200 (■), 400 (▲), and 1000 (▼) mg/dL concentrations of glucose. [48]

2.1.3 Diffraction Response

Hydrogels have also been coupled to the diffraction from photonic crystals by either encapsulation of a photonic crystal inside a hydrogel network, or by the direct assembly of photonic crystals using microgels as building blocks. These systems are

potentially advantageous sensing constructs because the Bragg diffraction they display, which is due to the periodicity of the crystal, is tunable/responsive to gel swelling. Therefore if a hydrogel/photonic crystal hybrid is designed in which the interparticle spacing changes due to the presence of an analyte, a label-free colorimetric sensor is obtained.

One key example of photonic crystal sensors are embodied by polymerized crystalline colloidal arrays (PCCA) studied by the Asher group at the University of Pittsburgh. PCCAs are colloidal crystals embedded in a responsive hydrogel network as shown in **Figure 2.4**. A number of different sensing applications have been attacked using PCCAs including glucose sensing.[45,49-52] For this application acrylamide-based hydrogels were modified to contain boronic acid units that bind to glucose; therefore, when glucose is present, multiple acid groups complex the glucose molecule thereby cross-linking the gel. The deswelling caused by this induced cross-linking causes the interparticle spacing of the colloidal crystalline array to decrease, thereby blue-shifting the Bragg diffraction.[49,50,52] The blue shift response is seen in when the ionic strength of the medium is high enough to shield Coulombic repulsion between the negatively charged glucose-boronic acid complexes. Conversely, when the ionic strength is lower, electrostatic repulsion in the gel causes a swelling response, increasing the interparticle spacing and inducing a red shift in the diffraction spectrum (**Figure 2.4**).[51] The different responses due to different ionic strengths may be problimatic if you do not have great contol over the ionic strength of the system.

PCCAs have also been employed for nerve agent sensing.[53,54] In this

methodology, an enzyme is covalently attached to the hydrogel network allowing binding of the analyte to the enzyme. Upon analyte binding or enzyme conversion, the charge in the network is either increased or decreased and swelling or deswelling occurs. The analytes in two specific cases were organophosphorus (OP) compounds.[53,54] In one case the enzyme acetylcholinesterase was bound to the

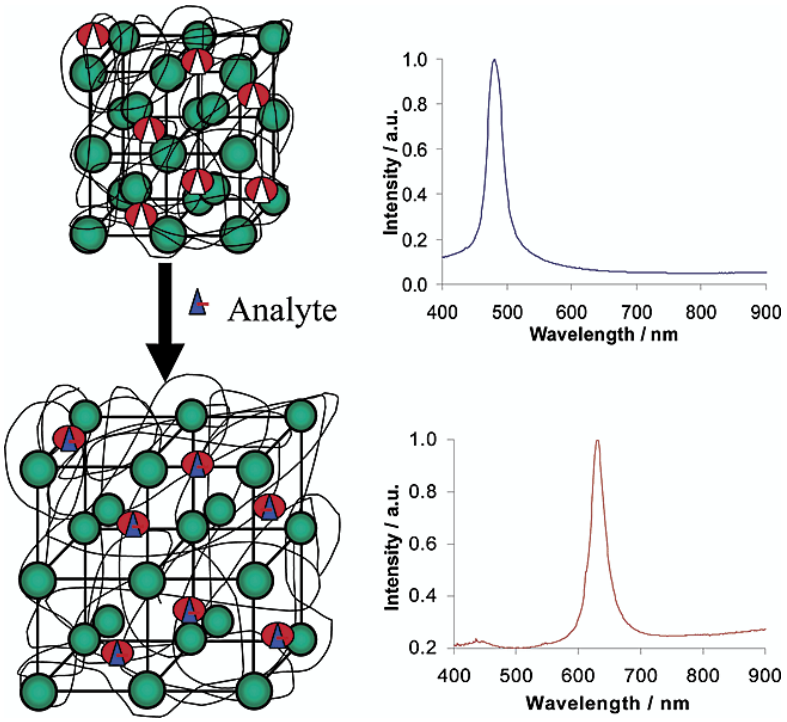

Figure 2.4. Scheme (left) and corresponding diffraction spectra (right) of a PCCA in the absence (top) and presence (bottom) of analyte.[51]

hydrogel network and upon OP binding an anionic complex was formed, causing the hydrogel to swell, increasing particle spacing, and shifting the Bragg diffraction peak.[53] In a similar case, organophosphorous hydrolase was attached to the hydrogel along with a phenol moiety.[54] When the analyte was introduced at a pH of 9.7, which is above the pK_a of the pendant phenol groups, those moieties became deprotonated

and charged. When the OP was introduced and hydrolyzed by the enzyme, protons were released, thereby lowering the local pH below the phenol pK_a and protonating the phenols. As a result, the internal network charge, electrostatic repulsion, interparticle spacing, and diffraction wavelength were all decreased. The PCCA method has been widely applied to other sensing applications, including metal ion,[55] ammonia,[56] and creatinine sensing.[57] These PCCA systems are nice contructs that have been shown to be responsive to many different analytes; however, does not seem to be excelent for any given analyte.

A different diffraction construct in which the colloidal crystal is directly formed from microgels has been studied as a glucose sensor.[58] In this approach, 3-acrylamidophenylboronic acid (APBA) was incorporated into pNIPAm microgels. The APBA is in equilibrium between neutral species and the hydrolyzed negatively charged species. Upon addition of glucose, the glucose binds to the charged form, yielding two water molecules and shifting the equilibrium towards the hydrolyzed products. This increases the number of locally charged species and the internal electrostatic repulsion, thereby causing a swelling of the microgels. Since these microgels are in assembled into a colloidal crystal, the expansion of the particles yields an increase in the interparticle distance and an increase in the Bragg diffraction wavelength and therefore a color change, shown in **Figure 2.5**. This is an important example because it is one of the only colloidal crystal sensing example in which the building blocks are microgels. This system, however, operates only above physicological pH so for real samples it might not work as well. The reason for the higher pH is that some of the APBA needs to be ionized in order to bind glucose. In a

more recent result, an etalon which is a device fabricated in a mirror-dielectric-mirror sandwich and causes constructive and desrtuctive interferance when light pass through it in the dielectic layer. The wavelength maximum is based on the distance between the two mirrors. In this case, microgels were used as the dielectric layer and were made to be glucose responsive. As they swell or deswell, the wavelength max changes creating a nice sensing mechanism .[59]

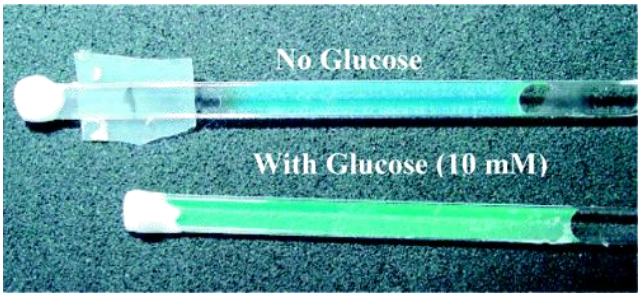

Figure 2.5. Glucose sensing microgel colloidal crystals with and without glucose.[58]

2.1.4 Direct Optical Response

This section focuses on hydrogel-based materials that change their optical properties due to a change in network swelling. Primary amongst these examples are microlenses that change their optical properties due to a change in refractive index or radius of curvature. The swelling response is therefore conveniently read out by observing the focusing power of the microlens by simply projecting an image through the microlens. Applying a stimulus that changes the focal length of the lens is observed as a focusing or defocusing of the projected image. There have only been a few examples of such optically responsive hydrogel materials. Most of the work done on such materials has been developed by our group using a microgel construct and will be discussed in detail. However, a few bulk hydrogel examples have also been reported.

The primary example of a “bulk” hydrogel approach to responsive microlenses involved microlenses synthesized by polymerizing a hydrogel precursor solution onto a glass substrate in the form of a “microdome”.[60] The microdome was an acryalamide-based gel that incorporated both covalently attached CaM and phenothiazine, which bind to each other creating a non-covalent cross-link in the gel. When the competing ligand chlorpromazine (CPZ) is present in the surrounding solution, it binds to CaM and displaces phenothiazine, thereby disrupting the cross-link, which induces gel swelling. The swelling response changes the curvature of the microdome as well as the refractive index. Therefore, the focal length changes and a focused image becomes defocused.

Another microlens construct was developed using a hydrogel ring to manipulate the curvature of a water/oil interface.[61] This construct was made to possess pH and temperature responsivity by incorporating acid or amino groups and thermo-responsive monomers into the hydrogel ring, respectively. In the temperature responsive system the hydrogel ring was polymerized with NIPAm. Similarly, in the pH-responsive case the gel contained acrylic acid or 2-(dimethylamino)ethyl methacrylate (DMAEMA). These microlenses were fabricated by sandwiching a hydrogel ring between a solid glass surface and a surface containing a hole aligned with the hole in the ring. Water was incorporated into this region of the device, and oil was sandwiched between the top surface that containing the hole and another glass surface. This created a system that had a water/oil interface in the middle of the hydrogel ring. The curvature of this interface was then tuned by swelling or deswelling the gel by inducing a pH change or change in temperature.

In our group a different type of microlens structure has been developed using well defined microgels as the building block. These microgels are synthesized via free radical polymerization of NIPAm and acrylic acid (AAc) with *N,N'*-methylene(bisacrylamide) (BIS) as a typical covalent cross-linker. The microgels are then adsorbed to a surface and have been shown to act as individual optical elements following adsorption and deformation into hemispherical structures.[62] A typical optical response is shown in **Figure 2.6**.[63] Given the incorporation of temperature and pH responsive monomers, the resultant microlenses are similarly responsive to changes in temperature[64] and pH.[63] The optical response shown in **Figure 2.6** is due to a change in pH, which changes the degree of AAc protonation and therefore the degree of Coulombic repulsion in the gel. Decreasing the pH of the surrounding media protonates the acid groups in the gel, causing deswelling that increases the refractive index which decreases the lens focal length. In the thermo-responsive case, a rise in temperature causes a contraction of the polymer network and a subsequent decrease in focal length.

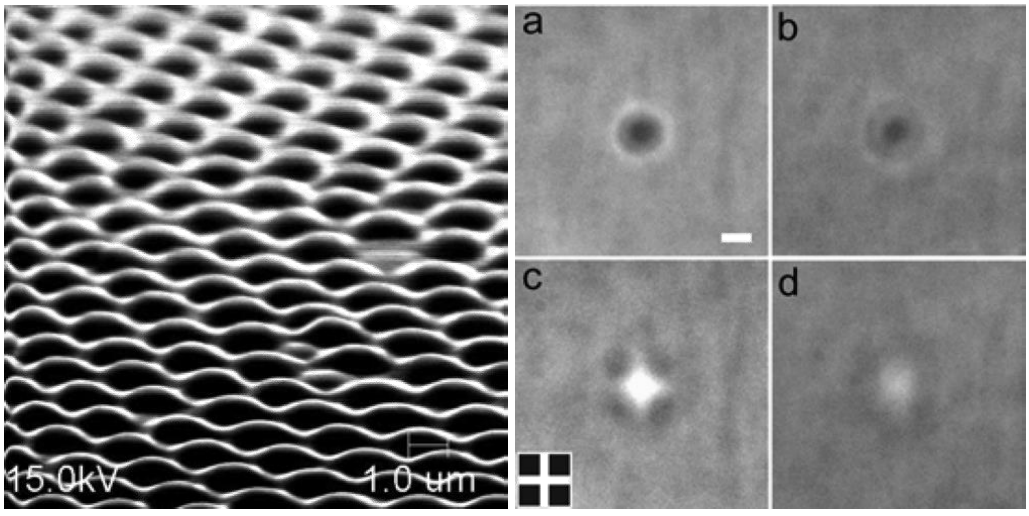

Figure 2.6. Microgel microlenses: SEM image (left panal) at a grazing angle of an array of microlenses a)-d) DIC microscopy images at pH 3.0 (a) and 6.5 (b) with the corresponding projection images (c) and (d). Scale bar = 1 μm.[63]

Following on the examples described above, the Lyon group designed microlenses that would display changes in refractive index that was induced via protein binding for use in sensing applications.[65-68] Specifically, microlenses have been designed for two different pathways for sensing: a direct binding-induced response and a displacement-induced response (**Scheme 2.1**[66]). To illustrate each method, the small vitamin biotin was conjugated to the acrylic acid groups on the microgels. For the first binding induced method (**Scheme 2.1, Route A**), avidin or anti-biotin (antibody) was added to the solution around the microlens, resulting in binding of the protein to the microlens surface. Since both avidin (four binding sites)

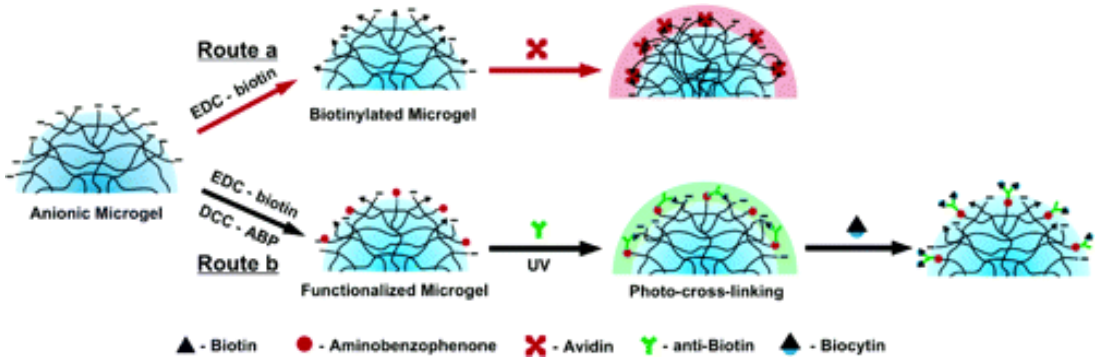

Scheme 2.1. Scheme showing the microlens sensing strategies: the binding-induced deswelling method (Route a) and displacement-induced swelling method (Route b).[66]

and anti-biotin (two binding sites) are able to bind multiple equivalents of biotin, the protein binding events increase the surface cross-linking of the microlens. This cross-linking induced a refractive index change and a visual signal was observed as shown in **Figure 2.7**.[65] In this example, the lenses transition from a single square projection to almost double image response while in projection mode, which is achieved by simply placing a pattern in between the light source and analyzer in an inverted

microscope. This method is simple and could be applied to many different protein-binding applications. A displacement-induced method can be achieved by designing a reversible antibody-antigen cross-linking construct. In this case, a photoaffinity approach is used to couple a bound antibody to the antigen-laden microlens. When the free biotin disrupts the cross-links via displacement, the microlens swells and the focal length increases accordingly. A biotin-free buffer wash removes the the free biotin, allowing for re-cross-linking of the gel and regeneration of the sensor.[68]

Using microgels as microlenses is attractive because of the ability to use many different solution based bioconjugation methods and the ease of assembly with simple electrostatic adsorption. Also unlike the bulk gels post-synthesis modifications can help ensure uniformity of the lens structure among different bioconjugations. The microgel examples, however, do need to be extended to more relevent antibodies or other biomolecule sensing as well as be applied to multi-sensing applications.

Here, we have shown examples of different hydrogel constructs that have potential for use in sensing applications. We have highlighted examples of hydrogels that give different responses due to the presence of analyte. These responses include simple physical changes in gel size or shape, colorimetric responses such as fluorescence intensity changes or diffraction wavelength change, and finally optical responses that occur due to focal length changes in microlenses. In some cases, as with the well-developed PCCA approach, the pathway to true sensing systems is well established. However, other methods are very much still in the materials discovery and development stage; coupling of these approaches to commercially applicable sensor constructs remains as a logical next step in device development.

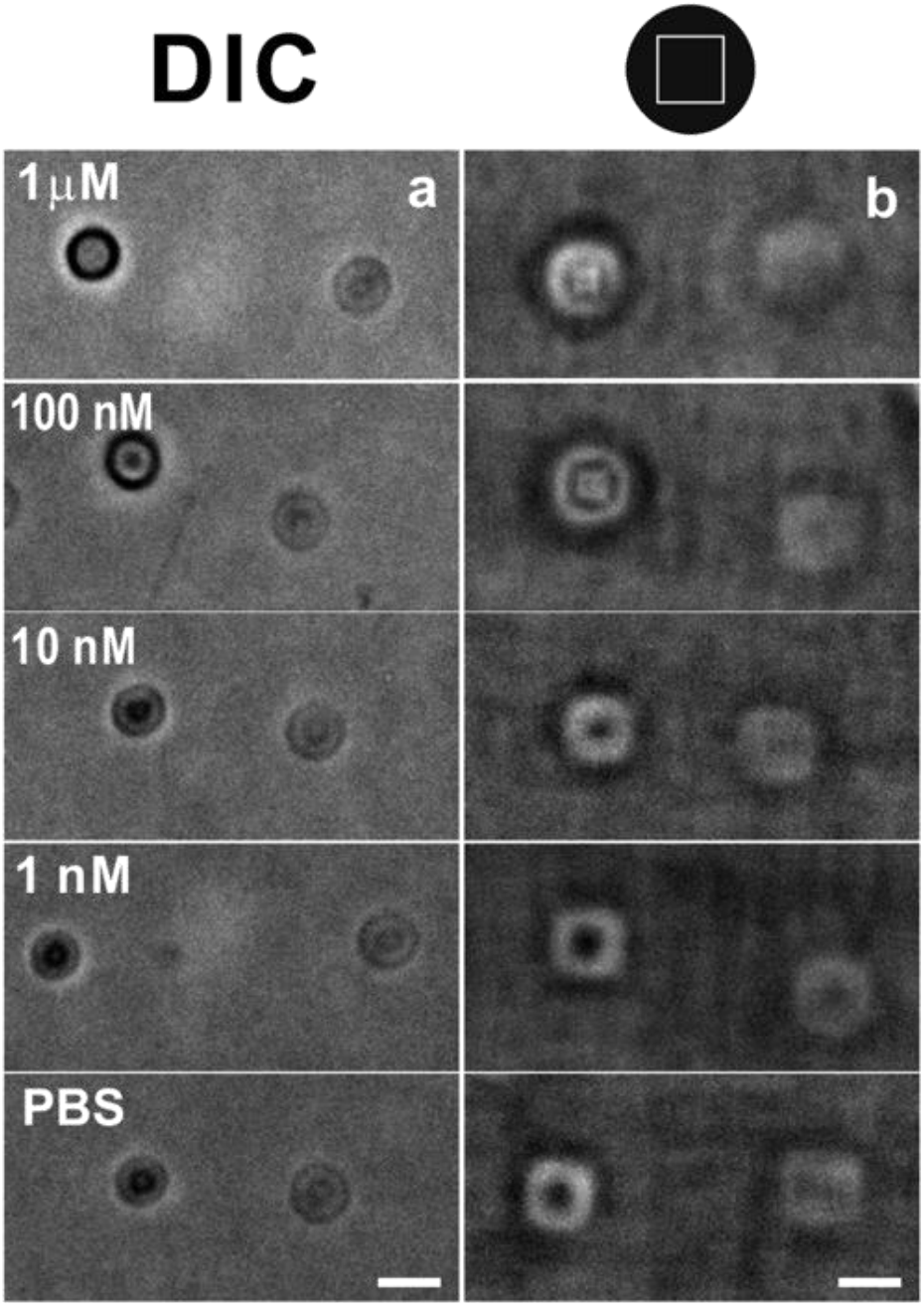

Figure 2.7. Microlens response to increasing amounts of avidin showing the DIC (left panels) and projection images (right panels) with particles with (left) an without (right) biotin. Scale bar = 2 μm.[65]

The efforts were two fold. First, a new generation of microlenses needed to be verified as responsive to not only similar probes as had been tested before but also extended to new probes such as nucleic acids. It was found that these new microlenses did respond to similar probes, however, the response was different. Secondly, extension of the microlens platform to a microfluidic device was performed in order to achieve the specific goal of making a device that could easily be extended to targeting multiple probes at the same time. The specific probes to be targeted were, in this case, autoantibodies which had been shown to be potential early detection cancer markers.[69-74]

2.2 Experimental

2.2.1 Materials

Monomers *N*-isopropylacrylamide (NIPAm; Aldrich) and *N*-isopropylmethacrylamide (NIPMAm) were recrystallized from hexanes (Fisher Scientific) before microgel synthesis. Cross-linker *N,N'*-methylenebis(acrylamide) (BIS; Aldrich), ammonium persulfate (APS; Aldrich), and acrylic acid (AAc; Fluka) were all used as received. The pH 7 buffer was a 10 mM (ionic strength (IS) = 100 mM) phosphate buffer and the pH 3 buffer was a 10 mM (IS = 100 mM) formate buffer. All water used in the experiments was purified to 18 mΩ (Barnstead E-pure system).

2.2.2 Microgel Synthesis

Large microgels were synthesized by precipitation polymerization of NIPAm, BIS (1 or 2 mol%), and AAc (10 mol%) with a total monomer concentration of 100 mM in 100 mL. All components were dissolved in distilled, deionized water and stirred under a nitrogen purge while heating to 68 °C. Then APS (0.01 mM) was added to initiate the

reaction. The reaction was allowed to stir under nitrogen at 68 °C overnight. All particle solutions were filtered and purified via centrifugation. The samples were then freeze-dried for storage.

2.2.3 Microgel Array Formation

In general, all samples were prepared by first silanizing glass cover slips. First, cleaning the glass cover slips was done by sonication in a series of solvents (Alconox solution, nanopure water, acetone, absolute ethanol, isopropyl alcohol, absolute ethanol). Then the cover slips were placed in a 1% 3-aminopropyltrimethoxysilane (APTMS) in absolute ethanol solution for 2 hours, rinsed with ethanol, and stored in absolute ethanol. When ready for use the glass slides were removed from the ethanol, dried under nitrogen, and gaskets were placed on top of the slides. A solution of microgel particles in PBS buffer (pH= 7.4) was added to the gaskets and particles were left to adsorb to the slide for 45 minutes. Most of the experiments were performed under adsorption conditions (particle concentration and time) which yielded sub-monolayers. Then the slide was rinsed with PBS buffer and dried under nitrogen.

2.2.4 Microgel Lensing

Micogels adsorbed to glass surfaces can act as individual lensing elements called microlenses. The curvature, refractive index contrast, and thickness of the microlens determine the lens focal length, therefore, you can tune that focal length by inducing a change in one or more of these quantities. Lensing is done by placing a microlens in the focal plane of an inverted microscope as shown in **Figure 2.8**. Here by manipulating the focus while observing the microlens through an objective using differential interference contrast microscopy, light can be more or less focused through the lens. Furthermore, a

light screen with a pattern can be placed in the same focal plane as the lens near the light source and that pattern can be focused through the microlens (**Figure 2.9**).

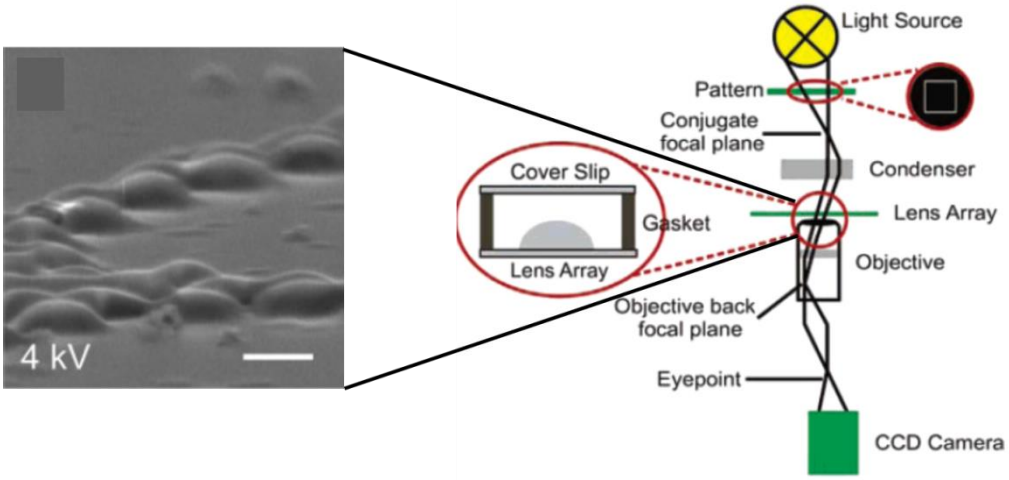

Figure 2.8. Left: SEM side view of microlenses on a glass surface.[oo] Right: Scheme of inverted microscope microlensing.[62]

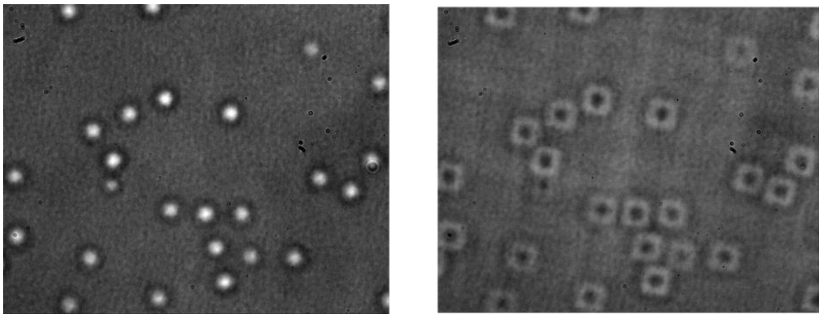

Figure 2.9. Left: Microlenses viewed using DIC imaging. Right: Microlenses after inserting a square pattern into the light path.

2.2.5 Biofunctionalization

For experiments where either avidin or anti-biotin were the target molecule the capture molecule was biotin. Biotin was conjugated to the particles using EDC (1-ethyl-3-(3-dimethylaminopropyl) carbodiimide hydrochloride) coupling which forms an amide bond between a carboxylic acid functionality and a primary amine (**Scheme 2.2**). This reaction is aided by a reactive intermediate formed by N-hydroxysuccinimide (NHS). This coupling was done between the acrylic acid groups on the particles and a biotin molecule with an amine moiety, biotin hydrazide. More specifically, lyophilized particles

were re-suspended in pH 5.5 MES (2-(N-morpholino)ethanesulfonic acid) buffer. Then excess NHS and EDC were dissolved in small amounts of the MES buffer and added to a mixed suspension of particles and the biotin hydrazide. These reacted at room temperature overnight and then the particles were washed in pH 7 PBS buffer by repeated centrifugation and re-suspension.

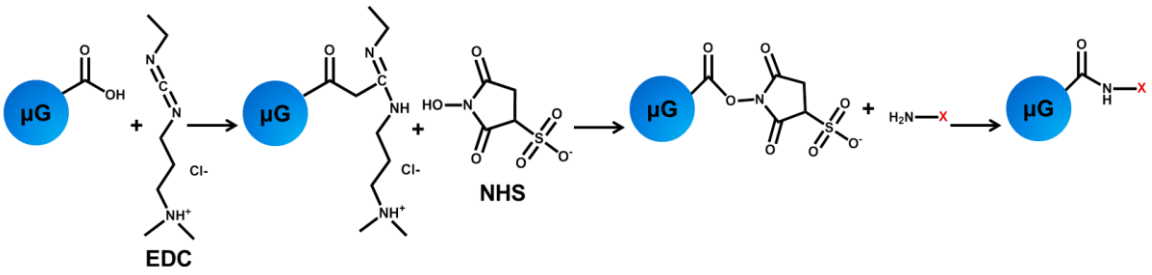

Scheme 2.2. Scheme of carbodiimide coupling of a primary amine to a carbocylic acid on a microgel (μG) mediated by N-hydroxysuccinimide (NHS).

2.2.6 Biosensing Experiments

Biosensing was carried by incubating the microgel suspension in solutions of either anti-biotin, avidin, or DNA. The change in refractive index was then monitored by optical microscopy. In some cases, a non-binding fluorescent microgel was included as an internal control.

2.2.7 Microfluidic Platform Experiments

In order to increase the capability of the microlens as a sensor these arrays were placed in microfluidic channels. Here, PDMS microfluidic devices (designed in the Hang Lu group in chemical engineering at the Georgia Institute of Technology) were added to the top of the already formed microgel array. These devices were simple Y-shaped microfluidic devices allowing for laminar flow between a two solutions in which 2 different solution conditions could be flowed at the same time and allowed for simultaneous monitoring of the optical properties in each condition.

2.2.8 Increasing Sensitivity Experiments

Five different stoichiometries were used to selectively label sets of particles with different amounts of biotin. First a 0.1 wt% solution of 2% BIS cross-linked microgels was made from a lyophilized sample and water. Next, six 2 mL aliquots of this solution were placed in centrifuge tubes and spun down and re-suspended in pH = 5.5 buffer. Then 100 μL of a 37 mg/ml solution of EDC and 100 μL of 42 mg/mL solution of N-hydroxysuccinimide (NHS) is added to the particles to for an excess of EDC and NHS. Then different volumes of a 12.9 mg/mL solution of biotin hydrazide were added to the activated particles. In each case a different desired stoichiometry of the acrylic acid groups was functionalized: 1:10 (3.8 μL), 1:4 (9.5 μL), 1:2 (19 μL), 3;4 (29 μL), 1:1 (38 μL), and 2:1 (78 μL). These solutions were allowed to shake at room temperature overnight and then centrifuged and re-suspended in pH = 7.4 PBS buffer. Then the HABA assay was performed to determine biotin concentration.

The HABA (4´-hydroxyazobenzene-2-carboxylic acid) assay is a spectroscopic assay to determine the amount of biotin in solution (**Scheme 2.3**). The basic idea is that when HABA is free in solution it only has a molar absorptivity of around 600 L/cm-mole at 500 nm; however, when it is bound to avidin its molar absorptivity is 34000 L/cm-mole. It also has a binding constant to avidin of around 10^5 where as biotin has a binding constant to avidin of around 10^{15}. Therefore, if a solution of saturated avidin with HABA is made and mixed with a solution of biotin the biotin will displace the HABA from the avidin thereby decreasing the absorbance at 500 nm.

In order for this assay to be successful it is very important that the solutions are stored in the fridge. First a solution of 10 mM HABA in a 0.1 M PBS buffer was made. Then 5 mg of avidin was dissolved in a few mL of PBS buffer and 300 μL of the HABA

solution was added and the total volume was made to 10 mL. This assay was attempted on the 10% acrylic acid particles with varying concentrations of biotin. Solutions of D-biotin were made to the concentration of biotin in the original conjugation solution and then diluted as reference solutions. Then the supernatant from the clean particles was collected and diluted to 10 mL. Next the HABA assay was performed by using 50 µL of the biotin solutions and 450 µL of the HABA/Avidin solution and then mixed. This ratio was decided on by trying some different ratios with the reference solutions. Lastly the absorbance of each solutions supernatant was taken and the resulting HABA/Avidin concentrations were calculated using Beer's Law. Then the resulting biotin concentration could be calculated and related back to the original concentration taking into account all of the dilutions.

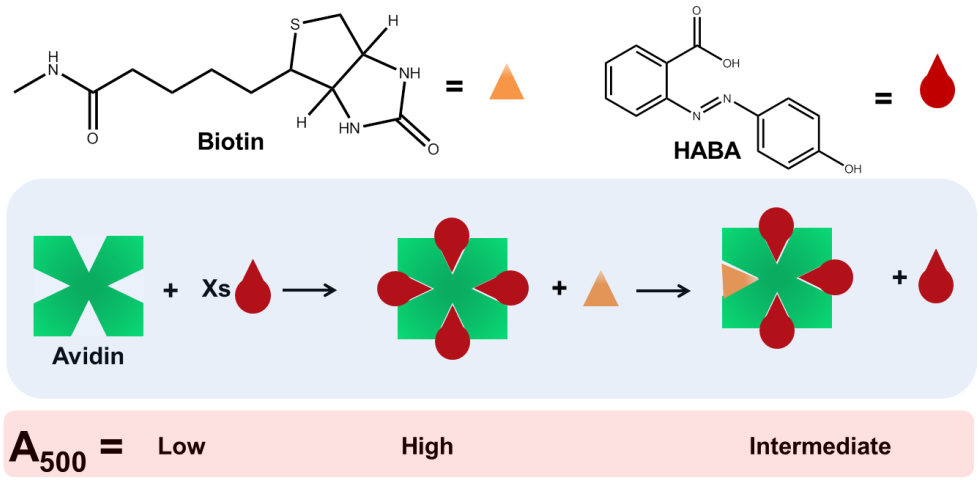

Scheme 2.3. HABA assay scheme with HABA and biotin structures and displacement scheme showing the relative absorbance of HABA at 500 nm in the different states.

2.3 Results and Discussion

The new generation of microlenses formed from single microgels adsorbed to a surface has been shown to be responsive to different stimuli such as pH (**Figure 2.10)**. The pH response is due to the incorporation of acrylic acid (10 mol%) during synthesis.

In the pH 7 buffer, the acid groups in the particle are mostly deprotonated, therefore, the microgel has imbibed counter ions and their associated water in order to balance charge causing swelling. This solution condition results in one microgel refractive index and a particular particle curvature. However, when the particles are subjected to a pH 3 buffer the acid groups are mostly protonated which allows for expulsion of some of these counter ions and the associated water thereby deswelling the microgel. This deswollen microgel now has a different refractive index and different curvature resulting in a different lens focal length. This in turn now allows for a tighter focus of the light passing through the lens. While responses to environmental conditions are informative of the responsivity of these lenses, they are merely representative of the microlens response desired in response to a biomolecule.

In **Scheme 2.4**, there are three different schemes representing the mode of action for the microlens biosensing. All three require conjugation of some target molecule to the particle and in case A and B it is the small vitamin biotin. In these two cases, the probe molecules were avidin and anti-biotin, respectively. Avidin is a ~66 kDa tetrameric protein in which each subunit binds biotin with a nearly covalent bond strength ($K_d = 10^{-15}$). The second target molecule anti-biotin is used as a less tightly binding mimic of a typical antibody. This molecule binds 2 biotin molecules with a $K_d = 10^{-10}$. Since it is unlikely that either protein penetrates the particle due to their sizes, the binding of the protein to the surface of the microlens causes cross-linking of the polymer network at the surface of the microgel. The cross-linking as well as the presence of the protein on the surface of the microgel changes the lens curvature, refractive index, and structure. Here most of the changes in refractive index and curvature happen at the surface of the microgel forming a more complex lens structure. This effect, however, results in a similar optical response as shown in **Figure 2.11** and **Figure 2.12**.

Although both of these sensing modalities had been observed in our group previously they needed to be verified with this microlenses. In the third biosensing

platform which was a new type of probe for our group, a biotiylated particle was also used, but here it was merely used as a linkage rather than the target. The target here was a biotiylated DNA oligomer. The microlenses were incubated with excess avidin allowing for near covalent binding to the microgel with open biotin binding to sites in the avidin. Then biotin conjugated DNA was added allowing for a microgel-biotin-avidin-biotin-DNA linkage. Then complementary probe DNA was added. Then ethidium bromide (EB) was added to indicate hybridization. The excess negative charge on the surface should change the swelling of the microgel and therefore the focal length of the microgels. As shown in **Figure 2.13**, there was DNA hybridization as shown by the probe ethidium bromide. In

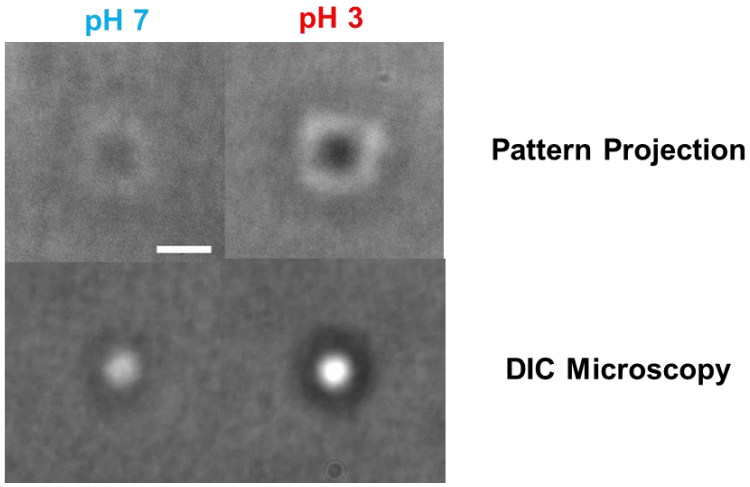

Figure 2.10. Carboxylated microlenses response to pH.

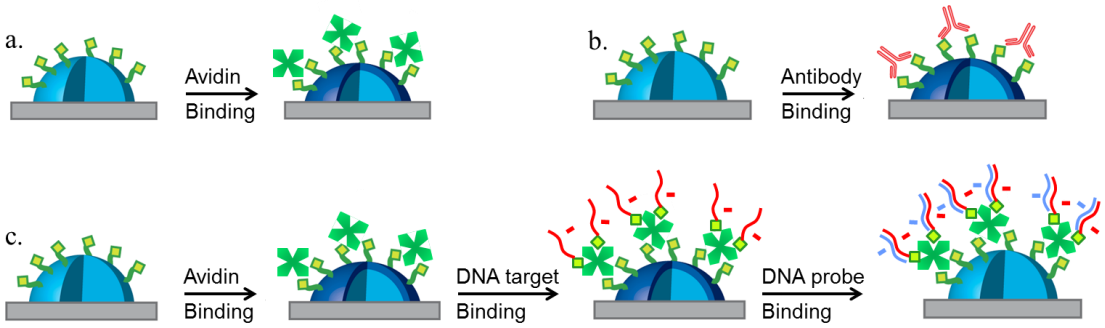

Scheme 2.4. Three different biosensing schemes: a. avidin binding (protein sensing), b. anti-biotin binding (antibody sensing), and c. DNA oligomer binding. Dark corona represents the change in focal length.

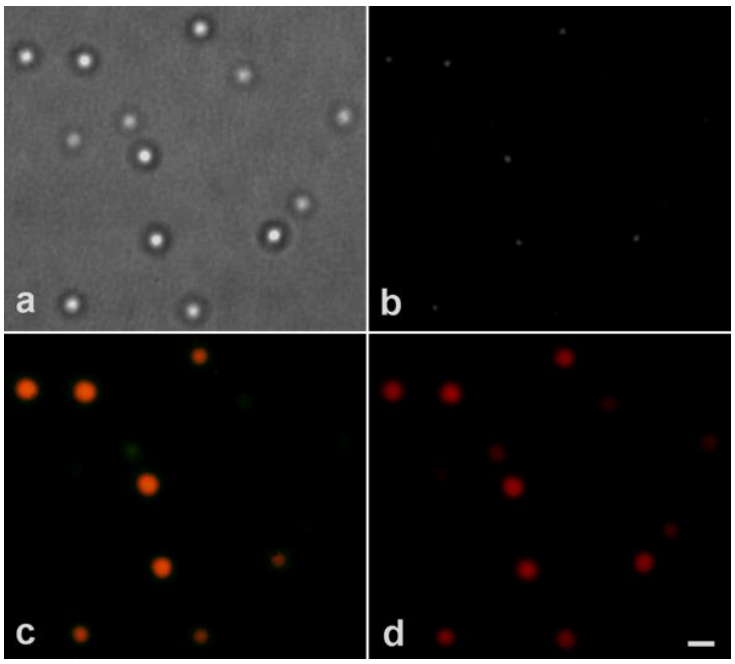

Figure 2.11. Avidin sensing with biotin labeled particles with some fluorescein labeled non-avidin binding standard particles. a) DIC microscopy after incubation with 500 nM Avidin-Texas Red b) Low light image showing only bound particles c) blue light excitation showing green fluorescence from standard particles d) green excitation showing avidin binding. Scale bar = 2 microns.

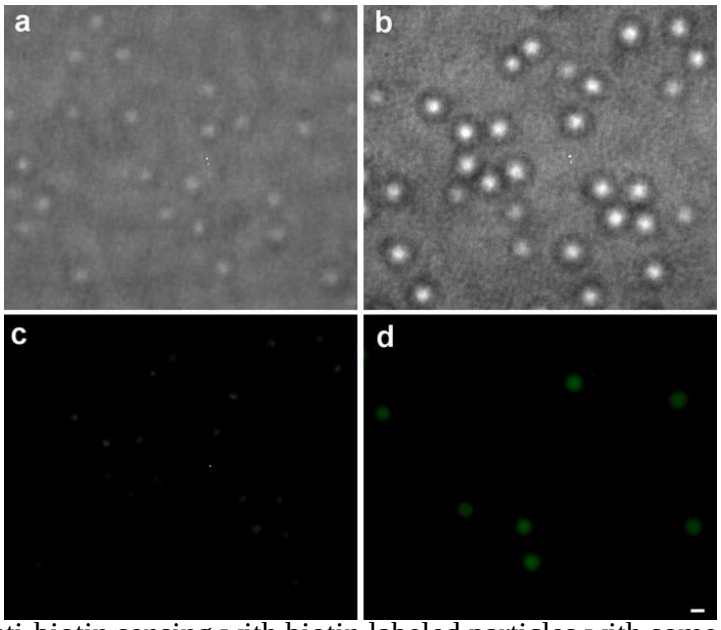

Figure 2.12. Anti-biotin sensing with biotin labeled particles with some fluorescein labeled non-binding standard particles. a) DIC microscopy before incubation with anti-biotin b) DIC microscopy after incubation with 300 nM anti-biotin c) low light image showing only the binding particles d) Blue light excitation showing the green standard particles. Scale bar = 2 microns.

this experiment some non-biotinylated microgels were adsorbed to the substrate as an internal control. These particles were labeled with fluorescein to identify them as the particles not conjugated with biotin. So, as shown in **Figure 2.13,** when avidin was added the expected lenses response was observed. Then as the negatively charged biotin conjugated target DNA was added the partcles restore a similar look to the original particles due to the increased swelling and necessary change in refractive index and curvature. Then after the probe DNA was added no optical change was observed. Although the binding methodology was successful, a strong optical change due to the probe DNA was not observed. Here, alternatives were discussed such as sensing a DNA hairpin using the hairpin as a cross-link to hopefully observe a change in the microlenses response, but efforts were quickly consumed by our second goal of extending this technology to a microfluidic platform sensing antibodies.

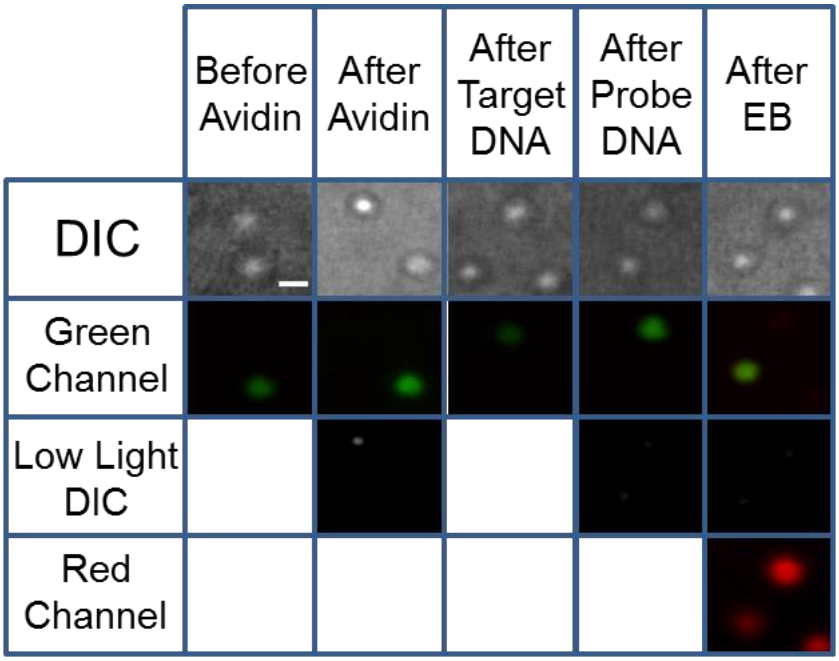

Figure 2.13. DIC and fluorescence microscopy images of DNA sensing platform. Scale bar = 2 microns.

Expanding the sensing platform to a microfluidic device should provide for more rapid diffusion to the particle surface under flow as well as facile extension to multiplex sample analysis. The first most basic device that was fabricated was a Y-shaped microfluidic device. In these devices two different liquids can be introduced, one on each branch of the Y. Then as these two liquids merge there is very little mixing of the liquids depending on flow rate, distance down the channel, and the dimensions of the channel. This phenomenon is called laminar flow. Therefore, as shown in **Figure 2.14**, different microlens responses can be observed in parallel based on solution conditions or biomolecule concentration for example. Here pH 3 and pH 7 buffers were flowed in parallel and their respective microlens response is observed. Then buffer and anti-biotin solutions were flowed in parallel and their respective responses can be observed across the channel as shown in **Figure 2.15**. The response over time can also be monitored as shown in **Figure 2.16**. In just 10-15 minutes, a noticeable response is observed.

So far we have shown that these microlenses have the ability to respond to solution conditions and few different types of biomolecules. They have been incorporated into microfluidic devices, which give a fast response and the ability to have an internal control and with more device engineering have the possibility to sense multiple biological probes. Although all of these experiments suggest a promising sensing platform, the question still remains can these devices be sensitive enough for the current probes of interest such as cancer markers.

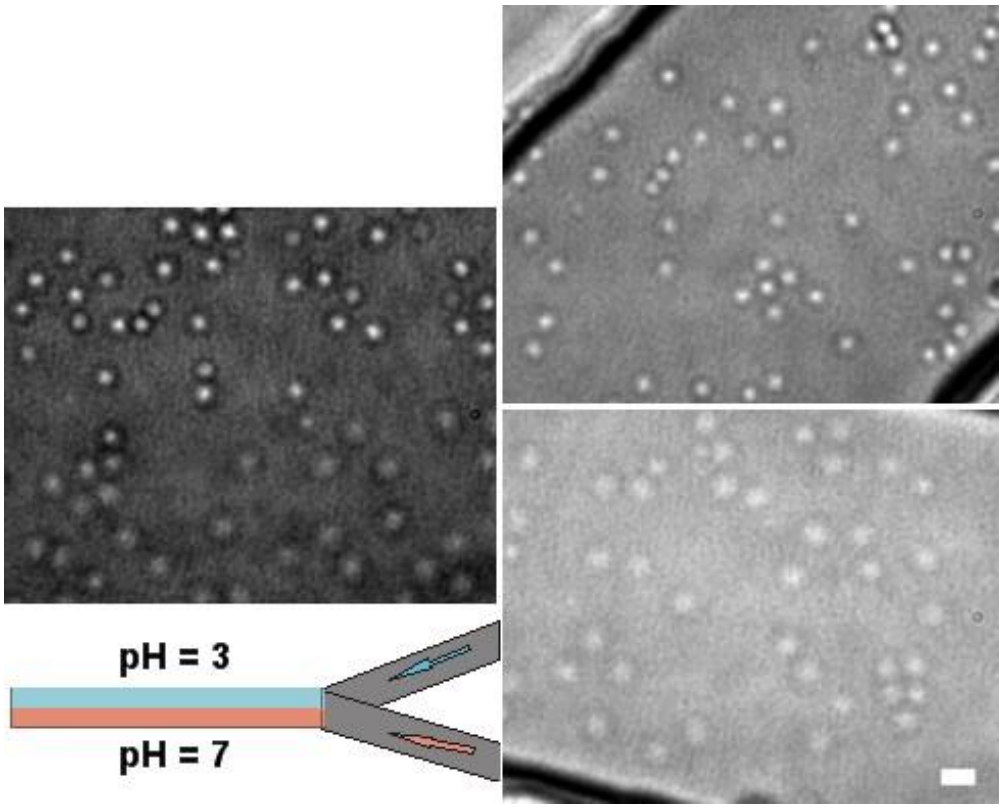

Figure 2.14. Microlens response to pH inside of a microfluidic channel. Top right: Image inside of the pH 3 buffer inlet. Bottom right: Image inside of the pH 7 buffer inlet. Middle left: inside the channel showing the response to both pH conditions. Bottom left: scheme of microfluidic channel. Scale bar = 2 microns.

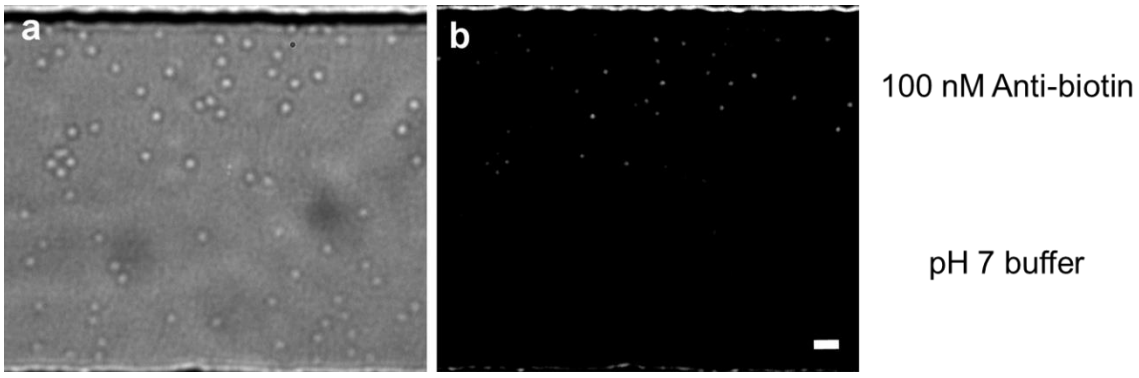

Figure 2.15. Microlens response to anti-biotin binding inside of a microfluidic channel. Image inside of a Y-channel microfluidic with 100 nM anti-biotin introduced through one Y and buffer in the other.

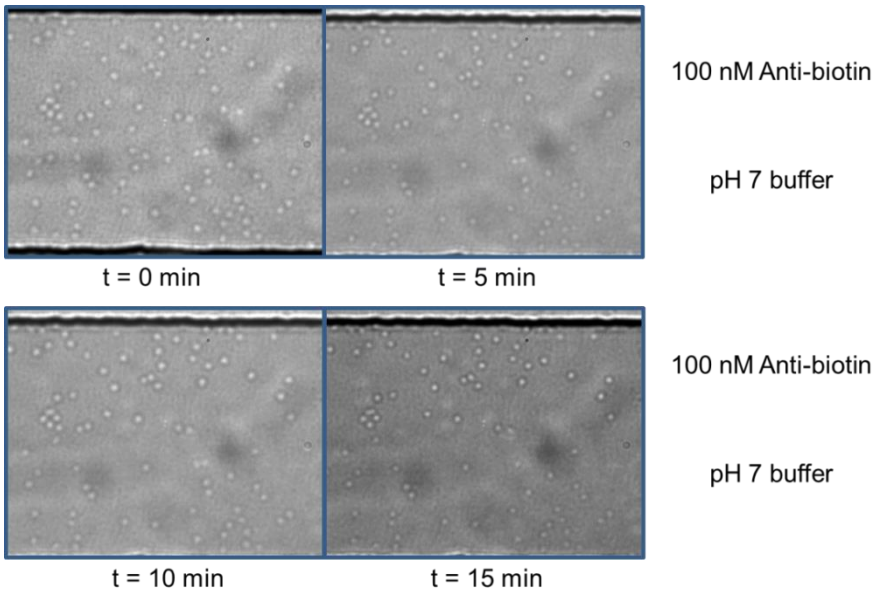

Figure 2.16. Microlens response to anti-biotin binding inside of a microfluidic channel over time. Image inside of a Y-channel microfluidic with 100 nM anti-biotin introduced through one Y and buffer in the other.

In order to get at the relative order of magnitude antibody sensitivity for each microlens, microgels were functionalized with different amounts of the biotin ligand. Here, biotin conjugation was done with biotin hydrazide added at 0, 10, 25, 50, 75, 100 and 200 mol % of the acid groups. Then a HABA assay as described above was performed and it was found that there is 0, 13, 45, 99, 151, 200, and 415 μg of biotin per mg of particles. Which if you use the approximate 1×10^9 g/mol molecular weight of the particles and the 244 g/mol molecular weight of biotin these values equal approximately 0, 0.05×10^6, 0.2×10^6, 0.4×10^6, 0.6×10^6, 0.8×10^6, and 2×10^6 biotin molecules per particle. Then experiments were done with each particle type to assess the magnitude of their response to antibiotin as shown in **Figure 2.17**. This is plotted in terms of particle center brightness difference from the background brightness as assessed on a free image analysis program called ImageJ. This is shown as a function of particle biotin concentration for each antibiotin solution concentration. As is shown, concentrations of around 100 nM were the lowest concentration which induce a substantial change in the lens.

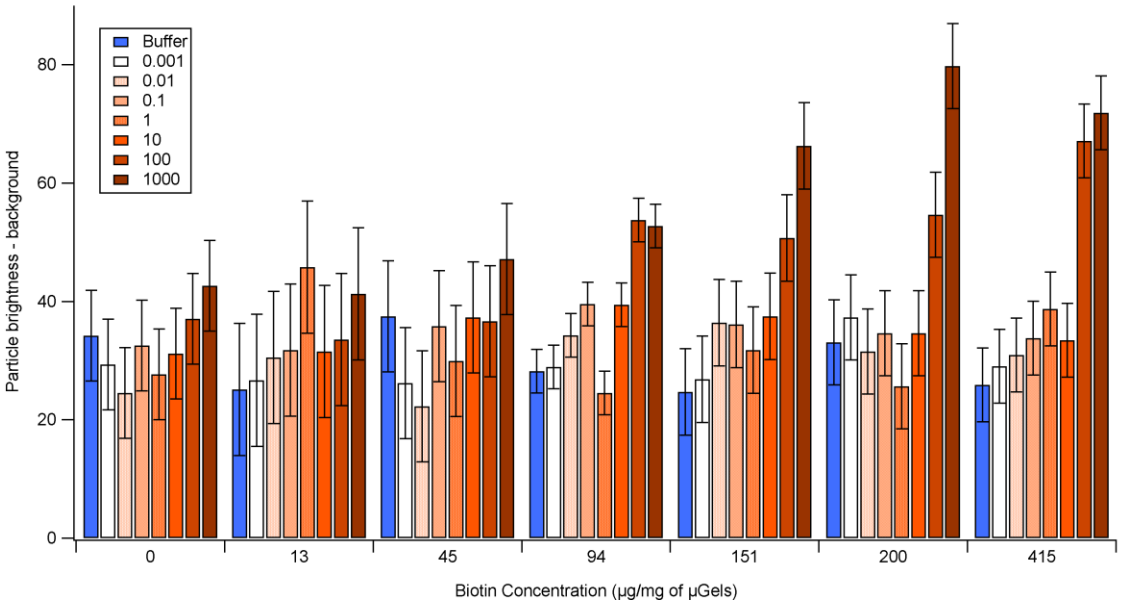

Figure 2.17. Biotinylated-microlens brightness differences between the middle of the particles and the background before and after incubation with buffer and various nM concentrations of anti-biotin. There are also microlenses with 7 different concentrations of biotin conjugated.

2.4 Conclusions and Outlook

The ability to sense small quantities of peptides, whole proteins such as antibodies, and nucleic acids in biological samples has become a very active area of research due to the increased emphasis on early detection and early diagnosis of diseases like cancer. One of the most desirable traits for such a platform would be the ability to analyze complex samples such as plasma, whole blood, or even macerated cells without further sample treatment. This attribute would reduce cost by reducing the amount of time and reagents needed for sample pre-treatment. This reduced cost could increase testing frequency of not only the entire population but also of an individual increasing the the likely hood of detection and peace of mind. Being able to detect multiple biomolecules at once would help increase diagnosis accuracy by assessing the individual's bimolecular profile rather than a single marker. Also, at least semi-quantitative information is paramount for an accurate diagnosis. This microlens platform

has been applied to different proteins including antibodies. These microlenses were also extended to a more user friendly and multiplexable microfluidic device. However, the most important factor is being able to sense molecules at biologically relevant concentrations (sensitivity) and being able to distinguish between safe and unsafe concentrations (accuracy). This method does not allow for the sensitivity or the quantitation that is necessary to sense autoantibodies or to compete with currently used techniques such as ELISA.

2.5 Implications of Softness

When designing a microgel to be used as a microlens, it is hard to underestimate the importance of the "softness" or compliance of the material. Here the microgel is asymmetrically deformed on the surface to create a physical shape that not only is capable of scattering light but also focusing light through it. I suggest that one could describe the optical properties of these particles as soft, meaning that the particle has a transparent or nearly optically clear refractive index that allows for visible light passage and focusing. Furthermore, the ability to have its refractive index, curvature and structure altered by multiple external sources could also be diagnostic of being soft. Although the physical and optical "softness" allow for an interesting sensor platform, it also makes it difficult to design the particle topology as well as to determine ligand or target placement and density. In terms of ligand placement, it seems reasonable that placing the target as close to the periphery of the particle as possible is logical. The Lyon group has been doing this for years using a core/shell structure and localizing the labile functional groups in the shell. This was attempted with modest results. It gets more unclear when discussing ligand density. The ligands need to be close enough together so that when an antibody binds it will bind either to two ligands thereby cross-linking the gel or binding one ligand with high enough protein density on the surface to change the refractive index enough to be visualized as a change in focusing power. However, the ligands need to be far enough

apart so that a single binding event makes a large difference in connectivity. Further complicating the situation is determining the optimal particle design in terms of cross-linking concentration and whether or not it should be a core/shell architecture. With such a soft and mobile platform, it is difficult to design these parameters and the most logical architectures that were attempted were did not yield more advantageous results.

2.6 References

[1] Moschou, E.A.; Madou, M.J.; Bachas, L.G.; Daunert, S. Voltage-Switchable Artificial Muscles Actuating at near Neutral Ph. *Sensors and Actuators B-Chemical* **2006**, *115*, 379-383.

[2] Moschou, E.A.; Peteu, S.F.; Bachas, L.G.; Madou, M.J.; Daunert, S. Artificial Muscle Material with Fast Electroactuation under Neutral Ph Conditions. *Chemistry of Materials* **2004**, *16*, 2499-2502.

[3] Seliktar, D.; Zisch, A.H.; Lutolf, M.P.; Wrana, J.L.; Hubbell, J.A. Mmp-2 Sensitive, Vegf-Bearing Bioactive Hydrogels for Promotion of Vascular Healing. *Journal of Biomedical Materials Research Part A* **2004**, *68A*, 704-716.

[4] Tae, G.; Kim, Y.J.; Choi, W.I.; Kim, M.; Stayton, P.S.; Hoffman, A.S. Formation of a Novel Heparin-Based Hydrogel in the Presence of Heparin-Binding Biomolecules. *Biomacromolecules* **2007**, *8*, 1979-1986.

[5] Wang, D.A.; Williams, C.G.; Yang, F.; Cher, N.; Lee, H.; Elisseeff, J.H. Bioresponsive Phosphoester Hydrogels for Bone Tissue Engineering. *Tissue Engineering* **2005**, *11*, 201-213.

[6] Yamaguchi, N.; Zhang, L.; Chae, B.S.; Palla, C.S.; Furst, E.M.; Kiick, K.L. Growth Factor Mediated Assembly of Cell Receptor-Responsive Hydrogels. *Journal of the American Chemical Society* **2007**, *129*, 3040-+.

[7] Gan, D.J.; Lyon, L.A. Synthesis and Protein Adsorption Resistance of Peg-Modified Poly(N-Isopropylacrylamide) Core/Shell Microgels. *Macromolecules* **2002**, *35*, 9634-9639.

[8] Nolan, C.M.; Reyes, C.D.; Debord, J.D.; Garcia, A.J.; Lyon, L.A. Phase Transition Behavior, Protein Adsorption, and Cell Adhesion Resistance of Poly(Ethylene Glycol) Cross-Linked Microgel Particles. *Biomacromolecules* **2005**, *6*, 2032-2039.

[9] Singh, N.; Bridges, A.W.; Garcia, A.J.; Lyon, L.A. Covalent Tethering of Functional Microgel Films onto Poly(Ethylene Terephthalate) Surfaces. *Biomacromolecules* **2007**, *8*, 3271-3275.

[10] De Geest, B.G.; Dejugnat, C.; Sukhorukov, G.B.; Braeckmans, K.; De Smedt, S.C.; Demeester, J. Self-Rupturing Microcapsules. *Advanced Materials* **2005**, *17*, 2357-+.

[11] Deng, Y.H.; Wang, C.C.; Shen, X.Z.; Yang, W.L.; An, L.; Gao, H.; Fu, S.K. Preparation, Characterization, and Application of Multistimuli-Responsive Microspheres with Fluorescence-Labeled Magnetic Cores and Thermoresponsive Shells. *Chemistry-a European Journal* **2005**, *11*, 6006-6013.

[12] Ehrick, J.D.; Deo, S.K.; Browning, T.W.; Bachas, L.G.; Madou, M.J.; Daunert, S. Genetically Engineered Protein in Hydrogels Tailors Stimuli-Responsive Characteristics. *Nature Materials* **2005**, *4*, 298-302.

[13] Gu, J.X.; Xia, F.; Wu, Y.; Qu, X.Z.; Yang, Z.Z.; Jiang, L. Programmable Delivery of Hydrophilic Drug Using Dually Responsive Hydrogel Cages. *Journal of Controlled Release* **2007**, *117*, 396-402.

[14] Rao, K.; Naidu, B.V.K.; Subha, M.C.S.; Sairam, M.; Aminabhavi, T.M. Novel Chitosan-Based Ph-Sensitive Interpenetrating Network Microgels for the Controlled Release of Cefadroxil. *Carbohydrate Polymers* **2006**, *66*, 333-344.

[15] Soppimath, K.S.; Kulkarni, A.R.; Aminabhavi, T.M. Chemically Modified Polyacrylamide-G-Guar Gum-Based Crosslinked Anionic Microgels as Ph-Sensitive Drug Delivery Systems: Preparation and Characterization. *Journal of Controlled Release* **2001**, *75*, 331-345.

[16] Tae, G.; Scatena, M.; Stayton, P.S.; Hoffman, A.S. Peg-Cross-Linked Heparin Is an Affinity Hydrogel for Sustained Release of Vascular Endothelial Growth Factor. *Journal of Biomaterials Science-Polymer Edition* **2006**, *17*, 187-197.

[17] Thornton, P.D.; Mart, R.J.; Ulijn, R.V. Enzyme-Responsive Polymer Hydrogel Particles for Controlled Release. *Advanced Materials* **2007**, *19*, 1252-+.

[18] Wheeldon, I.R.; Barton, S.C.; Banta, S. Bioactive Proteinaceous Hydrogels from Designed Bifunctional Building Blocks. *Biomacromolecules* **2007**, *8*, 2990-2994.

[19] Wood, K.C.; Chuang, H.F.; Batten, R.D.; Lynn, D.M.; Hammond, P.T. Controlling Interlayer Diffusion to Achieve Sustained, Multiagent Delivery from Layer-by-Layer Thin Films. *Proceedings of the National Academy of Sciences of the United States of America* **2006**, *103*, 10207-10212.

[20] Zhou, J.; Wang, G.N.; Zou, L.; Tang, L.P.; Marquez, M.; Hu, Z.B. Viscoelastic Behavior and in Vivo Release Study of Microgel Dispersions with Inverse Thermoreversible Gelation. *Biomacromolecules* **2008**, *9*, 142-148.

[21] Alarcon, C.D.H.; Pennadam, S.; Alexander, C. Stimuli Responsive Polymers for Biomedical Applications. *Chemical Society Reviews* **2005**, *34*, 276-285.

[22] Galaev, I.Y.; Mattiasson, B. 'Smart' Polymers and What They Could Do in Biotechnology and Medicine. *Trends in Biotechnology* **1999**, *17*, 335-340.

[23] Hoffman, A.S.; Stayton, P.S. Conjugates of Stimuli-Responsive Polymers and Proteins. *Progress in Polymer Science* **2007**, *32*, 922-932.

[24] Mart, R.J.; Osborne, R.D.; Stevens, M.M.; Ulijn, R.V. Peptide-Based Stimuli-Responsive Biomaterials. *Soft Matter* **2006**, *2*, 822-835.

[25] Li, J.; Li, X.; Ni, X.P.; Wang, X.; Li, H.Z.; Leong, K.W. Self-Assembled Supramolecular Hydrogels Formed by Biodegradable Peo-Phb-Peo Triblock Copolymers and Alpha-Cyclodextrin for Controlled Drug Delivery. *Biomaterials* **2006**, *27*, 4132-4140.

[26] Loh, X.J.; Goh, S.H.; Li, J. Hydrolytic Degradation and Protein Release Studies of Thermogelling Polyurethane Copolymers Consisting of Poly[(R)-3-Hydroxybutyrate], Poly(Ethylene Glycol), and Poly(Propylene Glycol). *Biomaterials* **2007**, *28*, 4113-4123.

[27] Deo, S.; Moschou, E.; Peteu, S.; Eisenhardt, P.; Bachas, L.; Madou, M.; Daunert, S. Responsive Drug Delivery Systems. *Anal. Chem.* **2003**, *75*, 207A-213A.

[28] Kikuchi, A.; Okano, T. Pulsatile Drug Release Control Using Hydrogels. *Adv. Drug Deliv. Rev.* **2002**, *54*, 53-77.

[29] Miyata, T.; Uragami, T.; Nakamae, K. Biomolecule-Sensitive Hydrogels. *Adv. Drug Deliv. Rev.* **2002**, *54*, 79-98.

[30] Ulijn, R.V.; Bibi, N.; Jayawarna, V.; Thornton, P.D.; Todd, S.J.; Mart, R.J.; Smith, A.M.; Gough, J.E. Bioresponsive Hydrogels. *Materials Today* **2007**, *10*, 40-48.

[31] Kiyonaka, S.; Sada, K.; Yoshimura, I.; Shinkai, S.; Kato, N.; Hamachi, I. Semi-Wet Peptide/Protein Array Using Supramolecular Hydrogel. *Nature Materials* **2004**, *3*, 58-64.

[32] Yang, Z.M.; Ho, P.L.; Liang, G.L.; Chow, K.H.; Wang, Q.G.; Cao, Y.; Guo, Z.H.; Xu, B. Using Beta-Lactamase to Trigger Supramolecular Hydrogelation. *Journal of the American Chemical Society* **2007**, *129*, 266-267.

[33] Yang, Z.M.; Xu, B. A Simple Visual Assay Based on Small Molecule Hydrogels for Detecting Inhibitors of Enzymes. *Chemical Communications* **2004**, 2424-2425.

[34] Miyata, T.; Jikihara, A.; Nakamae, K.; Hoffman, A.S. Preparation of Poly(2-Glucosyloxyethyl Methacrylate)Concanavalin a Complex Hydrogel and Its Glucose-Sensitivity. *Macromolecular Chemistry and Physics* **1996**, *197*, 1135-1146.

[35] Miyata, T.; Jikihara, A.; Nakamae, K.; Hoffman, A.S. Preparation of Reversibly Glucose-Responsive Hydrogels by Covalent Immobilization of Lectin in Polymer Networks Having Pendant Glucose. *Journal of Biomaterials Science-Polymer Edition* **2004**, *15*, 1085-1098.

[36] Miyata, T.; Asami, N.; Uragami, T. Preparation of an Antigen-Sensitive Hydrogel Using Antigen-Antibody Bindings. *Macromolecules* **1999**, *32*, 2082-2084.

[37] Miyata, T.; Asami, N.; Uragami, T. A Reversibly Antigen-Responsive Hydrogel. *Nature* **1999**, *399*, 766-769.

[38] Miyata, T.; Jige, M.; Nakaminami, T.; Uragami, T. Tumor Marker-Responsive Behavior of Gels Prepared by Biomolecular Imprinting. *Proceedings of the National Academy of Sciences of the United States of America* **2006**, *103*, 1190-1193.

[39] Ye, L.; Cormack, P.A.G.; Mosbach, K. Molecular Imprinting on Microgel Spheres. *Analytica Chimica Acta* **2001**, *435*, 187-196.

[40] Yoshimatsu, K.; Lesel, B.K.; Yonamine, Y.; Beierle, J.M.; Hoshino, Y.; Shea, K.J. Temperature-Responsive "Catch and Release" of Proteins by Using Multifunctional Polymer-Based Nanoparticles. *Angewandte Chemie-International Edition* **2012**, *51*, 2405-2408.

[41] Bai, W.; Gariano, N.A.; Spivak, D.A. Macromolecular Amplification of Binding Response in Superaptamer Hydrogels. *Journal of the American Chemical Society* **2013**, *135*, 6977-6984.

[42] Ulijn, R.V. Enzyme-Responsive Materials: A New Class of Smart Biomaterials. *Journal of Materials Chemistry* **2006**, *16*, 2217-2225.

[43] Plunkett, K.N.; Berkowski, K.L.; Moore, J.S. Chymotrypsin Responsive Hydrogel: Application of a Disulfide Exchange Protocol for the Preparation of Methacrylamide Containing Peptides. *Biomacromolecules* **2005**, *6*, 632-637.

[44] Sui, Z.J.; King, W.J.; Murphy, W.L. Dynamic Materials Based on a Protein Conformational Change. *Advanced Materials* **2007**, *19*, 3377-+.

[45] Murphy, W.L.; Dillmore, W.S.; Modica, J.; Mrksich, M. Dynamic Hydrogels: Translating a Protein Conformational Change into Macroscopic Motion. *Angewandte Chemie-International Edition* **2007**, *46*, 3066-3069.

[46] Moschou, E.A.; Sharma, B.V.; Deo, S.K.; Daunert, S. Fluorescence Glucose Detection: Advances toward the Ideal in Vivo Biosensor. *Journal of Fluorescence* **2004**, *14*, 535-547.

[47] McCurley, M.F. An Optical Biosensor Using a Fluorescent, Swelling Sensing Element. *Biosensors & Bioelectronics* **1994**, *9*, 527-533.

[48] Russell, R.J.; Pishko, M.V.; Gefrides, C.C.; McShane, M.J.; Cote, G.L. A Fluorescence-Based Glucose Biosensor Using Concanavalin a and Dextran Encapsulated in a Poly(Ethylene Glycol) Hydrogel. *Anal. Chem.* **1999**, *71*, 3126-3132.

[49] Alexeev, V.L.; Das, S.; Finegold, D.N.; Asher, S.A. Photonic Crystal Glucose-Sensing Material for Noninvasive Monitoring of Glucose in Tear Fluid. *Clinical Chemistry* **2004**, *50*, 2353-2360.

[50] Alexeev, V.L.; Sharma, A.C.; Goponenko, A.V.; Das, S.; Lednev, I.K.; Wilcox, C.S.; Finegold, D.N.; Asher, S.A. High Ionic Strength Glucose-Sensing Photonic Crystal. *Anal. Chem.* **2003**, *75*, 2316-2323.

[51] Asher, S.A.; Alexeev, V.L.; Goponenko, A.V.; Sharma, A.C.; Lednev, I.K.; Wilcox, C.S.; Finegold, D.N. Photonic Crystal Carbohydrate Sensors: Low Ionic Strength Sugar Sensing. *Journal of the American Chemical Society* **2003**, *125*, 3322-3329.

[52] Ben-Moshe, M.; Alexeev, V.L.; Asher, S.A. Fast Responsive Crystalline Colloidal Array Photonic Crystal Glucose Sensors. *Anal. Chem.* **2006**, *78*, 5149-5157.

[53] Walker, J.P.; Asher, S.A. Acetylcholinesterase-Based Organophosphate Nerve Agent Sensing Photonic Crystal. *Anal. Chem.* **2005**, *77*, 1596-1600.

[54] Walker, J.P.; Kimble, K.W.; Asher, S.A. Photonic Crystal Sensor for Organophosphate Nerve Agents Utilizing the Organophosphorus Hydrolase Enzyme. *Analytical and Bioanalytical Chemistry* **2007**, *389*, 2115-2124.

[55] Holtz, J.H.; Asher, S.A. Polymerized Colloidal Crystal Hydrogel Films as Intelligent Chemical Sensing Materials. *Nature* **1997**, *389*, 829-832.

[56] Kimble, K.W.; Walker, J.P.; Finegold, D.N.; Asher, S.A. Progress toward the Development of a Point-of-Care Photonic Crystal Ammonia Sensor. *Analytical and Bioanalytical Chemistry* **2006**, *385*, 678-685.

[57] Sharma, A.C.; Jana, T.; Kesavamoorthy, R.; Shi, L.J.; Virji, M.A.; Finegold, D.N.; Asher, S.A. A General Photonic Crystal Sensing Motif: Creatinine in Bodily Fluids. *Journal of the American Chemical Society* **2004**, *126*, 2971-2977.

[58] Lapeyre, V.; Gosse, I.; Chevreux, S.; Ravaine, V. Monodispersed Glucose-Responsive Microgels Operating at Physiological Salinity. *Biomacromolecules* **2006**, *7*, 3356-3363.

[59] Sorrell, C.D.; Serpe, M.J. Glucose Sensitive Poly (N-Isopropylacrylamide) Microgel Based Etalons. *Analytical and Bioanalytical Chemistry* **2012**, *402*, 2385-2393.

[60] Ehrick, J.D.; Stokes, S.; Bachas-Daunert, S.; Moschou, E.A.; Deo, S.K.; Bachas, L.G.; Daunert, S. Chemically Tunable Lensing of Stimuli-Responsive Hydrogel Microdomes. *Advanced Materials* **2007**, *19*, 4024-+.

[61] Dong, L.; Agarwal, A.K.; Beebe, D.J.; Jiang, H.R. Adaptive Liquid Microlenses Activated by Stimuli-Responsive Hydrogels. *Nature* **2006**, *442*, 551-554.

[62] Serpe, M.J.; Kim, J.; Lyon, L.A. Colloidal Hydrogel Microlenses. *Advanced Materials* **2004**, *16*, 184-+.

[63] Kim, J.; Serpe, M.J.; Lyon, L.A. Hydrogel Microparticles as Dynamically Tunable Microlenses. *Journal of the American Chemical Society* **2004**, *126*, 9512-9513.

[64] Kim, J.; Serpe, M.J.; Lyon, L.A. Photoswitchable Microlens Arrays. *Angewandte Chemie-International Edition* **2005**, *44*, 1333-1336.

[65] Kim, J.; Nayak, S.; Lyon, L.A. Bioresponsive Hydrogel Microlenses. *Journal of the American Chemical Society* **2005**, *127*, 9588-9592.

[66] Kim, J.; Singh, N.; Lyon, L.A. Influence of Ancillary Binding and Nonspecific Adsorption on Bioresponsive Hydrogel Microlenses. *Biomacromolecules* **2007**, *8*, 1157-1161.

[67] Kim, J.S.; Singh, N.; Lyon, L.A. Label-Free Biosensing with Hydrogel Microlenses. *Angewandte Chemie-International Edition* **2006**, *45*, 1446-1449.

[68] Kim, J.S.; Singh, N.; Lyon, L.A. Displacement-Induced Switching Rates of Bioresponsive Hydrogel Microlenses. *Chemistry of Materials* **2007**, *19*, 2527-2532.

[69] Anderson, N.E.; Rosenblum, M.K.; Graus, F.; Wiley, R.G.; Posner, J.B. Autoantibodies in Para-Neoplastic Syndromes Associated with Small-Cell Lung-Cancer. *Neurology* **1988**, *38*, 1391-1398.

[70] Dalmau, J.; Furneaux, H.M.; Rosenblum, M.K.; Graus, F.; Posner, J.B. Detection of the Anti-Hu Antibody in Specific Regions of the Nervous-System and Tumor from Patients with Paraneoplastic Encephalomyelitis Sensory Neuronopathy. *Neurology* **1991**, *41*, 1757-1764.

[71] Levine, T.D.; Gao, F.B.; King, P.H.; Andrews, L.G.; Keene, J.D. Hel-N1 - an Autoimmune Rna-Binding Protein with Specificity for 3' Uridylate-Rich Untranslated Regions of Growth-Factor Messenger-Rnas. *Molecular and Cellular Biology* **1993**, *13*, 3494-3504.

[72] Luque, F.A.; Furneaux, H.M.; Ferziger, R.; Rosenblum, M.K.; Wray, S.H.; Schold, S.C.; Glantz, M.J.; Jaeckle, K.A.; Biran, H.; Lesser, M.; Paulsen, W.A.; River, M.E.; Posner, J.B. Anti-Ri - an Antibody Associated with Paraneoplastic Opsoclonus and Breast-Cancer. *Annals of Neurology* **1991**, *29*, 241-251.

[73] Peterson, K.; Rosenblum, M.K.; Kotanides, H.; Posner, J.B. Paraneoplastic Cerebellar Degeneration .1. A Clinical Analysis of 55-Anti-Yo Antibody-Positive Patients. *Neurology* **1992**, *42*, 1931-1937.

[74] Scanlan, M.J.; Chen, Y.T.; Williamson, B.; Gure, A.O.; Stockert, E.; Gordan, J.D.; Tureci, O.; Sahin, U.; Pfreundschuh, M.; Old, L.J. Characterization of Human Colon Cancer Antigens Recognized by Autologous Antibodies. *International Journal of Cancer* **1998**, *76*, 652-658.

CHAPTER 3

PARTICLE SUSPENSION PASSAGE THROUGH MEMBRANES

Adapted from:

Hendrickson, G. R.; Lyon, L. A. Microgel Translocation Through Pores Under Confinement. *Angewandte Chemie, International Edition* **2010**, 49, 2193.

3.1 Introduction

In applications utilizing synthetic biomaterials, such as drug delivery,[1-4] bioimaging,[5,6] and tissue engineering,[7-11] the material mechanical properties represent an important set of design parameters.[12] Most studies of mechanical properties in biomaterials have focused on how cells interact with or move on surfaces of different rigidity in the context of mechanotransduction[7,10,11] and cell proliferation or differentiation.[8,9] However, few studies have investigated the effects of the mechanical softness of nanoparticles in nano- or micro-biological environments. It has been suggested, however, that the softness of nanoparticles may be relevant in processes such as phagocytosis or endocytosis.[13,14] This indicates that not only are cells affected by the mechanics of large surfaces or interfaces, but also by the rigidity of individual nanoparticles. The *in vivo* performance of nanoparticles is strongly dependent on a variety of biological processes, including, lymphatic drainage, endocytosis, extravasation, and kidney filtration. It stands to reason that any process that has a rigid size dependence may also be dependent on mechanical flexibility of the biomaterial.[15] Therefore, it is necessary to consider mechanics when outlining the nanoparticle size restrictions relevant for certain processes. This might especially be important when the process involves passage through small, well-defined pores, such as in renal filtration.

Renal or glomerular filtration is one of two routes of clearance of biomaterials from the body for particles smaller than 500 nm.[12,15,16] The other clearance route is biliary clearance through the liver; however, in nanomedicine applications biliary clearance is generally bypassed due to the small particle sizes typically used.[16] Therefore, renal clearance is an advantageous mechanism of nanoparticle excretion. This mechanism requires passage through approximately 8-nm diameter pores (as defined by endothelial gaps) under a pressure differential of 40 to 80 mmHg (0.7 to 1.5 psi).[17-21] Obviously, for most carrier systems these figures of merit are not easily met and require the integration of degradability into the nanoparticle design or rigorous control over small particle sizes.[22-25] In some cases these modifications may negatively alter drug loading/release, circulation times, cell uptake, and cytotoxicity. Therefore, it may be desirable to develop a carrier system that has the ability to be excreted without additional design complexity. For a hard sphere system, such as quantum dots, this implies a strict particle size limit,[26] which may negatively impact payload or may result in clearance through lymphatic drainage.[27] However, soft conformable nanoparticles that are able to deliver a large cargo yet are flexible enough to fit through small pores are a potentially attractive alternative. One example of such a construct is that of hydrogel colloids (i.e. nanogels or microgels), which are nanoparticles that can be dramatically compressed, due to their significant network flexibility.[28]

Herein, we describe the first demonstration of microgel translocation through cylindrical pores under pressure differentials relevant to renal filtration. We observe that microgel particles easily pass through such pores, even when the opening is >10 fold smaller than the unperturbed microgel diameter. For this study, track-etch membranes

were used as the model for pores in the renal system. As shown in **Scheme 3.1**, track-etch membranes were placed into gasket-sealed syringe filter holders and placed onto a luer-lock syringe that was enclosed at one end. A fluorescently-labeled microgel dispersion was added to the syringe and ~0.5 psi of hydrostatic pressure was applied from a compressed air cylinder to the head space of the syringe. Eluant was then be collected and analyzed by steady-state fluorescence.

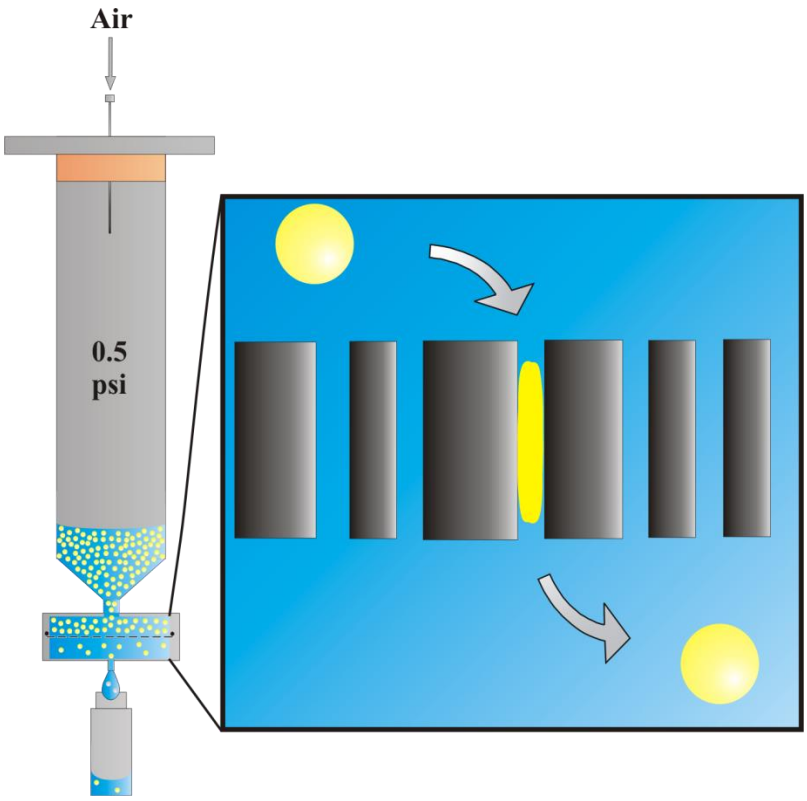

Scheme 3.1. Scheme of filtration setup and microgel filtration through a track-etch membrane.[29]

3.2 Experimental

3.2.1 Materials

Monomers *N*-isopropylacrylamide (NIPAm; Aldrich) and *N*-isopropylmethacrylamide (NIPMAm) were recrystallized from hexanes (Fisher Scientific) before microgel synthesis. The fluorescent monomer 4-acrylamidofluorescein

(AFA) was previously synthesized.[30] Cross-linker *N,N'*-methylenebis(acrylamide) (BIS; Aldrich), ammonium persulfate (APS; Aldrich), and acrylic acid (AAc; Fluka) were all used as received. The polystyrene (PS) standards (Duke Scientific) were diluted in a 0.003 wt% surfactant (sodium dodecyl sulfate (SDS; Aldrich)) solution. The track-etch membranes were purchased from Sterlitech (Kent, WA). The pH 7 buffer was a 10 mM (IS = 100 mM) phosphate buffer and the pH 3 buffer was a 10 mM (IS = 100 mM) formate buffer. All water used in the experiments was purified to 18 mΩ (Barnstead E-pure system).

3.2.2 Microgel Synthesis

The larger microgels were synthesized by precipitation polymerization of NIPAm, BIS (1 or 3 mol%), AFA (0.02 mol%), and AAc (10 mol%) with a total monomer concentration of 100 mM in 100 mL. All components were dissolved in distilled, deionized water and stirred under a nitrogen purge while heating to 68 °C. Then APS (0.01 mM) was added to initiate the reaction. The reaction was allowed to stir under nitrogen at 68 °C overnight. For the smaller microgel synthesis, NIPMAm was used with BIS and AFA, in the same manner except 8 mM SDS was added to stabilize the l particles, the syntheses were performed at 70 °C, and 8 mM APS was used.[31] All particle solutions were filtered and purified via centrufucation. The samples were then freeze-dried for storage.

3.2.3 Microgel Characterizations

Dynamic light scattering (DLS) was used to determine the hydrodynamic radius (R_h) under different pH conditions as described earlier.[32,33] This was done with a Wyatt Technologies DynaPro plate reader DLS using a laser wavelength of 830 nm. Scattering intensity fluctuations were detected for 10 s per reading by an avalanche photodiode at and angle of 158° (back scattering) from the incident laser. Dynamics software (Wyatt

Technologies Corp.) was used to calculate and fit an autocorrelation function plotted from the random fluctuations in scattering intensity. These fits of the autocorrelation functions were used to calculate the diffusion coefficients and then through the Stokes-Einstein equation, the R_h. The plate reader DLS provided the opportunity to use small volumes (50 μL) of particle solution and to run different aliquots in series without further sample preparation. Particle electrophoretic mobility measurements were carried out in 5 mM ionic strength HEPES (pH 7.4) and formate (3.0) buffers by electrophoretic light scattering with a Malvern Instruments Zetasizer.

3.2.4 Passage Experiments

Syringes (30 mL) were used for the filtration experiments by removing the plunger. Epoxy was used to seal a septum stopper in the top of the syringe. A manufacturer-supplied, luer lock membrane holder was used to hold the 25-mm radius membranes at the end of the syringe. The holders and syringes were sonicated and rinsed with a dilute Alconox solution and distilled, deionized water before assembly and use. After clamping the syringe vertically, a particle solution (~ 4 mL) was injected through the septum at the top of the syringe. Lastly a needle attached to a step-down (0 - 15 psi) regulator was placed into the septum to control the hydrostatic pressure. A particle solution of approximately 2 mL was collected which took anywhere from 4 to 8 hrs for the 100 nm pore experiments and 24 hrs to 48 hrs for the 10-nm pore experiments. After collection, all solutions were analyzed on a steady-state fluorescence spectrometer (Photon Technology International), equipped with a Model 814 PMT photon counting detector. For all microgels containing fluorescein the excitation wavelength was set to 490 nm and emission was detected between 500-600 nm. For the polystyrene standards, excitation was set to 468 nm and emission was collect from 480-600 nm based on the literature from the manufacturer. Then the fluorescence at peak max [515 nm (μGels) 508 nm (pS)] of the solutions was recorded. Readings of particles in pH 3 buffer were done

by spiking and aliquot of 0.5 mL of sample with 50 μL of a 100 mM pH 9 borate buffer to raise the pH to ~ 8 so that fluorescence would not be quenched. All data was analyzed by a Q-test and outliers at the 95% confidence interval were removed from the data set. The Q-test was done to remove any statistically irrelevant data. Also, the stars in the data sets represent data that is statistically different from the 88-nm pStyrene control at a 95% confidence level determined by a t-test. Standard curves for each particle type and pH condition were made by serial dilutions around the concentrations that passed through the membrane. Then using linear regression the background-subtracted fluorescence from the filtration experiments was used to calculate concentrations.

3.3 Results and Discussion

The microgels used in this study were prepared via co-polymerization of *N*-isopropylacrylamide (NIPAm), acrylic acid (AAc, 10 mol%), and 4-acrylamidofluorescein (AFA, 0.02 mol %) with *N,N'*-methylenebis(acrylamide) (BIS) as a cross-linker. The microgel sizes as a function of pH (pH dependence arises from the AAc co-monomer) are shown in **Table 3.1**. The 1% cross-linked particles were approximately 1140 nm in diameter fully swollen at pH 7, whereas the 3% cross-linked microgels were smaller (648 nm) as expected due to the increased cross-linking. Also, the deswelling due to protonation of the AAc at pH = 3 was 43% for the 1% and 30% for the 3% cross-linked microgels. Thus, these two microgel types provided two different sizes with two different pH-dependent compressabilities to investigate the generality of the phenomenon. Note that the cross-linking density difference only should account for a small difference in swollen particle elastic modulus (~8 kPa vs. ~13 kPa) based on previous bulk gel literature.[34] More important than the differences in the microgels is the fact that both are significantly larger than the 100 nm track-etch membrane pores. For comparison, volume conserving, rigid polystyrene beads with diameters of 200 nm

(negative control) and 88 nm (positive control) were used in identical filtration experiments.

As shown in **Figure 3.1**, after filtration the unfiltered solutions and the resulting eluants were analyzed by steady-state fluorescence spectroscopy, fluorescence microscopy, and bright field microscopy. The spectra of 3% particle solution unfiltered, filtered, and a buffer solution are shown. Also shown in **Figure 3.1**, a more concentrated solution of the same microgels was filtered through the 100 nm track-membranes and the solutions before and after filtration were dried on glass cover slips and analyzed via optical microscopy. Since the track-etch membranes have an extremely small pore density (100 nm pores: 4 pores/μm^2; 10 nm pores: 6 pores/μm^2), they do not allow for a high flux of particles, even if they are smaller than the pores. Therefore, steady-state fluorescence was used for quantification of the polymer mass passed through the filter. The fluorophore loading of the microgels and control polystyrene particles is not equal, however the unfiltered solutions contained the same polymer weight percent (wt%). Therefore, calculation of the particle wt% in the filtered solution allowed for fair comparison of particle flux. The background-subtracted fluorescence was converted to polymer wt% by creating standard curves of background-subtracted fluorescence to wt% for each particle at each pH condition.

Table 3.1. Hydrodynamic radii (R_h) and swelling properties of microgels under different pH conditions.

Particle Type	R_h (nm) pH 7.4	R_h (nm) pH 3.0	ζ (mV) pH 7.4	ζ (mV) pH 3.0	D %*
1% x-link µGel	570	324	− 20.5	− 4.1	43
3% x-link µGel	433	303	− 17.3	− 3.3	30
88 nm PS	48	46	N/A	N/A	N/A**
200 nm PS	101	96	N/A	N/A	N/A**

All R_h values were determined by DLS @ 25 °C.
All ζ potentials were determined by electrophoretic light scattering
*pH dependent deswelling percentage.
**No statistical difference in radii between pH 3 and 7. (t-test 95%)

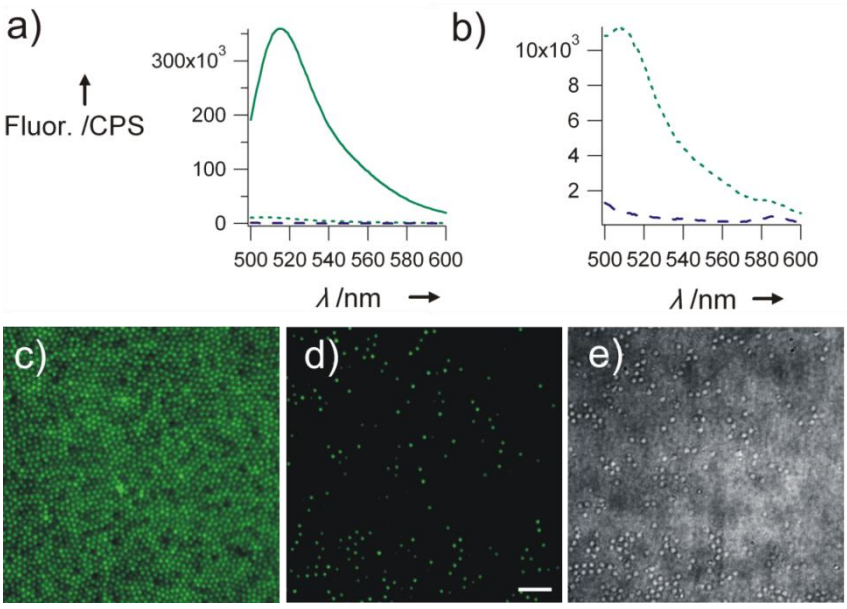

Figure 3.1. Fluorescence spectra, a) and b), of a 0.01 wt% solution of 3% cross-linked microgels (D_h = 648 nm) before (green) and after (green dotted) filtration through 100 nm pores at pH 7. The blue-dashed line represents pH 7 buffer. The spectrum of the filtrate is an average of 4 spectra. Panels (c), (d), and (e) are fluorescence microscopy images before and after flitration and a bright field microscopy image after filtration of the same microgels. Scale bar = 5 μm

The data in **Figure 3.2** display the surprising result that the flux of both microgel types at pH = 7 was equal to that of the much smaller PS positive control. A greater difference between the microgels and the PS control is observed when the overall particle concentration is increased, **Figure 3.3**. We tentatively ascribe this concentration dependence to jamming of the PS particles in the pores (*vide infra*). It appears, however, that the deformable microgel particles do not display jamming effects at pH = 7, presumably due to their conformational flexibility and Columbic interparticle repulsion (see **Table 3.1** for measured ζ potentials) during passage.

Two pH conditions were studied to evaluate the influence of microgel swelling on passage through the pores. At low concentration (**Figure 3.2**), the flux of the 1% cross-linked microgels at pH 3 is indistinguishable from the background. However, at pH 7 the 1% microgels pass readily through the pores, presumably due to the increased flexibility

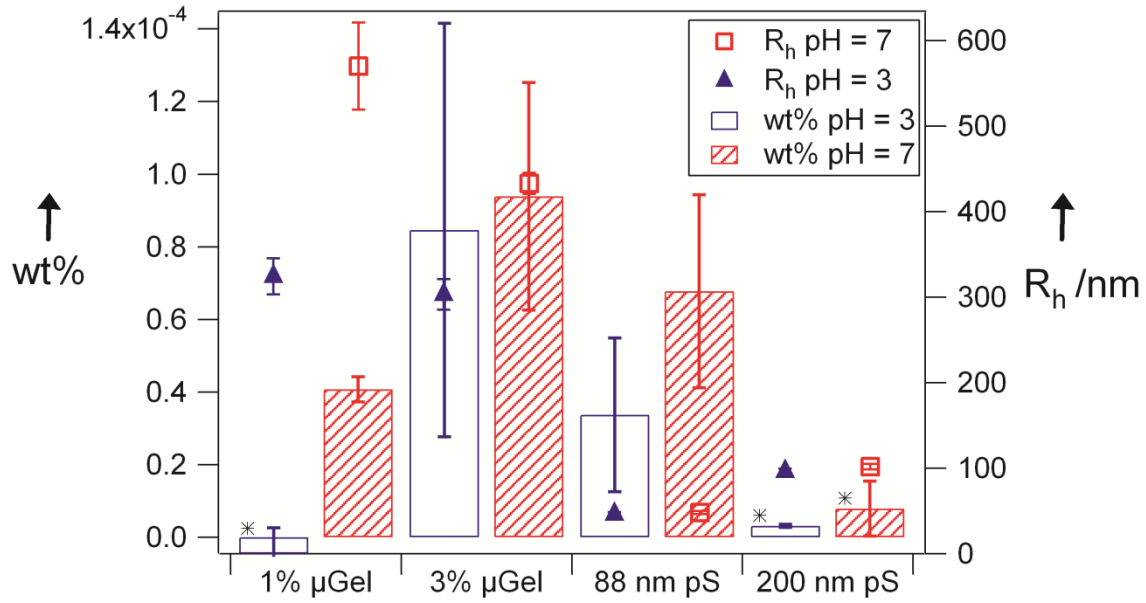

Figure 3.2. Filtration comparison of 1% and 3% microgels, 88 nm polystyrene, and 200 nm polystyrene particles (0.001 wt%). Error bars represent the uncertainty over 3 or 4 filtration experiments. Stars represent statistically significant data at the 95% confidence interval relative to 88 nm polystyrene at pH 7. Red squares are the hydrodynamic radii of particles at pH 7. Blue triangles are hydrodynamic radii of particles at pH 3.

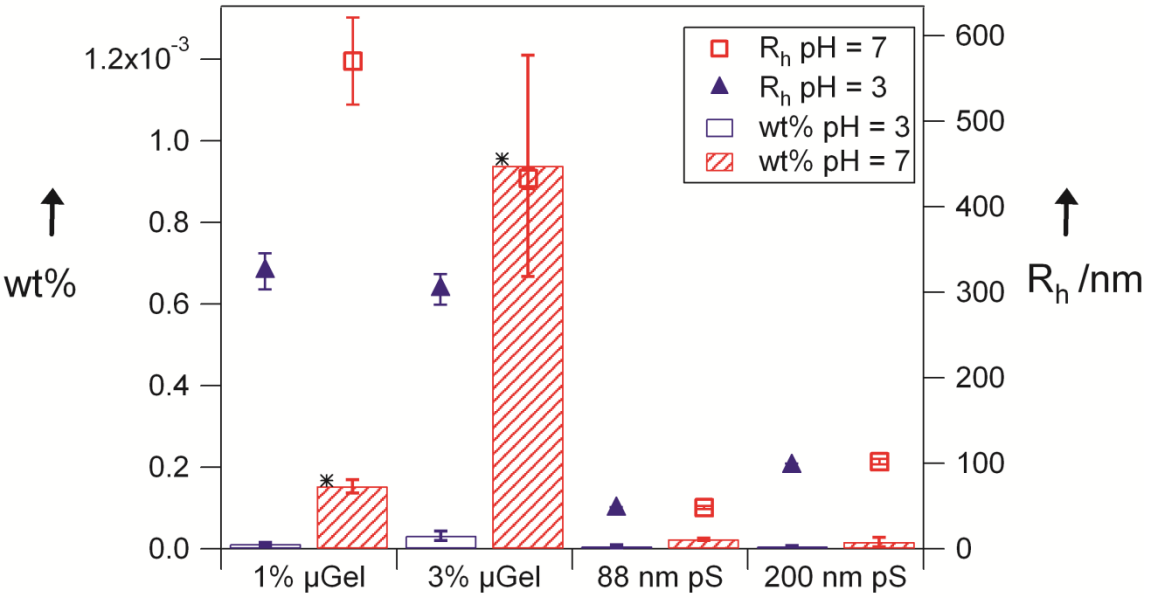

Figure 3.3. Filtration comparison of 1% and 3% microgels, 88 nm polystyrene, and 200 nm polystyrene particles (0.01 wt%). Error bars represent the uncertainty over 3 or 4 filtration experiments. Stars represent statistically significant data at the 95% confidence interval relative to 88 nm polystyrene at pH 7. Open circles are the hydrodynamic radii of all particles at pH 7. Filled triangles are hydrodynamic radii of all particles at pH 3.

of the swollen microgel, and decreased jamming due to Coulombic particle-particle repulsion. In the case of the 3% cross-linked microgels, there seems to be no difference between the two pH conditions. This is curious since both microgel types have a similar size at pH 3. Therefore, it could be the case that for this concentration and size, a jamming limit is being approached, and subtle differences in microgel modulus and interparticle potential produce large changes in pore passage. This is almost certainly the case when the concentration is increased further (**Figure 3.3**, 10-fold concentration increase); the observed flux for the microgels at pH 3 is much lower than that of the microgels at pH 7. This again suggests a jamming effect when the more rigid and less repulsive microgels try to fit through the small pores. This effect is emphasized by increasing the concentration another order of magnitude to 0.1 wt%, as shown in **Figure 3.4**. This figure shows that as the feed concentration increases only the flux of the 3% cross-linked particles in there fully swollen state (pH 7) increases, suggesting that the pS and deswollen microgels are jamming. It should be noted, however, that when the concentration is increased to 1 wt%, the passage increases for the microgels at both pH 7 and pH 3. The origin of this observation is still under investigation, but given our previous studies of microgel phase behavior at such concentrations,[35-37] it is likely that particle-particle interactions strongly perturb the actual hydrodynamic radii under these conditions. It should also be noted that the particle to pore size ratio of ~10:1 appears to be the rough limit for these particles, as larger microgels ($D_h \geq 1.5$ μm) did not appear to pass through 100 nm pores.

Having observed that pNIPAm-AAc microgels are able to translocate through pores 10 times smaller in diameter, we investigated the generality of this phenomenon to smaller pore sizes with more biologically relevant dimensions. Here, track-etch membranes with 10 nm pores were used in the same experimental setup (**Scheme 3.1**) with the same applied pressure differential of ~0.5 psi. The particles used in this

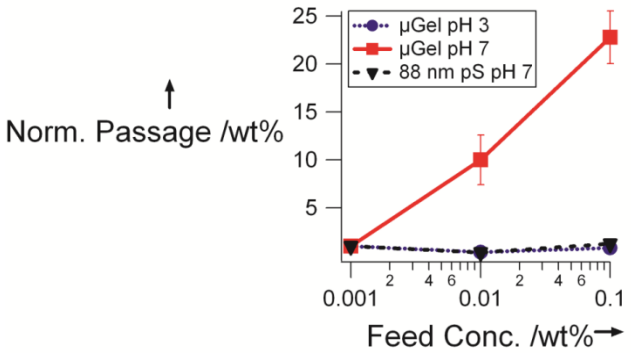

Figure 3.4. Normalized wt% passed versus feed concentration of 3% microgels at pH 3 and pH 7 and 88 nm pS at pH 7. The wt% passed was normalized to that as the lowest feed concentration.

experiment were fluorescent pNIPMAm microgels with a dilute solution diameter of 116 nm; 88 nm diameter fluorescently-labeled polystyrene beads were used as a negative control. The synthesis of the microgels has been published previously and is discussed briefly in the experimental section.[31] As shown in **Figure 3.5**, even at these smaller dimensions, the microgels still pass through the pores (pH 7) while the negative control does not. These data are compelling due to the similarity in pores size and pressures between those found in the kidney and used in these experiments. Also, it should be noted that when various FITC-dextran (fluorescein isothiocyanate–dextran) samples (MW = 20 or 150 kDa) were used as a positive control, they readily passed through the pores, as expected for a random chain flexible polymer.

Although the fundamental mechanisms underlying these observations are not understood quantitatively, the biology and physiology community has studied the glomerular filtration rate of macromolecules for many years.[17-20,38,39] It has been found that linear polysaccharides such as dextran have a much greater filtration rate and larger hydrodynamic radius cutoff than do proteins, due to the rigidity and well-defined secondary structure of the latter.[17]

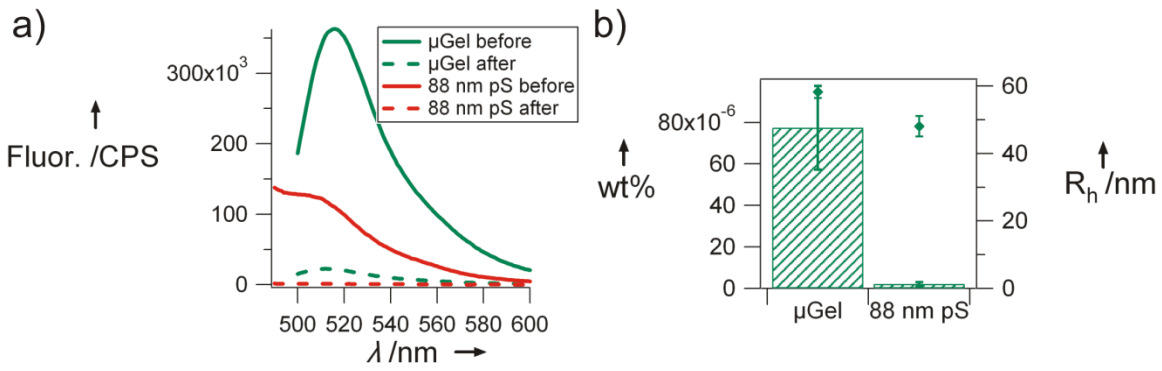

Figure 3.5. a) Fluorescence spectra of 0.001 wt% solutions before (solid) and after (dotted) filtration through 10 nm pores of 116 nm microgels (black) and 88 nm polystyrene beads (gray). After filtration spectra is an average of 4 spectra. b) Filtered wt% comparison of 116 nm microgels and 88 nm polystyrene. Diamonds are hydrodynamic radii of particles at pH 7.

Also, the soft matter community has extensively studied the passage of polymers through pores.[40-43] Translocation of a linear polymer through pores or in confined spaces is generally most probable if the polymer can go end first through the pore (as opposed to folding). Likewise, it has been found that a branched polymer has a higher probability of passage through a pore if more than one chain end can find the pore opening.[15] Therefore, a polymer nanoparticle with low connectivity and many different chain ends may have the conformational freedom to pass through a pore much smaller than its dilute solution diameter, due to the high number of energetically degenerate conformations with statistically identical passage probabilities. Also, the compressibility of these particles should be considered. For example, it has been shown that the combination of polymer and colloidal osmotic pressures, in a colloidal crystal of pNIPAm microgels was able to induce the dramatic deswelling of a much larger microgel "defect".[28] In that case the "defect" was compressed to a volume 15 times smaller than its dilute solution equilibrium volume, without imposing any direct mechanical force to the particle. It is therefore not unreasonable to hypothesize that similar microgels could adopt a configuration in which many chains enter the pore under a driving pressure differential,

followed by particle collapse/compression, and subsequent re-swelling as it emerges from the other side of the membrane.

3.4 Conclusions and Outlook

We have observed phenomena that illustrate the ability of hydrogel microparticles to pass through pores at least 10-fold smaller in size under hydrostatic pressures relevant to renal filtration. This extremely surprising result can be rationalized by considering the extreme softness of these nano-objects and conformational flexibility of the polymer chains comprising the particles. Importantly, we have illustrated the generality of the phenomenon to absolute pore sizes that are relevant to renal filtration by using nanogels appropriate in size for injectable drug delivery formulations. These studies illustrate the importance of considering the mechanical flexibility as a critical design component of nano-biomaterials. This network flexibility and compressibility of microgels is not only interesting in terms of their performance as biomaterials for drug delivery but is also of fundamental interest, as soft colloid physics has become a vibrant field of study. Indeed, both the fundamental physics of microgel softness and the biological impacts thereof have been and continue to be an active area of investigation within our research group.

3.5 Implications of Softness

Obviously, here the idea of softness is referring to the ability of a microgel to squeeze into and through small areas. These microgels do have a low modulus, probably in the 10-1000 Pa range based on previous studies.[44] However, this is the modulus assuming the volume is conserved and all chains are fully hydrated, but the ability for a microgel to fit into a small space not only involves deformation but also has the possibility of deswelling. The ability of the particles to deswell and deform comes from the fact that a microgel is comprised of hydrated flexible chains and gives these types of particles a different meaning of softness.

3.6 References

[1] Jain, T.K.; Reddy, M.K.; Morales, M.A.; Leslie-Pelecky, D.L.; Labhasetwar, V. Biodistribution, Clearance, and Biocompatibility of Iron Oxide Magnetic Nanoparticles in Rats. *Molecular Pharmaceutics* **2008**, *5*, 316-327.

[2] Jie, P.; Venkatraman, S.S.; Min, F.; Freddy, B.Y.C.; Huat, G.L. Micelle-Like Nanoparticles of Star-Branched Peo-Pla Copolymers as Chemotherapeutic Carrier. *Journal of Controlled Release* **2005**, *110*, 20-33.

[3] Shirota, K.; Kato, Y.; Suzuki, K.; Sugiyama, Y. Characterization of Novel Kidney-Specific Delivery System Using an Alkylglucoside Vector. *Journal of Pharmacology and Experimental Therapeutics* **2001**, *299*, 459-467.

[4] Tabata, T.; Murakami, Y.; Ikada, Y. Tumor Accumulation of Poly(Vinyl Alcohol) of Different Sizes after Intravenous Injection. *J. Controlled Release* **1998**, *50*, 123-133.

[5] He, X.X.; Nie, H.L.; Wang, K.M.; Tan, W.H.; Wu, X.; Zhang, P.F. In Vivo Study of Biodistribution and Urinary Excretion of Surface-Modified Silica Nanoparticles. *Anal. Chem.* **2008**, *80*, 9597-9603.

[6] Schipper, M.L.; Iyer, G.; Koh, A.L.; Cheng, Z.; Ebenstein, Y.; Aharoni, A.; Keren, S.; Bentolila, L.A.; Li, J.Q.; Rao, J.H.; Chen, X.Y.; Banin, U.; Wu, A.M.; Sinclair, R.; Weiss, S.; Gambhir, S.S. Particle Size, Surface Coating, and Pegylation Influence the Biodistribution of Quantum Dots in Living Mice. *Small* **2009**, *5*, 126-134.

[7] Chen, C.S.; Mrksich, M.; Huang, S.; Whitesides, G.M.; Ingber, D.E. Geometric Control of Cell Life and Death. *Science* **1997**, *276*, 1425-1428.

[8] Engler, A.J.; Griffin, M.A.; Sen, S.; Bonnetnann, C.G.; Sweeney, H.L.; Discher, D.E. Myotubes Differentiate Optimally on Substrates with Tissue-Like Stiffness: Pathological Implications for Soft or Stiff Microenvironments. *Journal of Cell Biology* **2004**, *166*, 877-887.

[9] Engler, A.J.; Sen, S.; Sweeney, H.L.; Discher, D.E. Matrix Elasticity Directs Stem Cell Lineage Specification. *Cell* **2006**, *126*, 677-689.

[10] Shen, H.; Tan, J.; Saltzman, W.M. Surface-Mediated Gene Transfer from Nanocomposites of Controlled Texture. *Nature Materials* **2004**, *3*, 569-574.

[11] Ingber, D.E. Cellular Mechanotransduction: Putting All the Pieces Together Again. *Faseb Journal* **2006**, *20*, 811-827.

[12] Mitragotri, S.; Lahann, J. Physical Approaches to Biomaterial Design. *Nature Materials* **2009**, *8*, 15-23.

[13] Beningo, K.A.; Wang, Y.L. Fc-Receptor-Mediated Phagocytosis Is Regulated by Mechanical Properties of the Target. *Journal of Cell Science* **2002**, *115*, 849-856.

[14] Banquy, X.; Suarez, F.; Argaw, A.; Rabanel, J.M.; Grutter, P.; Bouchard, J.F.; Hildgen, P.; Giasson, S. Effect of Mechanical Properties of Hydrogel Nanoparticles on Macrophage Cell Uptake. *Soft Matter* **2009**, *5*, 3984-3991.

[15] Fox, M.E.; Szoka, F.C.; Frechet, J.M.J. Soluble Polymer Carriers for the Treatment of Cancer: The Importance of Molecular Architecture. *Accounts of Chemical Research* **2009**, *42*, 1141-1151.

[16] Nel, A.E.; Madler, L.; Velegol, D.; Xia, T.; Hoek, E.M.V.; Somasundaran, P.; Klaessig, F.; Castranova, V.; Thompson, M. Understanding Biophysicochemical Interactions at the Nano-Bio Interface. *Nat. Mater.* **2009**, *8*, 543-557.

[17] Asgeirsson, D.; Venturoli, D.; Rippe, B.; Rippe, C. Increased Glomerular Permeability to Negatively Charged Ficoll Relative to Neutral Ficoll in Rats. *Am. J. Physiol. Renal Physiol.* **2006**, *291*, F1083-F1089.

[18] Deen, W.M.; Lazzara, M.J.; Myers, B.D. Structural Determinants of Glomerular Permeability. *Am. J. Physiol. Renal Physiol.* **2001**, *281*, F579-F596.

[19] Rippe, C.; Rippe, A.; Torffvit, O.; Rippe, B. Size and Charge Selectivity of the Glomerular Filter in Early Experimental Diabetes in Rats. *Am. J. Physiol. Renal Physiol.* **2007**, *293*, F1533-F1538.

[20] Salmon, A.H.J.; Toma, I.; Sipos, A.; Muston, P.R.; Harper, S.J.; Bates, D.O.; Neal, C.R.; Peti-Peterdi, J. Evidence for Restriction of Fluid and Solute Movement across the Glomerular Capillary Wall by the Subpodocyte Space. *Am. J. Physiol. Renal Physiol.* **2007**, *293*, F1777-F1786.

[21] Lau, C.; Sudbury, I.; Thomson, M.; Howard, P.L.; Magil, A.B.; Cupples, W.A. Salt-Resistant Blood Pressure and Salt-Sensitive Renal Autoregulation in Chronic Streptozotocin Diabetes. *Am. J. Physiol. Regul. Integr. Comp. Physiol.* **2009**, *296*, R1761-R1770.

[22] Atzet, S.; Curtin, S.; Trinh, P.; Bryant, S.; Ratner, B. Degradable Poly(2-Hydroxyethyl Methacrylate)-Co-Polycaprolactone Hydrogels for Tissue Engineering Scaffolds. *Biomacromolecules* **2008**, *9*, 3370-3377.

[23] Hua, N.; Sun, J. Body Distribution of Poly(D,L-Lactide-Co-Glycolide) Copolymer Degradation Products in Rats. *J. Mater. Sci.: Mater. Med.* **2008**, *19*, 3243-3248.

[24] Park, J.H.; Gu, L.; von Maltzahn, G.; Ruoslahti, E.; Bhatia, S.N.; Sailor, M.J. Biodegradable Luminescent Porous Silicon Nanoparticles for in Vivo Applications. *Nature Materials* **2009**, *8*, 331-336.

[25] Troutman, T.S.; Barton, J.K.; Romanowski, M. Biodegradable Plasmon Resonant Nanoshells. *Advanced Materials* **2008**, *20*, 2604-+.

[26] Choi, H.S.; Liu, W.; Misra, P.; Tanaka, E.; Zimmer, J.P.; Ipe, B.I.; Bawendi, M.G.; Frangioni, J.V. Renal Clearance of Quantum Dots. *Nature Biotechnology* **2007**, *25*, 1165-1170.

[27] Parungo, C.P.; Soybel, D.I.; Colson, Y.L.; Kim, S.W.; Ohnishi, S.; DeGrand, A.M.; Laurence, R.G.; Soltesz, E.G.; Chen, F.Y.; Cohn, L.H.; Bawendi, M.G.; Frangioni, J.V. Lymphatic Drainage of the Peritoneal Space: A Pattern Dependent on Bowel Lymphatics. *Ann. Surg. Oncol.* **2007**, *14*, 286-298.

[28] Iyer, A.S.; Lyon, L.A. Self-Healing Colloidal Crystals. *Angew. Chem., Int. Ed.* **2009**, *48*, 4562-4566.

[29] Hendrickson, G.R.; Lyon, L.A. Microgel Translocation through Pores under Confinement. *Angewandte Chemie-International Edition* **2010**, *49*, 2193-2197.

[30] Serpe, M.J.; Jones, C.D.; Lyon, L.A. Layer-by-Layer Deposition of Thermoresponsive Microgel Thin Films. *Langmuir* **2003**, *19*, 8759-8764.

[31] Blackburn, W.H.; Lyon, L.A. Size-Controlled Synthesis of Monodisperse Core/Shell Nanogels. *Colloid Polym. Sci.* **2008**, *286*, 563-569.

[32] Debord, J.D.; Lyon, L.A. Thermoresponsive Photonic Crystals. *Journal of Physical Chemistry B* **2000**, *104*, 6327-6331.

[33] Yi, Y.D.; Bae, Y.C. Volume-Phase Transition of Submicron-Sized N-Isopropylacrylamide/N-Tert-Butylacrylamide Particles by Photon Correlation Spectroscopy. *Journal of Applied Polymer Science* **1998**, *67*, 2087-2092.

[34] Matzelle, T.R.; Geuskens, G.; Kruse, N. Elastic Properties of Poly(N-Isopropylacrylamide) and Poly(Acrylamide) Hydrogels Studied by Scanning Force Microscopy. *Macromolecules* **2003**, *36*, 2926-2931.

[35] Meng, Z.; Cho, J.K.; Breedveld, V.; Lyon, L.A. Physical Aging and Phase Behavior of Multiresponsive Microgel Colloidal Dispersions. *J. Phys. Chem. B* **2009**, *113*, 4590-4599.

[36] Meng, Z.Y.; Cho, J.K.; Debord, S.; Breedveld, V.; Lyon, L.A. Crystallization Behavior of Soft, Attractive Microgels. *J. Phys. Chem. B* **2007**, *111*, 6992-6997.

[37] St John, A.N.; Breedveld, V.; Lyon, L.A. Phase Behavior in Highly Concentrated Assemblies of Microgels with Soft Repulsive Interaction Potentials. *J. Phys. Chem. B* **2007**, *111*, 7796-7801.

[38] Fissell, W.H.; Manley, S.; Dubnisheva, A.; Glass, J.; Magistrelli, J.; Eldridge, A.N.; Fleischman, A.J.; Zydney, A.L.; Roy, S. Ficoll Is Not a Rigid Sphere. *Am. J. Physiol. Renal Physiol.* **2007**, *293*, F1209-F1213.

[39] Tanner, G.A.; Rippe, C.; Shao, Y.Z.; Evan, A.P.; Williams, J.C. Glomerular Permeability to Macromolecules in the Necturus Kidney. *Am. J. Physiol. Renal Physiol.* **2009**, *296*, F1269-F1278.

[40] de Gennes, P.G., in *Polymers in Confined Environments, Vol. 138*, **1999**, pp. 91-105.

[41] Muthukumar, M. Translocation of a Confined Polymer through a Hole. *Physical Review Letters* **2001**, *86*, 3188-3191.

[42] Papisov, M.I. Modeling in-Vivo Transfer of Long-Circulating Polymers (2 Classes of Long Circulating Polymers and Factors Affecting Their Transfer in-Vivo). *Adv. Drug Deliv. Rev.* **1995**, *16*, 127-139.

[43] Wong, C.T.A.; Muthukumar, M. Polymer Translocation through a Cylindrical Channel. *Journal of Chemical Physics* **2008**, *128*.

[44] Wiedemair, J.; Serpe, M.J.; Kim, J.; Masson, J.-F.; Lyon, L.A.; Mizaikoff, B.; Kranz, C. In-Situ Afm Studies of the Phase-Transition Behavior of Single Thermoresponsive Hydrogel Particles. *Langmuir* **2007**, *23*, 130-137.

CHAPTER 4

RESISTIVE PULSE ANALYSIS: BACKGROUND AND EXPERIMENTAL

4.1 Introduction

4.1.1 General Principle

Resistive pulse analysis (RPA) is a technique based on electrochemical cell in which two electrolyte solutions are separated by a single pore. An electrode is placed in each solution and an electrical bias is placed between them. This creates an ion flow between the two electrodes through the pore and the magnitude of the current is determined by the electrical bias and the characteristics of the pore such as size, shape, surface charge, and electrolyte concentration. The main principle is based on the passage of an object, which could be a protein, cell, or colloidal particle, through the pore interfering with the current flow by occupying a percentage of the pore volume. Successful detection of the desired species is dependent on the ratio of pore volume to volume of the analyte; large volume exclusion from the pore changes the measured current flow. The name of this technique comes from the fact that as this species passes through the pore it most often suppresses current creating a brief resistive pulse in the current versus time trace (**Scheme 4.1**).

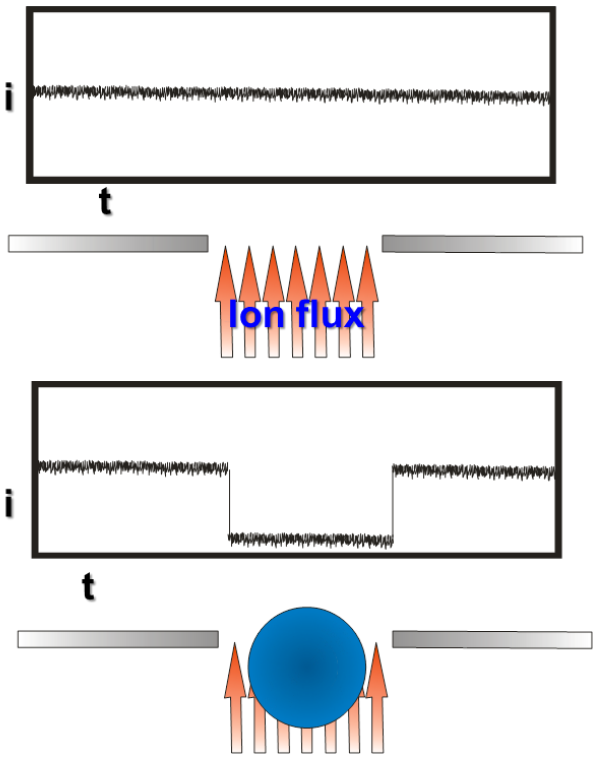

Scheme 4.1. Scheme of Resistive Pulse Analysis (RPA).

4.1.2 Brief History

The principle briefly described above is called the Coulter principle, patented by Wallace Coulter in 1953 (**Scheme 4.2**).[1] He and his brother, Joe, started the Coulter Corporation which marketed and sold the first commercial Coulter counter in 1956 for counting microparticles and cells.[2] The company was then bought by Beckman Instruments, Inc. in 1997 and is now known as Beckman Coulter, Inc. According to the Beckman Coulter, Inc website, the current Coulter counters can count and size particles from 0.4 μm to 1600 μm. Some of the first counters to focus on particles were developed by Deblois and co-workers.[3-9] Many different researchers since then have made home-built systems to study their particular analyte of interest. As described below, much of the

development here was to study particles or molecules smaller than the commercial instruments can detect. It should also be noted that the first commercial device with a tunable pore size is on the market called the qNano manufactured by Izon, Inc.[10] This allows for the analysis of a wide range of sizes without changing the pore itself which is common in most instruments where the pore dimensions are fixed.

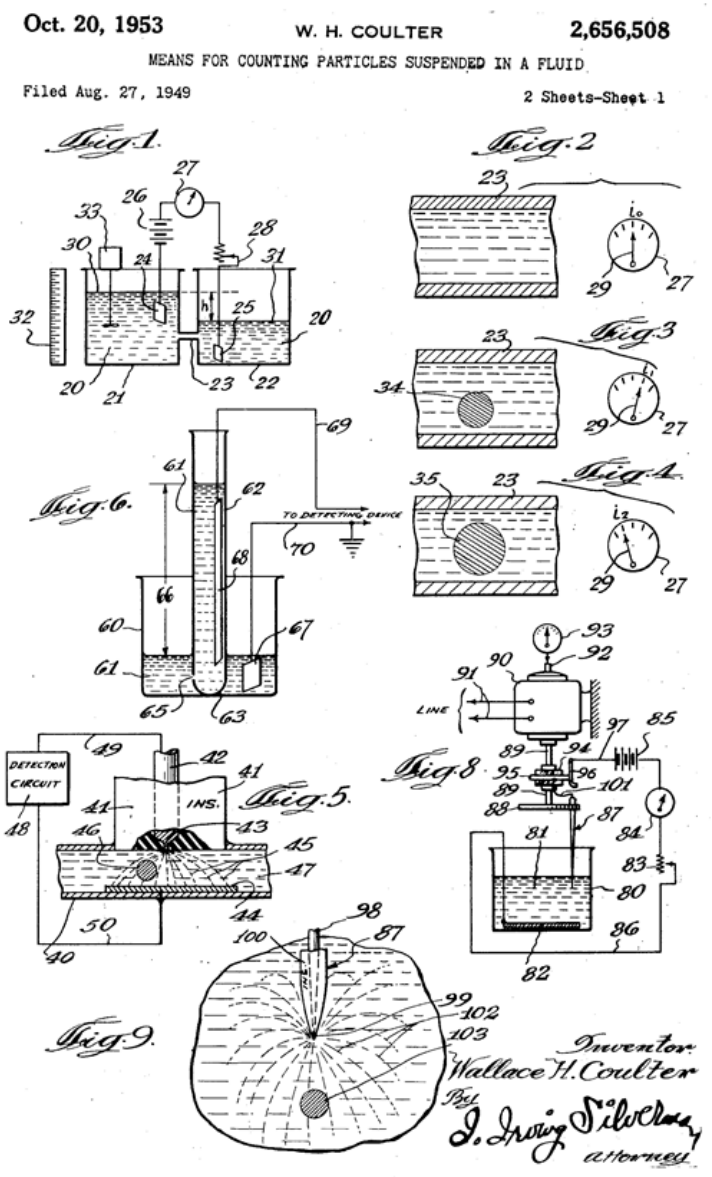

Scheme 4.2. Schemes from Walace Coulters 1953 patent. US Patent 2656508.[1]

4.1.3 Devices and Applications

Although, a commercial Coulter Counter has been on the market for over 60 years, many researchers have been developing ways of studying their particular flavor of analyte by developing their own system.[11-16] These systems push the limits of the currently commercially available systems by tuning sensitivity, selectivity, sample preparation or sample introduction. In most cases, in order to achieve these goals a new pore platform was introduced. **Scheme 4.3**, published in a nice review by Kozak et.al., outlines the developments over the years.[16] This scheme shows different pore types, platforms, and analytes that have been considered. In the following sections, examples of synthetic pores and biological pores and their respective analytes will be discussed.

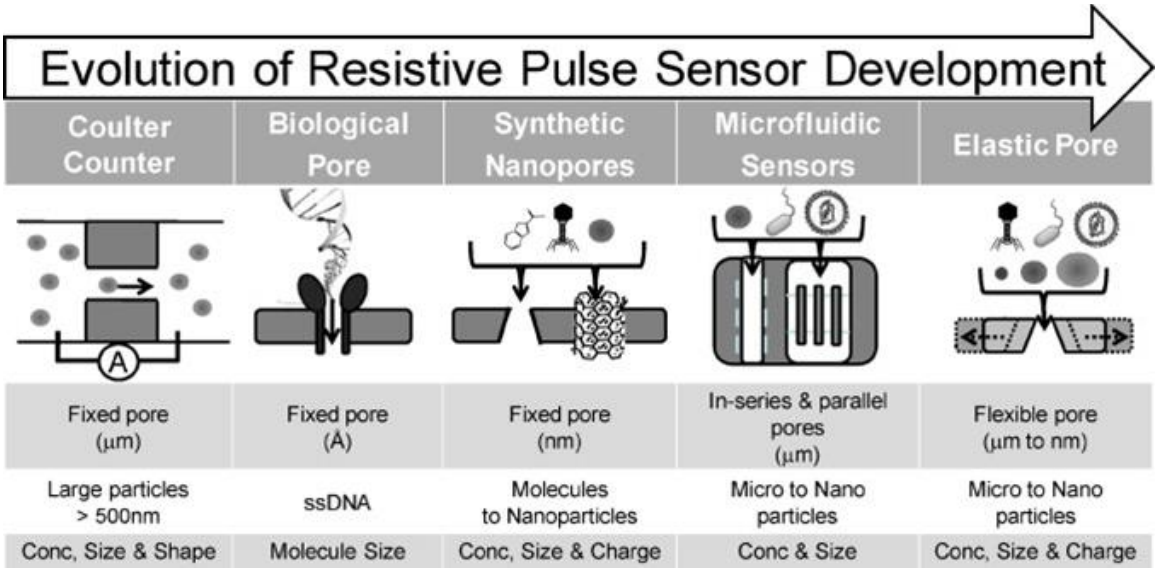

Scheme 4.3. Scheme showing the development of RPA systems.[16]

4.1.3.1 Synthetic Pores

There are many different types of synthetic resistive pulse devices including SiN pores,[17] polymer pores,[18] micropipette pores,[19] carbon nanotube pores,[20-23] graphene

pores,[24] flexible pores,[25] pores incorporated into microfluidic devices,[26] and glass capillary pores.[27] A very nice recent review of all nanoscale electrochemical techniques was published in Analytical Chemistry by Oja, et al.[28] Here, some examples of each pore type will be discussed.

The first example of a silicon nitride pore was made by using a focused ion beam (FIB) to mill a small cavity (60 nm) in one side of a Si_3N_4 membrane deposited over a small hole in a silicon substrate. Then an Ar^+ ion beam with a larger focus was used to mill away the opposite side of the membrane until a small few nanometer hole was created at the bottom of the previous formed cavity.[29] Then these pores were used to analyze translocation events of different length dsDNA.[30] Passage events where the DNA passed straight through the pore one end at a time and events where the two ends of the DNA entered together as it passed through were characterized. Recently, similar pores fabricated using e-beam lithography and reactive ion etching was used to fabricate silicon nitride pores which were then coated with Au.[31] The gold surface was then used as a substrate to attach receptors for proteins which allowed for detection of specific proteins in a mixed sample as well as the ability to determine dissociation rates.[32]

One interesting polymer pore was formed by first forming a thin polymer membrane over a 2 mm hole in a Teflon substrate using a thermoplastic.[18] Then after punching a large 200 μm hole in the membrane, laser heating was used to melt the plastic and therefore shrink the pore to diameters of ~ 8 nm. These pores were then used to detect DNA passage. Modified polymer track-etch membranes have also been used as nanopore devices.[33,34] In this case, tracked membranes were purchased prior to their chemical etching into the cylindrical pores. This etching was performed in-house where a

special single-side plasma etch was performed in order to create a conical pore opening.[33] This etching was optimized to create conical pores with small side openings of less than 100 nm.[35] Gold plating and subsequent PEG-thiol functionalization to the interior of these pores has been done and the transport properties of proteins through these pores has been studied.[34]

Methods have also been developed using pulled pipettes as pores. DNA has been detected using pulled pipettes as well as ion binding to a functionalized nanopipette tip.[19,36-38] A technique using pipette pulling has also been develop to for a glass nanochannel by sealing a small piece of the pulled pipette into another micropipette.[39] These pores were 100 nm to 5 nm in diameter and the transport properties of DNA and polystyrene particles were studied.

Carbon nanotube Coulter counter devices have been fabricated by embedding a single carbon nanotube in epoxy developed by Crooks and co-workers.[23] It was shown that the electrokinetic mobility, particle count, diameter, and transport times of charged polystyrene spheres of approximately 60 nm in diameter could be determined using this technique.[20-22] A detailed comparison with common nanoparticle characterization techniques such as dynamic light scattering (DLS) and transmission electron microscopy (TEM) was also done highlighting the advantages to single particle measurements in solution.[20]

Single or multiple sheets of graphene with single pores created by an electron beam have also been created.[24,40-42] These device have the advantage of not only having sub-10 nm pores but also being extremely thin. This small thickness provides an extremely small and therefore sensitive sensing zone. Graphene devices have been

applied to the study of transients of different conformations of DNA as it passes through the pore.[41] It was also shown that due to the ultrathin graphene a single base enters and leaves the sensing zone one at a time suggesting that it might be possible to perform *in situ* sequencing.[42]

A very interesting idea for increasing the utility of a pore and its dynamic range is to create a tunable pore.[25,43-47] The pores are advantageous because a fixed pore only has a small range of possible analyte sizes. In addition it allows for an easier clearance mechanism for clogs that occur in the pore. Microparticle, nanoparticles and viruses have been sensed using these pores. These conical pores are formed in a cross-shaped thermoplastic by mechanically puncturing it with an electrochemically sharpened W rod. The pore size is adjusted by mechanically pulling on the 4 ends of the cross, which stretches the pore.

Another interesting advancement in resistive pulse analysis has been its incorporation into microfluidic platforms.[26] As with most technologies that have been incorporated into microfluidics this platform allows potential for low sample volume, high sample throughput, multiplexed sample analysis, increased statistics, and portability. In one case, a device was fabricated with the idea of being able to mix cells with different molecules and then analyze the resulting sample.[48] As a demonstration they showed that the device could count and distinguish between 5 μm, 10 μm, and 15 μm particles as well as between fibroblast cells and microspheres. In a similar application multiple Coulter counter pores in a microfluidic device were used to improve accuracy of differentiating between different sized PMA (polymethacrylate) particles and two different types of pollen.[49] The same group also developed a device with parallel apertures that allowed for

a 300% increase in polystyrene particle counting rate for a high throughput counting device.[50] A similar device was able to distinguish between PMA particles and pollen at the same counting rate.[51] The idea of using multiple apertures was extended also to virus counting.[52] In another device, a particle analysis of 500,000 particles per second was performed using mixtures of 3 different sized polystyrene particles and then mixtures of phage and polystyrene particles.[53] Here, phage infected whole mouse blood could also be distinguished from uninfected whole mouse blood. This demonstrates the ability to recognize contaminates with a high background. The authors also pointed out that because of the high throughput nature of this device statistics on rare events could be collected. In another case it was shown that soluble antibodies could be detected by monitoring the size of an antigen functionalized colloid.[54] As antibody bound the colloid the apparent size of the particle increased. Also, antibodies have been functionalized to the pore to detect proteins on the surface of a cell.[55] As the cells flowed by the resonance time in the sensing zone increased if there were specific interactions between the cell and the pore bound antibodies. These microfluidic devices may be a great option for fast characterization and have the potential for commercial use.

The last example is the one developed by the White group at the University of Utah. This method is the one described in detail in this chapter and is one which creates a single pore in the end of glass capillary.[27] The White group has studied nanoparticle transport through these pores.[56] In collaboration with our group, we studied the transport of microgels that were larger than the pores and these experiments will be the subject of **Chapter 5**.[57,58] This concept was then extended to multi-laminer liposomes by the White group.[59]

4.1.3.2 Biological Pores

An interesting alternative to trying to fabricate very small pores for applications like nucleotide recognition, is to use a biological pore, These pores have very small and well defined geometries and sizes. One of the most common examples is α-hemolysin.[60] This is a toxin secreted by bacteria that will form a water filled pore in a cell lipid bilayer membrane and can increase water flow and ion flow resulting in osmotic death of a cell. There are three advantageous properties of this channel. First, the smallest point is 1.4 nm wide meaning that it has the potential to distinguish between very small differences between analytes. Second, the small channel is hydrophilic meaning that it is easy to hydrate. Third, this channel is a self-assembly of 7 protein subunits that will assemble only in a lipid bilayer allowing for dissolution of the subunits into a continuous phase and spontaneous assembly into a supported lipid bilayer. There are many example of using the α-hemolysin channel to detect and possibly sequence DNA.[61-65] More recently, the White group at the University of Utah developed a method of suspending a lipid bilayer over the opening of a glass capillary nanopore and monitoring α-hemolysin ion channel formation in the bilayer.[66] They then monitored protein binding to the channel.[66,67] Next, this group tracked the effects of multiple channels forming in the bilayer and passage of oligios of a single nucleotide base.[68-71] Then detection of single base mutations has been attempted by detection of different adducts in a long chain of bases.[72] Then oxidative mutations were detected by hybridizing a small probe DNA stand which then depending on the strength of binding would unzip at different rates as it passed through the channel.[73,74] Mutations were also detected by functionalizing the mutated bases with a crown ether and then as it passes through the channel the bulky and cation bound ether

could be detected as a larger blockage.[75,76] Other strategies to slow down the DNA translocation for a better chance at increasing the differences between bases passing through the pore have included different modifications to the α-hemolysin channel.[77-80] Also, functionalization of different molecules to the channel has allowed for detection of other organic molecules.[3,8,9] Evident is the effort from researchers to create a strategy to detect mutations and ultimately sequence DNA using RPA which is an inexpensive and fast analysis technique.

4.2 Experimental Setup

4.2.1 Conductivity Experiments

Scheme 4.4 shows our RPA setup. For conductivity experiments, a Dagan Corporation Chem-Clamp voltameter-amperometer with a preamplifier (0.05-1 nA/V) supplied the constant voltage bias and monitored the sample current. Data was collected at 1 x 10^5 Hz and averaged over 1 x 10^4 points. The Dagan voltameter was interfaced with a PC through a NI-PCIe-6320, X-series DAQ with a BNC-2120 shielded connector block and experiments were run in a LabView program written in house by the White group. The nanopore conductivity was monitored by placing an electrolyte solution inside and outside of a nanopore capillary with an Ag/AgCl (1 mm) electrode in the interior and exterior solutions. Then a constant bias (usually 100 mV) was placed between the two solutions and the current flow was monitored. In the pressure driven experiments a special air-tight capillary holder was used that housed both the capillary and the Ag/AgCl electrode. Then the pressure was changed by attaching a 10 mL syringe and either pulling or pushing to change the pressure differential between the inside and outside of the capillary. The pressure was monitored by a digital pressure gauge. This allowed samples to be pulled into or driven out of the nanopore. Keeping the nanopore clean is very

important and so prior to and after experiments the pore was rinsed with a number of solvents and electrolyte solutions including: ethanol, methanol, nanopure H_2O, and the electrolyte solution used for the experiment. Also, very gentle sonication in water can be done to try and clear the nanopore of debris.

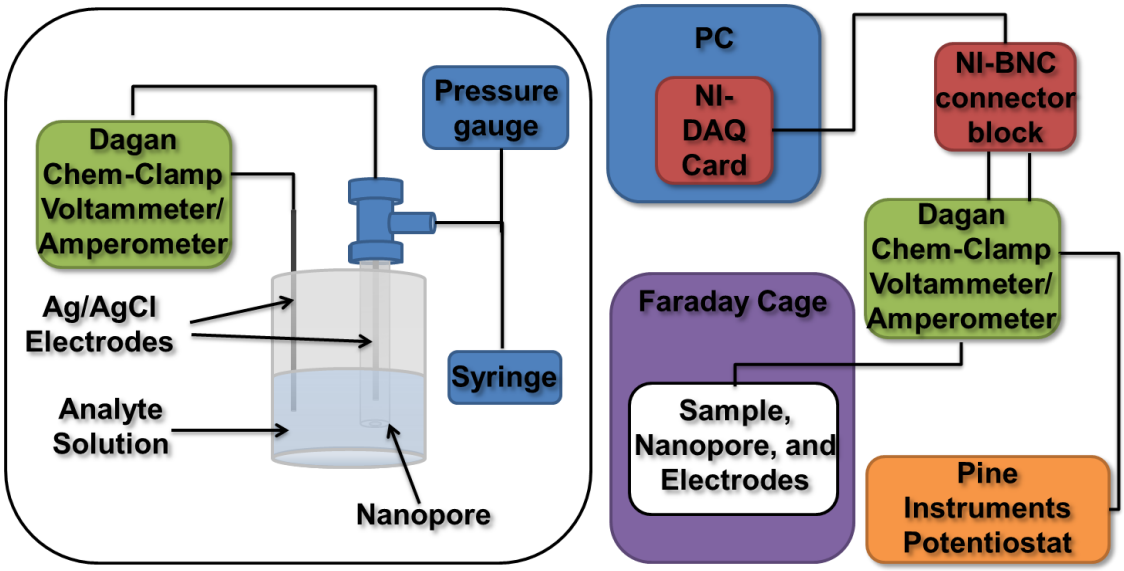

Scheme 4.4. Scheme showing the development of overall RPA setup.

4.2.2 Voltammetry Experiments

Voltammetry was mainly performed to diagnosis the nanopore size as well as the Pt electrode size that is created during nanopore fabrication as described in **Section 4.3.3**. The voltammetry experiments were also performed using the Dagan Chem-Clamp voltammeter except the voltage sweep was supplied to the Chem-Clamp device by a Pine Instruments potentiostat. The signals were sent to the PC through the same DAQ and monitored using LabView. Here, a two electrode setup was used. In the case of measuring the size of the Pt disk electrode created during nanopore fabrication, an Ag/AgCl (3M NaCl) electrode and the Pt disk electrode were used in a ferrocene in

acetonitrile solution. However, when measuring the nanopore size, two Ag/AgCl electrodes were used one inside and one outside of the capillary in a KCl solution.

4.2.3 Pt Etching

Two steps in the fabrication of nanopores calls for Pt etching. In one step Pt wire is etched to sharpen the tip and in another the Pt wire sealed in glass is etched out to create the nanopore. In both cases, an Agilent waveform generator is used and both setups are shown in **Scheme 4.5**. Briefly, for sharpening the Pt tip a NaCN, KOH solution is used with a Pt counter electrode. In the case of etching the Pt out of the nanopore a $CaCl_2$ solution was used with a Pt counter electrode.

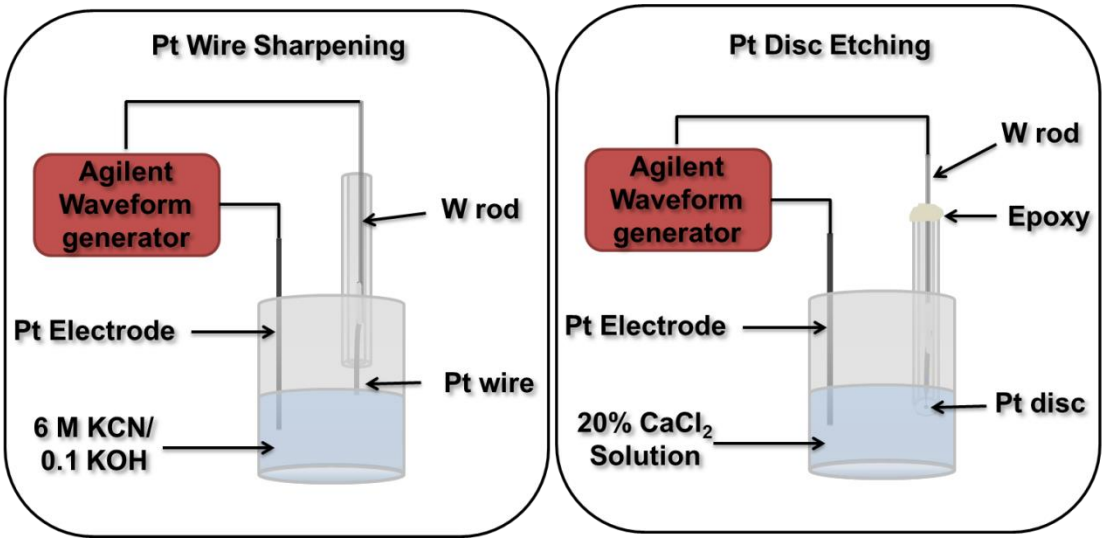

Scheme 4.5. Scheme showing the Pt etching setups.

4.3 Nanopore Fabrication

4.3.1 Materials

For pore fabrication, Pt wire (99.95% purity; 25 μm diameter; Alfa Aesar), tungsten rods (0.010 in diameter; 3 in in length; FHC, Inc), and glass capillaries (1.65 mm O.D.; 0.75 mm I.D.; softening point 700 °C; composition 67.7% SiO_2, 2.8% BaO,

15.6% Na_2O, 5.6% CaO, 4% MgO, 1.5% B, and 0.6% K_2O%; Dagan Corporation (SB16)), and Ag paint (FHC, Inc) were used. During fabrication the following chemicals are used for various tasks as outlined below: NaCN, KOH, and $CaCl_2$ all used as received from Sigma. A Loctite® 0151™ Hysol two-part epoxy was also used. Polishing materials from Buehler were used and more specifically Microcut silicon carbide wet and dry grinding paper, (P800, P2400, P4000), Microcloth PSA (2-7/8 inchs), and Micropolish II (0.05 μm). After pore fabrication, ferrocene (100%, Alfa Aesar), Tetra-*n*-butylammonium hexafluorophosphate (TBAPF6, Sigma), acetonitrile (Sigma), KCl (Sigma), bleach and Ag wire (1 mm diameter, Sigma) were all used during different diagnostic steps. All water used in experiments is DI water run through a Barstead Nanopure filtration system until the resistance is 18 MΩ.

4.3.2 Fabrication

To fabricate glass nanopores a method developed by the White group at University of Utah was used.[27] Here, the particular methods used in our group and for the experiments discussed in **Chapter 5** will be described and are outlined in **Scheme 4.6.**

First, a 1-2 cm long section of the 25 μm Pt wire is cut and attached with a small drop of Ag conductive paint to the end of a 3 in long by 0.010 in diameter tungsten rod. A small bend or kink should be put in the W rod. Next, the Pt wire/W rod assembly was threaded through a glass capillary (1.65 mm 0.D., 0.75 mm I.D.) with just the end of the Pt sticking out of the capillary (**Scheme 4.6**). The W rod allows for the maneuvering of the small piece of platinum wire inside and out of the end of the capillary and the kink in the rod does not allow for it to fall out of the capillary. Using a gloved finger the platinum wire is straightened and centered in the middle of the capillary. Here, you can

check the position and whether or not the tip of the platinum is bent with a microscope. The Pt wire being positioned in the exact center is not necessary; however, the wire should be as parallel to the walls of the capillary as possible. Now, there should be a centered Pt wire attached to the end of a bent tungsten rod inside of a glass capillary.

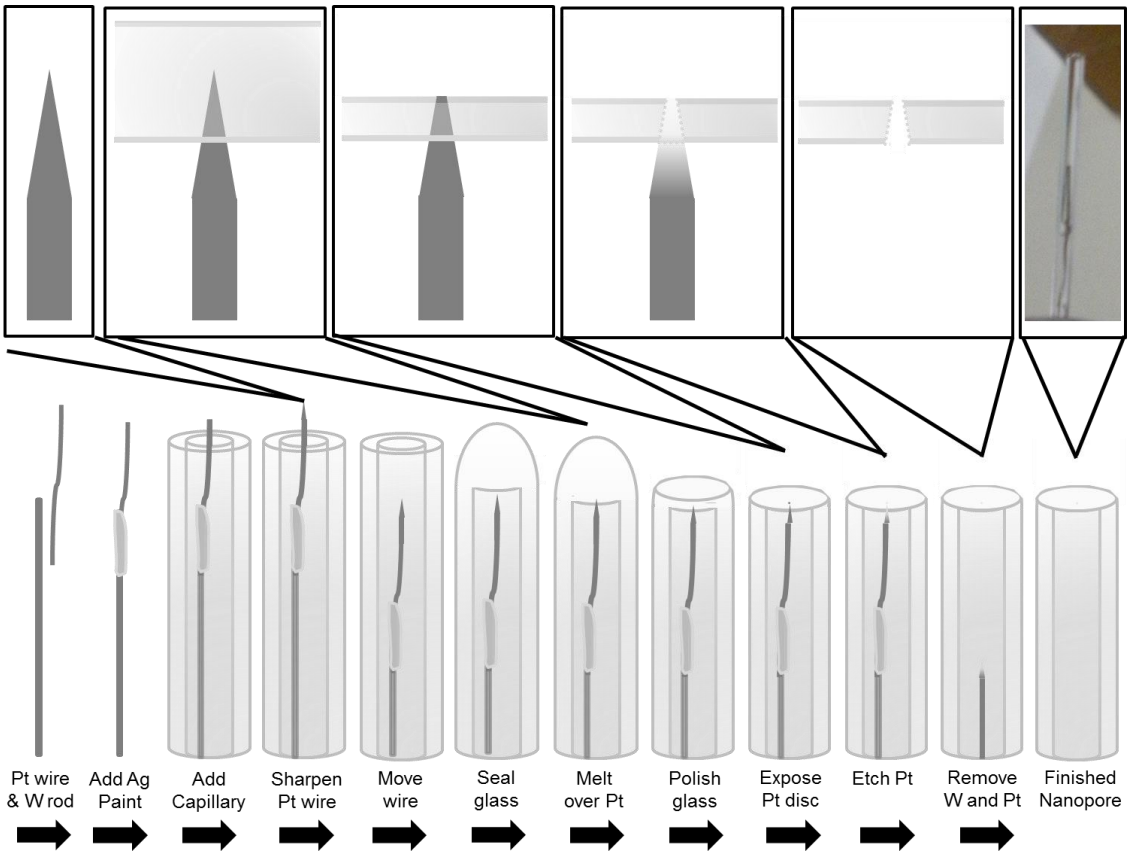

Scheme 4.6. Scheme showing the fabrication process of the glass nanopores. Top images are zoomed in versions of key steps and the photograph is of a completed pore with an Ag/AgCl electrode inside of it.

The Pt wire is now sharpened to create a small diameter tip. The wire is protruded through the end of the glass capillary and the whole assembly is placed in a holder which can be lowered with a micromanipulator. This process is very similar to how many scientists fabricate scanning tunneling microscopy (STM) tips.[81] A 6 M solution of NaCN in 0.1 M KOH is made to use as the sharpening solution. Then, a platinum electrode and

the Pt wire through W rod are hooked to different poles of a function generator as shown in **Scheme 4.5**. Then a sine function at 3.6 V amplitude and 100 Hz frequency is run between the two electrodes. Just before starting the AC sweep, the tip of the Pt wire is inserted into the solution. Then the AC sweep is turned on a as the Pt is etched away bubbles form when the bubbles stop forming the sweep is stopped and the tip is rinsed in water. An example of a sharpened platinum tip is shown in **Figure 4.1**.

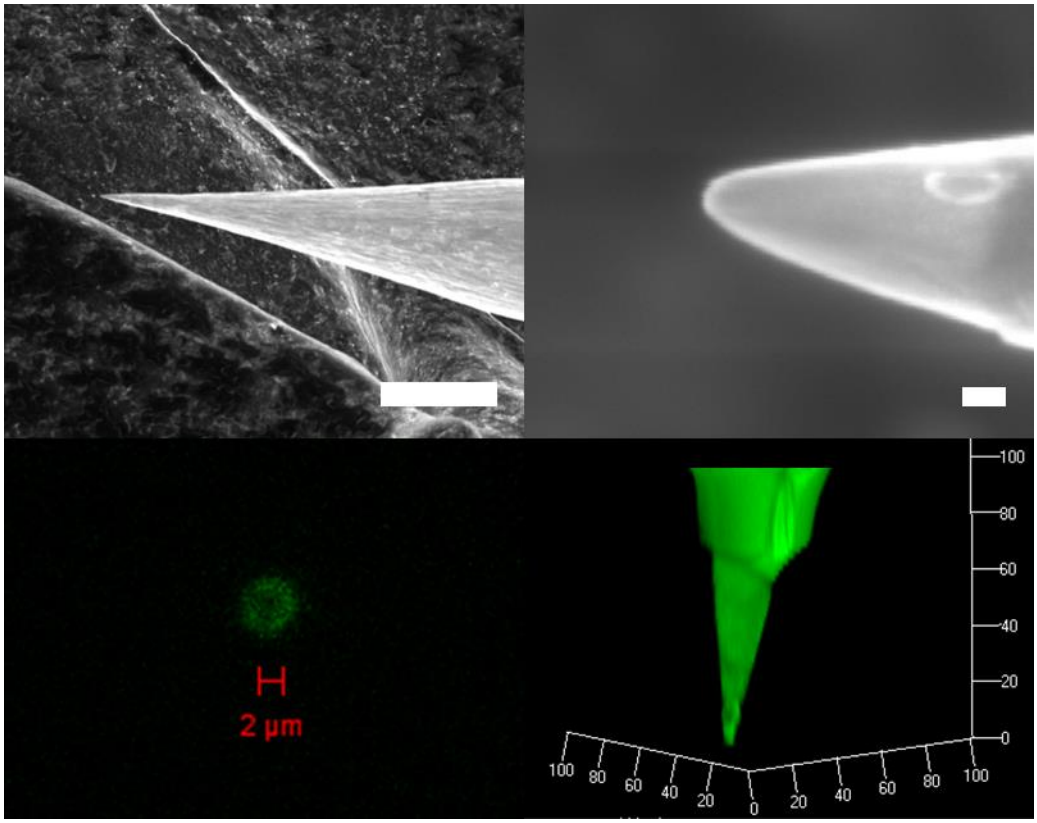

Figure 4.1. Top left: SEM image of the sharpened Pt tip (Scale bar: 20 µm) Top right: SEM image of sharpened tip (Scale bar: 100 nm) Bottom: Confocal imaging done of a nanopore filled with a fluorescein solution. Single plane at the pore opening shown on left and the 3D reconstruction shown on right (scale bar in µm).

Next the platinum tip is pulled back into the capillary using the tungsten rod. Then a hydrogen in air flame is used to melt the glass capillary around the sharpened platinum tip. The whole tip is not melted into the glass as to reduce the Pt etching

removal time. Next, the W rod is pushed into the capillary a little in order to reduce any strain on the Pt wire. Then a small amount of epoxy is placed around the W rod and open end of the capillary to hold the W rod in place. This is allowed to dry usually overnight.

Polishing is the most tedious and important step. Here, the melted end of the glass is carefully rubbed against grinding paper of increasing grit number until a smooth, flat, mirror-finish glass surface is achieved. Care needs to be taken to make sure that the length of the capillary stays as perpendicular to the polishing surface as possible. In fact, often the tip of the capillary would be polished in a figure eight pattern to ensure that even if the capillary is held at a small angle in one direction that the same angle is produced in the reverse direction in order to even out the polished surface. During this polishing the surface is frequently inspected under a microscope for both surface angle and smoothness. This surface is slowly polished until it approaches the tip of the Pt. As this happens since the glass surface is smooth it can reflect an image of the Pt tip if the whole assembly is held at the correct angle under a microscope. This allows for some feedback on how soon the Pt tip should be exposed. The Pt tip and its reflection should look like they are approaching each other as polishing continues. Once they appear close, a wet polishing pad with a small amount of polishing powder is used to remove a tiny amount of material each pass. Also, here a conductivity sensor is used in order to determine when the Pt has been exposed. One lead of the meter is placed under the pad on top of an insulating material. The other lead is hooked to the W rod. The polishing pad and powder are wet with a conductive solution (1M KCl), which allows for the resistance between the end of the capillary and the polishing pad to be sensed. Therefore, when the Pt wire is exposed the resistance drops and the conductivity meter can give a visual or

audio signal. The White group published the original conductivity meter design[27], however, Richard Bedell, (Electronics shop, Georgia Institute of Technology, School of Chemistry and Biochemistry) built and designed a similar unit in which the desired resistance level in could be tuned. Since the resistance is proportional the diameter of the Pt wire cross-section that is exposed and that circle represents the size of the nanopore, the polisher, in theory, can dial in the approximate relative resistance desired before polishing and polish until a light is seen and a beep is heard. Practically, however, the meter was set on the highest resistance in order to make the smallest pore. While polishing, it is important to wear gloves to insulate hands from the different surfaces, and the W rod should be touched to the polishing surface once in a while to make sure that the meter is still functional. This should give an immediate feedback since the resistance here is much lower than any of the threshold settings.

Once polishing is complete, the platinum can be etched (**Scheme 4.5**). A function generator is again used to etch the Pt out leaving a conical pore (**Scheme 4.6**). One lead is attached to a Pt electrode and the other is connected to the W rod of the polished Pt electrode. Then, the a ramp function is used from +3.0 to -2.9 V at 1 kHz. This can be left for up to a couple weeks depending on size of the Pt surface and therefore the size of the pore. Once the Pt has been etched out from where it was sealed in glass, the glass is scored with a file, broken, and the epoxy and W rod side of the capillary is removed. The glass capillary nanopore is immediately rinsed with water and placed into a small vial of water for storage until needed. A confocal 3D reconstruction of a pore is shown in **Figure 4.1**. The glass capillary was filled with fluorescein then cut down to be mounted pore side

down on an inverted microscope. Also pictured is the single plane confocal image taken at the pore opening.

4.3.3 Diagnostics

During fabrication of a nanopore there are two important diagnostics that can be performed. The first is to measure size of the Pt disc electrode that is created after polishing is finished. Here, the predictable redox chemistry of ferrocene is utilized. A 5 mM ferrocene solution with 0.1 M $TBAPF_6$ in acetonitrile was used with a Ag/AgCl counter electrode. One lead is connected to the Ag/AgCl electrode and one is connected to the W rod on the Pt disc electrode. Then a cyclic voltammagram (CV) is collected sweeping voltage from 0.2 to 0.7 V at 10 mV/s. This should produce a classic disc electrode CV with an oxidation and reduction at 0.4 V shown in **Figure 4.2**. The magnitude of this oxidation and reduction change is proportional to the size of disc electrode and can be calculated via **Equation 4.1**.

$$r = \frac{\Delta i}{4nFCD}$$

Equation 4.1. Calculation for radius of a disc electrode. n, F, C, and D are the number of electrons, Faraday's constant, ferrocene concentration, and ferrocene diffusion constant, respectively. Δi is the difference between the baseline and plateau of the CV.

The second diagnostic which is most important is sizing the actual nanopore after etching. This can be done by assessing the current flow through the pore using known ionic strength solutions. A high ionic strength solution (1 M KCl) is used to reduce the effects of any charge on the pore surface. Then current is passed through the pore by placing a Ag/AgCl electrode inside the capillary and outside the capillary with 1 M KCl solution in both. Then a voltage sweep was done from -0.1 V to +0.1 V and the current was monitored (**Figure 4.2**). These electrodes were fabricated by soaking a silver wire in a bleach solution for 15 or 20 min. To calculate pore diameter, **Equation 4.2** was used.

$$r_p = \frac{1}{\kappa R_p}\left(\frac{1}{tan\theta} + \frac{1}{4}\right)$$

Equation 4.2. Nanopore radius calculation. θ, R_p, and κ are the half-cone angle, pore resistance and solution conductivity, respectively. θ can be measured by SEM or optical microscopy.

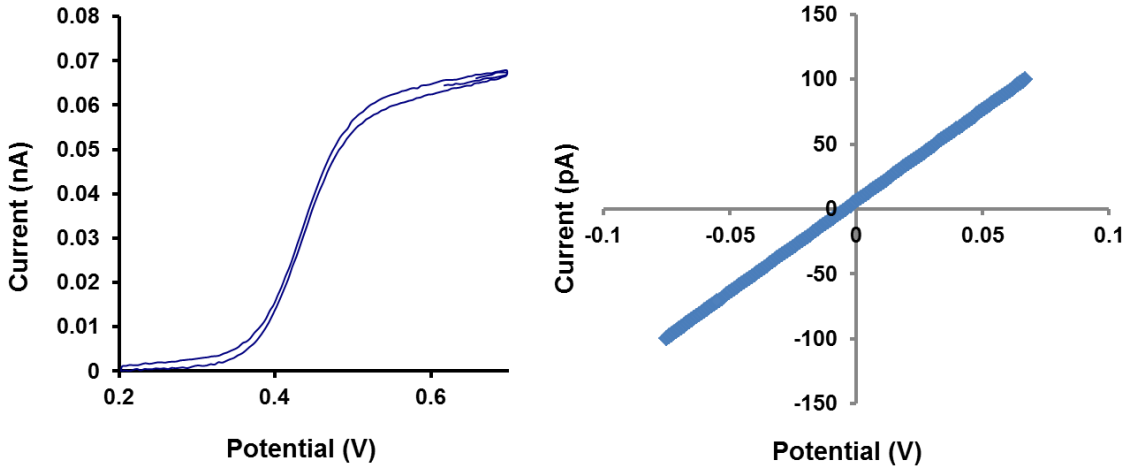

Figure 4.2. Example of the CV of ferrocene used to size the Pt. disc electrode (left) and the ion flux as a function of applied potential used to size the nanopore (right).

4.4 Summary

Resistive pulse techniques have been used nicely to count, size and identify different particles, cells, viruses, and proteins. In the coming chapter, efforts will be described using resistive pulse techniques to study the passage of microgels through glass nanopores that are smaller than their diameter. The mechanics of soft particles passing through small pores is an important characterization for use of these particles in biomedical applications.

4.5 References

[1] Coulter, W.H. Means for Counting Particles Suspended in Fluid. US2656508 **1953**.

[2] https://www.beckmancoulter.com/wsrportal/wsr/company/about-us/our-history/index.htm

[3] Bayley, H.; Braha, O.; Gu, L.Q. Stochastic Sensing with Protein Pores. *Advanced Materials* **2000**, *12*, 139-142.

[4] Deblois, R.W.; Bean, C.P. Counting and Sizing of Submicron Particles by Resistive Pulse Technique. *Review of Scientific Instruments* **1970**, *41*, 909-&.

[5] Deblois, R.W.; Bean, C.P.; Wesley, R.K.A. Electrokinetic Measurements with Submicron Particles and Pores by Resistive Pulse Technique. *Journal of Colloid and Interface Science* **1977**, *61*, 323-335.

[6] Deblois, R.W.; Mayyasi, S.A.; Schidlov.G; Wesley, R.; Wolff, J.S. Virus Counting and Analysis by Resistive Pulse (Coulter Counter) Technique. *Proceedings of the American Association for Cancer Research* **1974**, *15*, 104-104.

[7] Deblois, R.W.; Wesley, R.K.A. Sizes and Concentrations of Several Type-C Oncornaviruses and Bacteriophage-T2 by Resistive-Pulse Technique. *Journal of Virology* **1977**, *23*, 227-233.

[8] Gu, L.Q.; Braha, O.; Conlan, S.; Cheley, S.; Bayley, H. Stochastic Sensing of Organic Analytes by a Pore-Forming Protein Containing a Molecular Adapter. *Nature* **1999**, *398*, 686-690.

[9] Sanchez-Quesada, J.; Ghadiri, M.R.; Bayley, H.; Braha, O. Cyclic Peptides as Molecular Adapters for a Pore-Forming Protein. *Journal of the American Chemical Society* **2000**, *122*, 11757-11766.

[10] http://www.izon.com/

[11] Bayley, H.; Cremer, P.S. Stochastic Sensors Inspired by Biology. *Nature* **2001**, *413*, 226-230.

[12] Bayley, H.; Martin, C.R. Resistive-Pulse Sensing - from Microbes to Molecules. *Chemical Reviews* **2000**, *100*, 2575-2594.

[13] Deamer, D.W.; Branton, D. Characterization of Nucleic Acids by Nanopore Analysis. *Accounts of Chemical Research* **2002**, *35*, 817-825.

[14] Dekker, C. Solid-State Nanopores. *Nature Nanotechnology* **2007**, *2*, 209-215.

[15] Henriquez, R.R.; Ito, T.; Sun, L.; Crooks, R.M. The Resurgence of Coulter Counting for Analyzing Nanoscale Objects. *Analyst* **2004**, *129*, 478-482.

[16] Kozak, D.; Anderson, W.; Vogel, R.; Trau, M. Advances in Resistive Pulse Sensors: Devices Bridging the Void between Molecular and Microscopic Detection. *Nano Today* **2011**, *6*, 531-545.

[17] Stein, D. Nanopores - Molecular Ping-Pong. *Nature Nanotechnology* **2007**, *2*, 741-742.

[18] Wu, S.; Park, S.R.; Ling, X.S. Lithography-Free Formation of Nanopores in Plastic Membranes Using Laser Heating. *Nano Letters* **2006**, *6*, 2571-2576.

[19] Steinbock, L.J.; Stober, G.; Keyser, U.F. Sensing DNA-Coatings of Microparticles Using Micropipettes. *Biosensors & Bioelectronics* **2009**, *24*, 2423-2427.

[20] Ito, T.; Sun, L.; Bevan, M.A.; Crooks, R.M. Comparison of Nanoparticle Size and Electrophoretic Mobility Measurements Using a Carbon-Nanotube-Based Coulter Counter, Dynamic Light Scattering, Transmission Electron Microscopy, and Phase Analysis Light Scattering. *Langmuir* **2004**, *20*, 6940-6945.

[21] Ito, T.; Sun, L.; Crooks, R.M. Simultaneous Determination of the Size and Surface Charge of Individual Nanoparticles Using a Carbon Nanotube-Based Coulter Counter. *Anal. Chem.* **2003**, *75*, 2399-2406.

[22] Ito, T.; Sun, L.; Henriquez, R.R.; Crooks, R.M. A Carbon Nanotube-Based Coulter Nanoparticle Counter. *Accounts of Chemical Research* **2004**, *37*, 937-945.

[23] Sun, L.; Crooks, R.M. Single Carbon Nanotube Membranes: A Well-Defined Model for Studying Mass Transport through Nanoporous Materials. *Journal of the American Chemical Society* **2000**, *122*, 12340-12345.

[24] Garaj, S.; Hubbard, W.; Reina, A.; Kong, J.; Branton, D.; Golovchenko, J.A. Graphene as a Subnanometre Trans-Electrode Membrane. *Nature* **2010**, *467*, 190-U173.

[25] Vogel, R.; Willmott, G.; Kozak, D.; Roberts, G.S.; Anderson, W.; Groenewegen, L.; Glossop, B.; Barnett, A.; Turner, A.; Trau, M. Quantitative Sizing of Nano/Microparticles with a Tunable Elastomeric Pore Sensor. *Anal. Chem.* **2011**, *83*, 3499-3506.

[26] Zhang, H.P.; Chon, C.H.; Pan, X.X.; Li, D.Q. Methods for Counting Particles in Microfluidic Applications. *Microfluidics and Nanofluidics* **2009**, *7*, 739-749.

[27] Zhang, B.; Galusha, J.; Shiozawa, P.G.; Wang, G.L.; Bergren, A.J.; Jones, R.M.; White, R.J.; Ervin, E.N.; Cauley, C.C.; White, H.S. Bench-Top Method for Fabricating Glass-Sealed Nanodisk Electrodes, Glass Nanopore Electrodes, and Glass Nanopore Membranes of Controlled Size. *Anal. Chem.* **2007**, *79*, 4778-4787.

[28] Oja, S.M.; Wood, M.; Zhang, B. Nanoscale Electrochemistry. *Anal. Chem.* **2013**, *85*, 473-486.

[29] Li, J.; Stein, D.; McMullan, C.; Branton, D.; Aziz, M.J.; Golovchenko, J.A. Ion-Beam Sculpting at Nanometre Length Scales. *Nature* **2001**, *412*, 166-169.

[30] Li, J.L.; Gershow, M.; Stein, D.; Brandin, E.; Golovchenko, J.A. DNA Molecules and Configurations in a Solid-State Nanopore Microscope. *Nature Materials* **2003**, *2*, 611-615.

[31] Wei, R.; Pedone, D.; Zuerner, A.; Doeblinger, M.; Rant, U. Fabrication of Metallized Nanopores in Silicon Nitride Membranes for Single-Molecule Sensing. *Small* **2010**, *6*, 1406-1414.

[32] Wei, R.; Gatterdam, V.; Wieneke, R.; Tampe, R.; Rant, U. Stochastic Sensing of Proteins with Receptor-Modified Solid-State Nanopores. *Nature Nanotechnology* **2012**, *7*, 257-263.

[33] Li, N.C.; Yu, S.F.; Harrell, C.C.; Martin, C.R. Conical Nanopore Membranes. Preparation and Transport Properties. *Anal. Chem.* **2004**, *76*, 2025-2030.

[34] Sexton, L.T.; Mukaibo, H.; Katira, P.; Hess, H.; Sherrill, S.A.; Horne, L.P.; Martin, C.R. An Adsorption-Based Model for Pulse Duration in Resistive-Pulse Protein Sensing. *Journal of the American Chemical Society* **2010**, *132*, 6755-6763.

[35] Wharton, J.E.; Jin, P.; Sexton, L.T.; Horne, L.P.; Sherrill, S.A.; Mino, W.K.; Martin, C.R. A Method for Reproducibly Preparing Synthetic Nanopores for Resistive-Pulse Biosensors. *Small* **2007**, *3*, 1424-1430.

[36] Sa, N.; Fu, Y.; Baker, L.A. Reversible Cobalt Ion Binding to Imidazole-Modified Nanopipettes. *Anal. Chem.* **2010**, *82*, 9963-9966.

[37] Steinbock, L.J.; Otto, O.; Chimerel, C.; Gornall, J.; Keyser, U.F. Detecting DNA Folding with Nanocapillaries. *Nano Letters* **2010**, *10*, 2493-2497.

[38] Steinbock, L.J.; Otto, O.; Skarstam, D.R.; Jahn, S.; Chimerel, C.; Gornall, J.L.; Keyser, U.F. Probing DNA with Micro- and Nanocapillaries and Optical Tweezers. *Journal of Physics-Condensed Matter* **2010**, *22*.

[39] Zhang, B.; Wood, M.; Lee, H. A Silica Nanochannel and Its Applications in Sensing and Molecular Transport. *Anal. Chem.* **2009**, *81*, 5541-5548.

[40] Merchant, C.A.; Healy, K.; Wanunu, M.; Ray, V.; Peterman, N.; Bartel, J.; Fischbein, M.D.; Venta, K.; Luo, Z.; Johnson, A.T.C.; Drndic, M. DNA Translocation through Graphene Nanopores. *Nano Letters* **2010**, *10*, 2915-2921.

[41] Schneider, G.F.; Kowalczyk, S.W.; Calado, V.E.; Pandraud, G.; Zandbergen, H.W.; Vandersypen, L.M.K.; Dekker, C. DNA Translocation through Graphene Nanopores. *Nano Letters* **2010**, *10*, 3163-3167.

[42] Wells, D.B.; Belkin, M.; Comer, J.; Aksimentiev, A. Assessing Graphene Nanopores for Sequencing DNA. *Nano Letters* **2012**, *12*, 4117-4123.

[43] Sowerby, S.J.; Broom, M.F.; Petersen, G.B. Dynamically Resizable Nanometre-Scale Apertures for Molecular Sensing. *Sensors and Actuators B-Chemical* **2007**, *123*, 325-330.

[44] Willmott, G.R.; Moore, P.W. Reversible Mechanical Actuation of Elastomeric Nanopores. *Nanotechnology* **2008**, *19*.

[45] Willmott, G.R.; Parry, B.E.T. Resistive Pulse Asymmetry for Nanospheres Passing through Tunable Submicron Pores. *Journal of Applied Physics* **2011**, *109*.

[46] Willmott, G.R.; Platt, M.; Lee, G.U. Resistive Pulse Sensing of Magnetic Beads and Supraparticle Structures Using Tunable Pores. *Biomicrofluidics* **2012**, *6*.

[47] Willmott, G.R.; Vogel, R.; Yu, S.S.C.; Groenewegen, L.G.; Roberts, G.S.; Kozak, D.; Anderson, W.; Trau, M. Use of Tunable Nanopore Blockade Rates to Investigate Colloidal Dispersions. *Journal of Physics-Condensed Matter* **2010**, *22*.

[48] Wu, Y.; Benson, J.D.; Critser, J.K.; Almasri, M. Mems-Based Coulter Counter for Cell Counting and Sizing Using Multiple Electrodes. *Journal of Micromechanics and Microengineering* **2010**, *20*.

[49] Jagtiani, A.V.; Zhe, J.; Hu, J.; Carletta, J. Detection and Counting of Micro-Scale Particles and Pollen Using a Multi-Aperture Coulter Counter. *Measurement Science & Technology* **2006**, *17*, 1706-1714.

[50] Jagtiani, A.V.; Carletta, J.; Zhe, J. A Microfluidic Multichannel Resistive Pulse Sensor Using Frequency Division Multiplexing for High Throughput Counting of Micro Particles. *Journal of Micromechanics and Microengineering* **2011**, *21*.

[51] Zhe, J.; Jagtiani, A.; Dutta, P.; Hu, J.; Carletta, J. A Micromachined High Throughput Coulter Counter for Bioparticle Detection and Counting. *Journal of Micromechanics and Microengineering* **2007**, *17*, 304-313.

[52] Harms, Z.D.; Mogensen, K.B.; Nunes, P.S.; Zhou, K.; Hildenbrand, B.W.; Mitra, I.; Tan, Z.; Zlotnick, A.; Kutter, J.P.; Jacobson, S.C. Nanofluidic Devices with Two Pores in Series for Resistive-Pulse Sensing of Single Virus Capsids. *Anal. Chem.* **2011**, *83*, 9573-9578.

[53] Fraikin, J.-L.; Teesalu, T.; McKenney, C.M.; Ruoslahti, E.; Cleland, A.N. A High-Throughput Label-Free Nanoparticle Analyser. *Nature Nanotechnology* **2011**, *6*, 308-313.

[54] Saleh, O.A.; Sohn, L.L. Direct Detection of Antibody-Antigen Binding Using an on-Chip Artificial Pore. *Proceedings of the National Academy of Sciences of the United States of America* **2003**, *100*, 820-824.

[55] Carbonaro, A.; Mohanty, S.K.; Huang, H.; Godley, L.A.; Sohn, L.L. Cell Characterization Using a Protein-Functionalized Pore. *Lab on a Chip* **2008**, *8*, 1478-1485.

[56] Lan, W.-J.; Holden, D.A.; Liu, J.; White, H.S. Pressure-Driven Nanoparticle Transport across Glass Membranes Containing a Conical-Shaped Nanopore. *Journal of Physical Chemistry C* **2011**, *115*, 18445-18452.

[57] Holden, D.A.; Hendrickson, G.; Lyon, L.A.; White, H.S. Resistive Pulse Analysis of Microgel Deformation During Nanopore Translocation. *Journal of Physical Chemistry C* **2011**, *115*, 2999-3004.

[58] Holden, D.A.; Hendrickson, G.R.; Lan, W.-J.; Lyon, L.A.; White, H.S. Electrical Signature of the Deformation and Dehydration of Microgels During Translocation through Nanopores. *Soft Matter* **2011**, *7*, 8035-8040.

[59] Holden, D.A.; Watkins, J.J.; White, H.S. Resistive-Pulse Detection of Multilamellar Liposomes. *Langmuir* **2012**, *28*, 7572-7577.

[60] Song, L.Z.; Hobaugh, M.R.; Shustak, C.; Cheley, S.; Bayley, H.; Gouaux, J.E. Structure of Staphylococcal Alpha-Hemolysin, a Heptameric Transmembrane Pore. *Science* **1996**, *274*, 1859-1866.

[61] Akeson, M.; Branton, D.; Kasianowicz, J.J.; Brandin, E.; Deamer, D.W. Microsecond Time-Scale Discrimination among Polycytidylic Acid, Polyadenylic Acid, and Polyuridylic Acid as Homopolymers or as Segments within Single Rna Molecules. *Biophysical Journal* **1999**, *77*, 3227-3233.

[62] Henrickson, S.E.; Misakian, M.; Robertson, B.; Kasianowicz, J.J. Driven DNA Transport into an Asymmetric Nanometer-Scale Pore. *Physical Review Letters* **2000**, *85*, 3057-3060.

[63] Kasianowicz, J.J.; Brandin, E.; Branton, D.; Deamer, D.W. Characterization of Individual Polynucleotide Molecules Using a Membrane Channel. *Proceedings of the National Academy of Sciences of the United States of America* **1996**, *93*, 13770-13773.

[64] Meller, A.; Nivon, L.; Brandin, E.; Golovchenko, J.; Branton, D. Rapid Nanopore Discrimination between Single Polynucleotide Molecules. *Proceedings of the National Academy of Sciences of the United States of America* **2000**, *97*, 1079-1084.

[65] Vercoutere, W.; Winters-Hilt, S.; Olsen, H.; Deamer, D.; Haussler, D.; Akeson, M. Rapid Discrimination among Individual DNA Hairpin Molecules at Single-Nucleotide Resolution Using an Ion Channel. *Nature Biotechnology* **2001**, *19*, 248-252.

[66] White, R.J.; Ervin, E.N.; Yang, T.; Chen, X.; Daniel, S.; Cremer, P.S.; White, H.S. Single Ion-Channel Recordings Using Glass Nanopore Membranes. *Journal of the American Chemical Society* **2007**, *129*, 11766-11775.

[67] Ervin, E.N.; Kawano, R.; White, R.J.; White, H.S. Simultaneous Alternating and Direct Current Readout of Protein Ion Channel Blocking Events Using Glass Nanopore Membranes. *Anal. Chem.* **2008**, *80*, 2069-2076.

[68] Ervin, E.N.; White, R.J.; White, H.S. Sensitivity and Signal Complexity as a Function of the Number of Ion Channels in a Stochastic Sensor. *Anal. Chem.* **2009**, *81*, 533-537.

[69] Kawano, R.; Schibel, A.E.P.; Cauley, C.; White, H.S. Controlling the Translocation of Single-Stranded DNA through Alpha-Hemolysin Ion Channels Using Viscosity. *Langmuir* **2009**, *25*, 1233-1237.

[70] Schibel, A.E.P.; Edwards, T.; Kawano, R.; Lan, W.J.; White, H.S. Quartz Nanopore Membranes for Suspended Bilayer Ion Channel Recordings. *Anal. Chem.* **2010**, *82*, 7259-7266.

[71] Schibel, A.E.P.; Heider, E.C.; Harris, J.M.; White, H.S. Fluorescence Microscopy of the Pressure-Dependent Structure of Lipid Bilayers Suspended across Conical Nanopores. *Journal of the American Chemical Society* **2011**, *133*, 7810-7815.

[72] Schibel, A.E.P.; An, N.; Jin, Q.A.; Fleming, A.M.; Burrows, C.J.; White, H.S. Nanopore Detection of 8-Oxo-7,8-Dihydro-2 '-Deoxyguanosine in Immobilized Single-Stranded DNA Via Adduct Formation to the DNA Damage Site. *Journal of the American Chemical Society* **2010**, *132*, 17992-17995.

[73] Jin, Q.; Fleming, A.M.; Burrows, C.J.; White, H.S. Unzipping Kinetics of Duplex DNA Containing Oxidized Lesions in an Alpha-Hemolysin Nanopore. *Journal of the American Chemical Society* **2012**, *134*, 11006-11011.

[74] Schibel, A.E.P.; Fleming, A.M.; Jin, Q.; An, N.; Liu, J.; Blakemore, C.P.; White, H.S.; Burrows, C.J. Sequence-Specific Single-Molecule Analysis of 8-Oxo-7,8-Dihydroguanine Lesions in DNA Based on Unzipping Kinetics of

Complementary Probes in Ion Channel Recordings. *Journal of the American Chemical Society* **2011**, *133*, 14778-14784.

[75] An, N.; Fleming, A.M.; White, H.S.; Burrows, C.J. Crown Ether-Electrolyte Interactions Permit Nanopore Detection of Individual DNA Abasic Sites in Single Molecules. *Proceedings of the National Academy of Sciences of the United States of America* **2012**, *109*, 11504-11509.

[76] An, N.; White, H.S.; Burrows, C.J. Modulation of the Current Signatures of DNA Abasic Site Adducts in the Alpha-Hemolysin Ion Channel. *Chemical Communications* **2012**, *48*, 11410-11412.

[77] Hammerstein, A.F.; Jayasinghe, L.; Bayley, H. Subunit Dimers of Alpha-Hemolysin Expand the Engineering Toolbox for Protein Nanopores. *Journal of Biological Chemistry* **2011**, *286*, 14324-14334.

[78] Rincon-Restrepo, M.; Milthallova, E.; Bayley, H.; Maglia, G. Controlled Translocation of Individual DNA Molecules through Protein Nanopores with Engineered Molecular Brakes. *Nano Letters* **2011**, *11*, 746-750.

[79] Rotem, D.; Jayasinghe, L.; Salichou, M.; Bayley, H. Protein Detection by Nanopores Equipped with Aptamers. *Journal of the American Chemical Society* **2012**, *134*, 2781-2787.

[80] Stoddart, D.; Heron, A.J.; Klingelhoefer, J.; Mikhailova, E.; Maglia, G.; Bayley, H. Nucleobase Recognition in Ssdna at the Central Constriction of the Alpha-Hemolysin Pore. *Nano Letters* **2010**, *10*, 3633-3637.

[81] Melmed, A.J. The Art and Science and Other Aspects of Making Sharp Tips. *Journal of Vacuum Science & Technology B* **1991**, *9*, 601-608.

CHAPTER 5

RESISTIVE PULSE ANALYSIS OF MICROGEL PASSAGE THROUGH A NANOPORE

Adapted from:

Holden, D.A.;Hendrickson, G.;Lyon, L.A.;White, H.S. Resistive Pulse Analysis of Microgel Deformation During Nanopore Translocation. J. Phys. Chem. C 2011, 115, 2999-3004.

Holden, D.A.;Hendrickson, G.R.;Lan, W.J.;Lyon, L.A.;White, H.S. Electrical Signature of the Deformation and Dehydration of Microgels During Translocation through Nanopores. Soft Matter 2011, 7, 8035-8040.

5.1 Introduction

The work presented in this chapter is written based on research that was performed in collaboration with the White group at the University of Utah, which resulted in two publications.[1,2] Most of the experiments and data were performed and collected in the White labrotory; however, the conception of experiments, data interpretations, and synthesis and characterization of the polymeric materials were in large part our contribution.

Investigations into synthetic biomaterials for applications such as drug delivery, bioimaging, and tissue enginneeing have led to the construction of different design rules for these materials.[3,4] The most common design rules encompass size, shape, topology, charge, and mechanics. These design rules are formed by studying the effects of each of the design rules on properties such as circulation, cellular uptake, biological clearance, payload retention and delivery, and toxcicity. Until recently, the effects of the mechanical properties of the material had not been extensively studied. For 2- and 3- dimensional cellular substrates, studies have been

performed on the effects of their rigidity on cellular processes such as mechanotransduction, differentiation, adhesion, and proliferation.[5-9] Likewise for nanoparticulate biomaterials, the effects of material mechanics on phagocytosis or endocytosis have been studied.[10,11] A much more heavily investigated design rule for particles in particular has been size.[12-15] The size requirements for many different biological processes involved in biomaterial drug delivery have been extensively characterized as shown in **Scheme 5.1**.[3] For example, it has been shown for renal clearance of rigid quantum dots, the size limits are close to the 8 nm pores defined by endothelial gaps in the kidneys.[16] However, all of these sizes assume a rigid particle; the size design rules might be much different for a soft particle. The mechanical flexibility of a nanoparticle could allow particles that do not fit the currently accepted size restrictions for biological tight junctions to actually deform and squeeze though them. One of the smallest juctions is in the kidneys and is utilized for renal filtration, and since renal clearance is an advantagous clearance mechanism for a nanoparticle biomaterials it is of particluar interest.

As shown in **Chapter 3**, we have studied the passage of soft particles though track-etch membranes 10-fold smaller than the size of the particles in dilute solution.[17] In those studies, the soft, conformable particles were NIPAm-AAc microgels cross-linked by BIS. The particles were forced through the cylindrical track-etch pores under modest pressure differentials similar to those present in the kidney durring renal filtration (40-80 mmHg).[18-22] The experiments were perfomed with large (~1 μm) microgels passing through 100 nm pores as well as small (~100 nm) microgels passing through 10 nm pores. In the case of the small microgels, the 10

nm pores are close to the size of the pores in the kidneys (~8 nm), and the particles are similar to the nanogels our group has studied as siRNA drug delivery vehicles.[23-25] Although, these experiments are encouraging and provide insight into the flexibility of these microgels, they do not provide detailed information on the passage mechanism of a single particles.

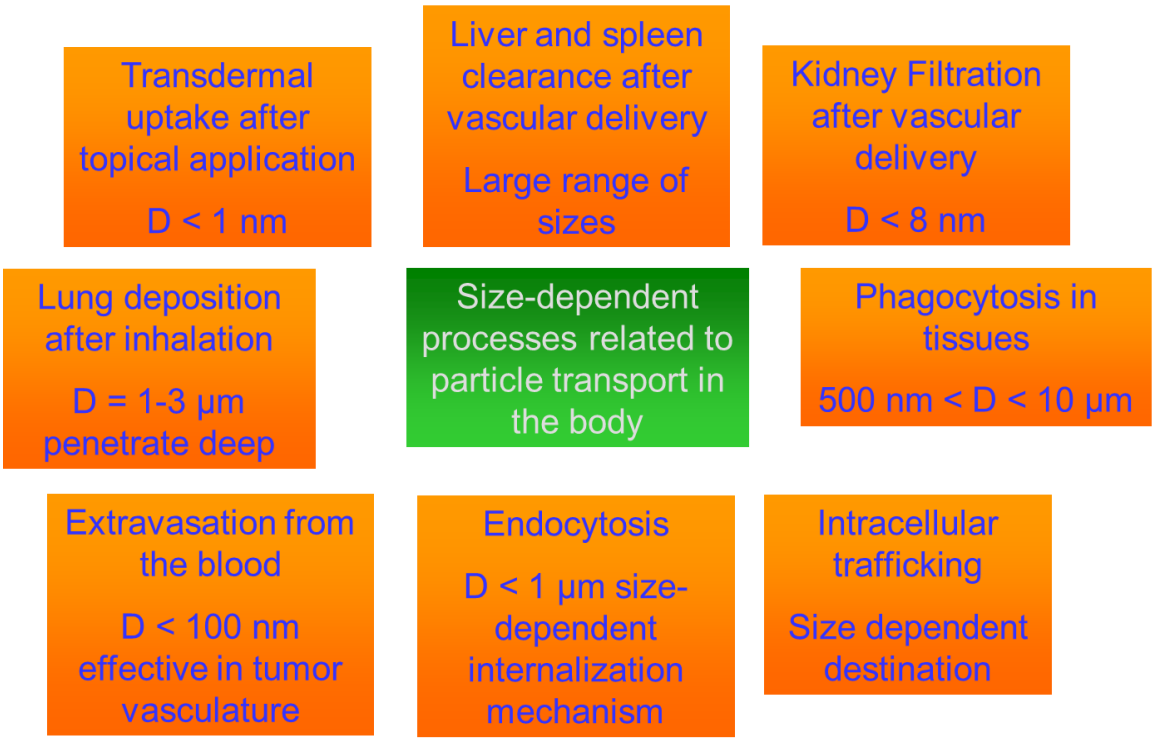

Scheme 5.1. Size restrictions in biological processes involved in drug delivery. Adapted from reference.[3]

To gain information about the passage of these particles through single pores, the resistive pulse analysis technique was applied to microgel passage through glass nanopores.[1,2] As described in detail in **Chapter 4**, resistive pulse analysis involves measuring the change ionic current as an object interferes with the current passing through a pore separating two electrolyte solutions.[26] This technique has been applied to "hard"particles like polystyrene or gold particles,[27-35] cells,[36-38] viruses,[30,39-43] and

biological molecules like protiens and nucleic acids.[44-50] For "solid" particles, cells, and viruses this technique has been used to count, size, and identify the analyte in simple and complex mixtures. In the cases of biomolecules, attempts to study binding to pore supported ligands, protien or nucleic acid folding, and even DNA sequencing have been made. Here, we studied the translocation, deformation, and dehydration of the microgels through nanopores. The particular pores used here are conical glass nanopores formed in the end of a glass capillary.[51]

5.2 Experimental

5.2.1 Materials

Materials for hydrogel microparticle (microgel) synthesis are the same as in **Chapter 3.** Buffers and electrolye solutions were made from KCl, K_2HPO_4, and KH_2PO_4 (Mallinckrodt Chemicals). Materials for nanopore fabrication include Pt wire (99.95% purity; 25 μm diameter; Alfa Aesar), tungsten rods (0.010 in diameter; 3 in in length; FHC, Inc), glass capillaries (1.65 mm O.D.; 0.75 mm I.D.; softening point 700 °C; composition 67.7% SiO2, 2.8% BaO, 15.6% Na2O, 5.6% CaO, 4% MgO, 1.5% B, and 0.6% K2O%; Dagan Corporation (SB16)), and Ag paint (FHC, Inc). All water used in experiments is DI water run through a Barstead Nanopure filtration system until the resistance is 18 MΩ.

5.2.2 Microgel Synthesis

Large microgels were synthesized by precipitation polymerization of NIPAm, BIS (1 mol %), and AAc (10 mol%) with a total monomer concentration of 100 mM in 100 mL. All components were dissolved in distilled, deionized water and stirred under a

nitrogen purge while heating to 68 °C. Then APS (0.01 mM) was added to initiate the reaction. The reaction was allowed to stir under nitrogen at 68 °C overnight. All particle solutions were filtered and purified via centrifugation. The samples were then freeze-dried for storage and then re-dispersed into desired concentrations. Dynamic light scattering (DLS) was used to determine the hydrodynamic radius (R_h) under different pH conditions.[52,53] This was done with a Wyatt Technologies DynaPro plate reader DLS using a laser wavelength of 830 nm. Scattering intensity fluctuations were detected for 10 s per reading by an avalanche photodiode at and angle of 158° (back scattering) from the incident laser. Dynamics software (Wyatt Technologies Corp.) was used to calculate and fit an autocorrelation function plotted from the random fluctuations in scattering intensity. These fits of the autocorrelation functions were used to calculate the diffusion coefficients and then through the Stokes-Einstein equation, the R_h. The plate reader DLS provided the opportunity to use small volumes (50 μL) of particle solution and to run different aliquots in series without further sample preparation. Zeta potential measurements were carried out in 5 mM ionic strength HEPES (pH 7.4) and formate (3.0) buffers by electrophoretic light scattering with a Malvern Instruments Zetasizer.

5.2.3 Nanopore Fabrication

Section 4.3 describes the nanopore fabrication in great detail and was adapted from the original steps published previously.[51] In general, the tip of an electrochemically sharpened Pt wire was placed in the center of a glass capillary. The glass was melted over the tip and the melted end of the glass capillary was polished until the tip of the Pt wire was exposed creating a Pt disc electrode. Lastly, the Pt was etched out of the glass leaving behind a conical glass nanopore.

5.2.4 Experimental Setup-Translocation Experiments

Scheme 5.2 shows the experimental setup for all translocation experiments. Here, a Ag/AgCl electrode was placed in the solution outside and inside the capillary. A +0.1 V bias was applied between the two electrodes and the current was monitored by a Dagan Chem-Clamp voltammeter/amperometer with a high-sensitivity preamplifier (0.05 to 10 nA/V) and filtered with a 10 kHz 3-pole low-pass Bessel Filter. A BNC 2120 board (National Instruments) and a PCI 6251 DAQ card (National Instruments) were used to interface with a PC and data was collected on in-house LabView virtual instrumentation. The glass nanopore capillary was held by a special pressure tight adapter supplied by Dagan Corporation in which pressure could be controlled by an external gas tight syringe. This pressure differential was used to drive particles in and out of the pore.

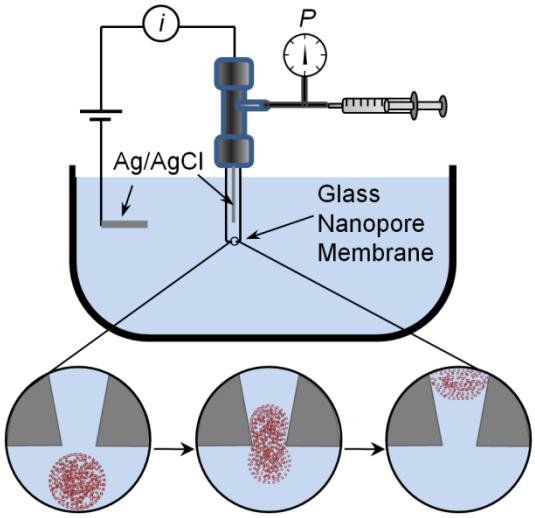

Scheme 5.2. Scheme of the glass nanopore setup and passage of a microgel particle. The glass nanopore membrane has a single pore separating two electrolyte solutions inside and outside of the capillary.[1]

5.3 Results and Discussion

Translocation of single microgels through a single pore was studied using the experimental setup shown in **Scheme 5.2**. A current flow was induced through a single conical pore formed in a glass membrane by placing a Ag/AgCl electrode in an electrolyte solution on either side of the pore and placing an electrical bias between the electrodes. The current flow was then interrupted by the passage of microgels through the pore as shown in **Figure 5.1**. These particles were driven through the pore using a gas-tight syringe to create a pressure differential between the inside of the capillary and the outside of the capillary. The microgels used here were NIPAm-AAc microgels that at pH 7 were negatively charged. The charged particles could be electrophoreticlly driven to the pore, but could not be pushed through the pore. Therefore, all experiments were performed under a pressure driven flow and the sign of the applied voltage did not affect microgel translocation.

The microgels studied were synthesized as described above, and were determined to be 570 nm in radius by DLS. As mentioned above these particles do contain acid moieties and therefore exhibit a pH-dependent ζ-potential. At pH 7 these particles have a -20.5 mV potential and at pH 3 they have a -4.1 mV potential. Although, the ζ-potential for microgel particles can be used as a relative measure of charge, since the particles have an ill-defined surface the absolute numbers may not be easily compared to other particle types. For microgels, both surface and buried charges could affect electrophoretic mobility. Since, all of the translocation studies were performed in a pH 7 buffered solutions particles were fully charged and swollen with charge balancing ions making the particle conductivity significant.

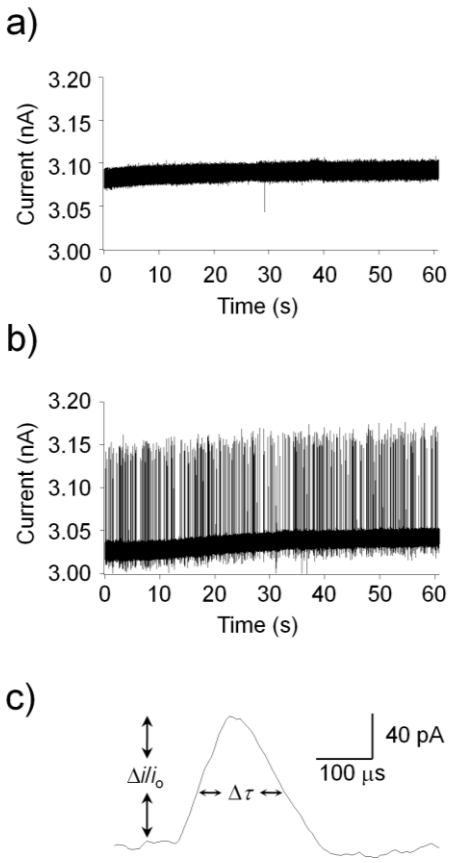

Figure 5.1. a) open pore current of a 433 nm radius pore b) pulses created by 570 nm microgels (0.001 wt%) pushed through the pore under a -50 mmHg (inside vs. outside) pressure differential c) Single translocation pulse showing the translocation time, Δτ, and relative difference in current intensity, Δi/i. Solutions were buffered 10 mM KCl solutions and applied voltage was +0.1 V (internal vs. external).[1]

As a microgel passes through the nanopore electrolyte solution is displaced and a change in current is detected. This change in current creates a pulse in the *i-t* plots as shown in **Figure 5.1**. From these plots, quantities such as the translocation time (Δτ) and the current change magnitude ($\Delta i/i_o$) can be measured for each pulse. Here, the pore was 433 nm in radius and the 570 nm radius microgel is passed through the pore under a modest pressure of 50 mmHg with a 0.001 wt% microgel concentration. Different from most RPA experiments, the microgels, increase the current as they pass through which suggests that the ion flux as the particle deforms through the pore increases as the particle

expels some ions. As observed in **Figure 5.1a**, an occasional baseline drift will be observed due to small changes in pressure.

In all cases, experiments were performed with particles starting only on the outside of the pore and then pulled into the pore. In order to verify that the observed signals were indeed particle passage events experiments were performed where the pressure differential was reversed to drive the captured particles back out of the pore (**Figure 5.2**). Here, events were observed for particles pulled into and then pushed back out of the pore suggesting complete particle translocation. This was observed for all pores greater than 375 nm in radius at 50 mmHg pressure differentials. In cases where the particles would not pass through the pores they might be "captured" in the pore and then dislodged by reversing the pressure as shown in **Figure 5.3**.

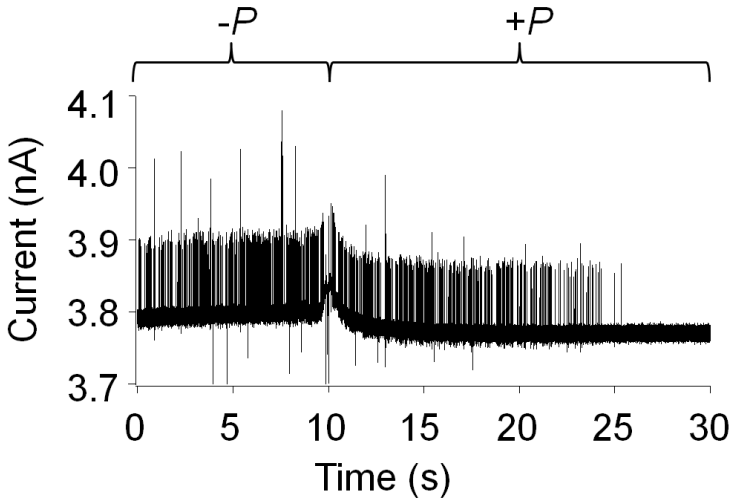

Figure 5.2. Current vs. time trace of microgel passage (570 nm radius, 0.001 wt%) through a 466 nm radius pore in a buffered 10 mM KCl solution when pressure was first applied to pull the particles into the pore (-50 mmHg (internal vs. external)) and then back out of the pore (+50 mmHg (internal vs. external)). Applied voltage was +0.1 V applied (internal vs. external).[1]

Passage events were analyzed for pores ranging from 73 nm to 915 nm in radius. For the pores greater than 700 nm in radius, particle passage events produced weak current changes due to the much larger sensing zone and could not be analyzed. Also, for pressure differentials of -50 mmHg (internal vs. external), passage events were not observed for pores smaller than 375 nm. However, for pores between 375 nm and 700 nm passage event rate increases as the pore size gets larger (**Figure 5.4**). Although, the event rate does increase as a third power to the radius, which agrees with the volumetric flow rate dependence on radius, it is a much lower event rate than expected. This is likely due to the Coulombic repulsion between the negatively charged glass pore and the negatively charged particle, as well as the fact that the particle has to deform to fit through the pore.

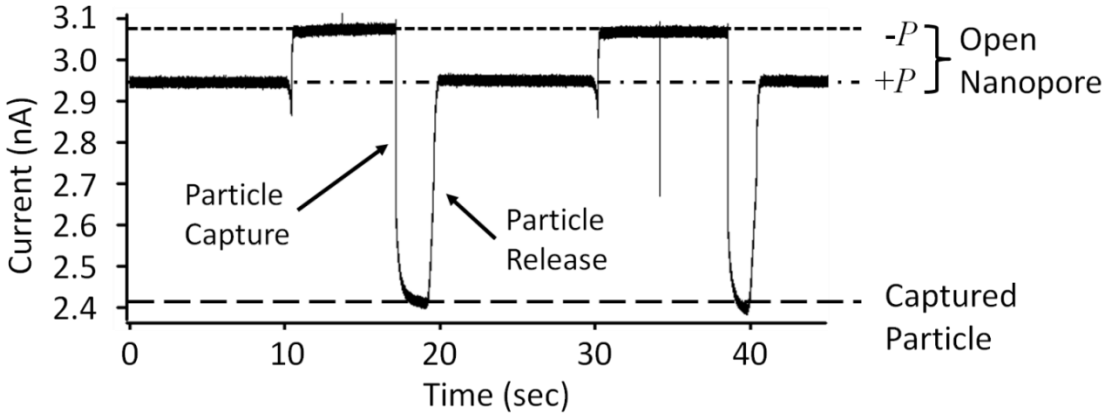

Figure 5.3. Example of an *i-t* trace where the pore (358 nm radius) was too small for the pressure (-50 mmHg (inside vs. outside)) being applied to force the particle through and therefore the particle was "captured" and then forced out again by reversing the pressure (+50 mmHg (inside vs. outside)). Applied voltage = +0.1 V. Particle solutions were in a buffered 10 mM KCl solution.[1]

In order to further characterize the ionic strength dependence, experiments were performed using solutions ranging from 10 mM KCl to 130 mM KCl using a constant pressure differential (-50 mmHg) and pore size (433 nm) (**Figure 5.5**). It was found that the magnitude of the current change decreased as the salt concentration increased until at

around 50 mM where passage events were not detected. Then, as the salt concentration increases further, the current sign was reversed and the current started decreasing as particles passed through the pore. This observation further reinforced the thought that the pulse is due to the release of the ions carried by the particle during translocation. If a line is fit to the data, the point at which the pulse height is zero is at 48 mM KCl which should have conductivity close to that of the microgel itself.

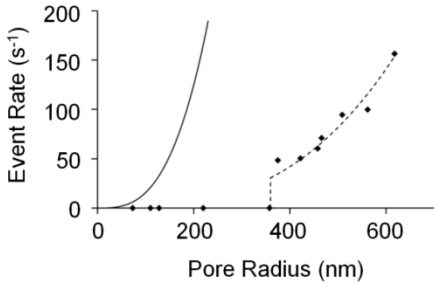

Figure 5.4. Event rates vs. pore size for passage experiments with 570 nm microgels at an applied voltage and pressure of +0.1 V and -50 mmHg, respectively. Experiments performed in buffered solutions of 10 mM KCl with 0.001 wt% microgel. Solid line is analytical theory on pressure driven translocation. Dashed line is analytical theory multiplied by a best fit constant (0.0418).[1]

Also shown in **Figure 5.5,** the translocation times decrease as salt concentration increases which is probably due to a combination of three factors. First, at higher salt concentrations these particles slightly deswell due to increased screening of charges within a microgel making the required deformation for passage smaller. Second, the increased salt concentration helps screen charges on the glass nanopore from the particle thereby increasing the speed of translocation. Lastly, due to the screening of charges within a particle, there is a lower barrier to deformation of the particle. It should be noted that the convergence to a single translocation time is due to the fact that passage times

faster than ~ 50 μs could not be observed due to the 10 kHz low-pass filter on the instrumentation.

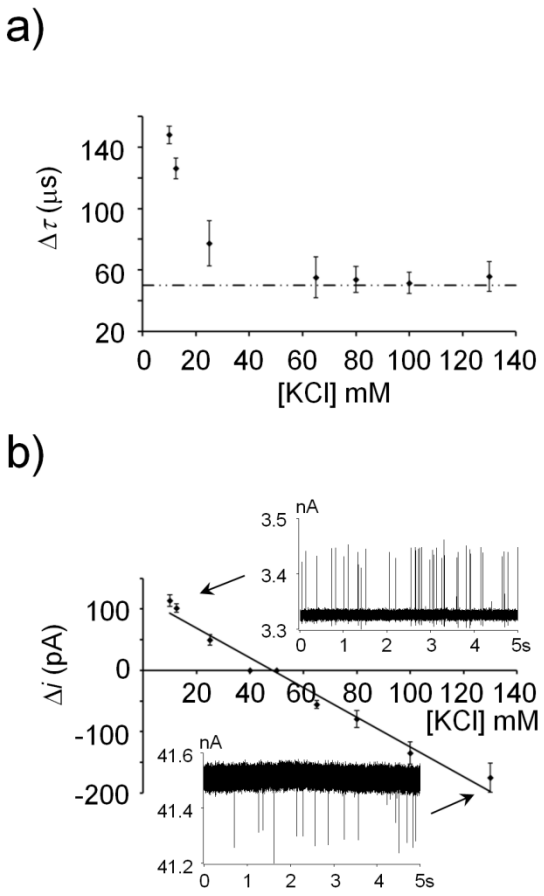

Figure 5.5. a) Translocation times and b) peak heights for 570 nm microgels translocation events at an applied voltage and pressure of +0.1 V and -50 mmHg, respectively. Pore radius was 433 nm. Experiments performed in buffered KCl solutions of different salt concentrations with 0.001 wt% microgel concentration. Dashed line in a) is the electronic limitation due to a low-pass filter. Solid line in b) is a best-fit line. Insets in b) are examples of positive and negative pulses as a result of translocation.[1]

Most of the pulses in these experiments are very uniform most likely due to the monodispersity of the particles; however, in some cases, there are a small number of variable peak heights (**Figure 5.2**). A Poisson statistical analysis was performed to

determine if these peaks were due to simultaneous single particle events or due to a particle aggregate. The method used has been described by Davis.[54] This treatment will give the probability of uncorrelated particle translocation events, λ, that occur over a given time, T. The expected number of events, *m* is given by **Equation 5.1**.

Equation 5.1. $$m = \lambda T$$

Since these events are stochastic, there is a finite probability that multiple events would overlap and appear as a single event. Therefore, the actual number of events might be higher than observed. The probability of multiple component events is determined by counting the observed events over time T. Then, if dt is defined as the time between the midpoint of events it follows that **Equation 5.2** defines the probability that dt is greater than the time needed to resolve events, t_o.

Equation 5.2. $$p(\mathrm{dt} > t_o) = \exp(-\lambda t_o)$$

If next the p is multiplied by the expected number of events, *m*, to give the number (N) of time intervals between observed events in which dt $>$ t_o. Then substitute mT for λ, rearrange, and **Equation 5.3** results.

Equation 5.3 $$\ln(N) = \ln(m) - m(\frac{t_o}{T})$$

Figure 5.6 shows a plot of ln(N) vs. t_o/T using data from **Figure 5.1b** where T = 60.85 s. Here, the expected number of events, *m*, can be calculated by both the slope (-*m*) and the intercept (ln(*m*)) which yield 427 and 431, respectively matching closely the actual number of events, 443. Now, **Equation 5.4** represents the probability that a single event represents more than one particle translocation.

Equation 5.4. $$N_n = \exp(-2mt_o/T)\left[1 - \exp(-mt_o/T)\right]^{(n-1)}$$

Using this equation for analysis of the same data set as above gives a probability of 99.6 % of any pulse being a single particle translocation event or the probability of a double or triple event is 2.1 x 10^{-3} or 4.4 x 10^{-6}, respectively. Since these events have prohibitively small probabilities, it is likely that any unusually high peak heights are due to actual particle aggregates, but most events are single particle translocations.

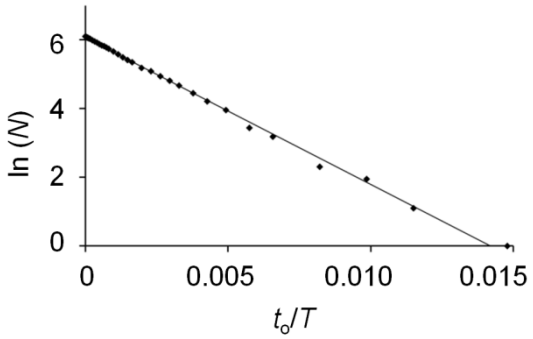

Figure 5.6. Plot of ln(N) vs. t_o/T for data in **Figure 5.1b** T = 60.85 s with 443 total translocation events. The line is a linear regression fit to data.[1]

Figure 5.7 shows a cluster plot of Δi/i and Δτ for microgels passing through a 375 nm, 509 nm, and 618 nm pores. As shown, the events are relatively monodisperse in change in current and translocation time. In particular, the distribution of Δi/i is around ~15 % which does correlate nicely to the expected polydispersity of these particles of ~10% by DLS. Also, the expected trends of smaller pores resulting in longer translocation times as well as larger of Δi/i are observed as well. The longer times are expected due to the larger deformation that must take place in order for a particle to pass through the smaller pore. The Δτ were 89 ± 17, 98 ± 11, and 117 ± 13 μs for the 618 nm, 509, and 375 nm pores, respectively. As far as the increase in current change, when the particle is larger in relation to the pore size the more of the sensing zone is occupied resulting in the larger current changes.

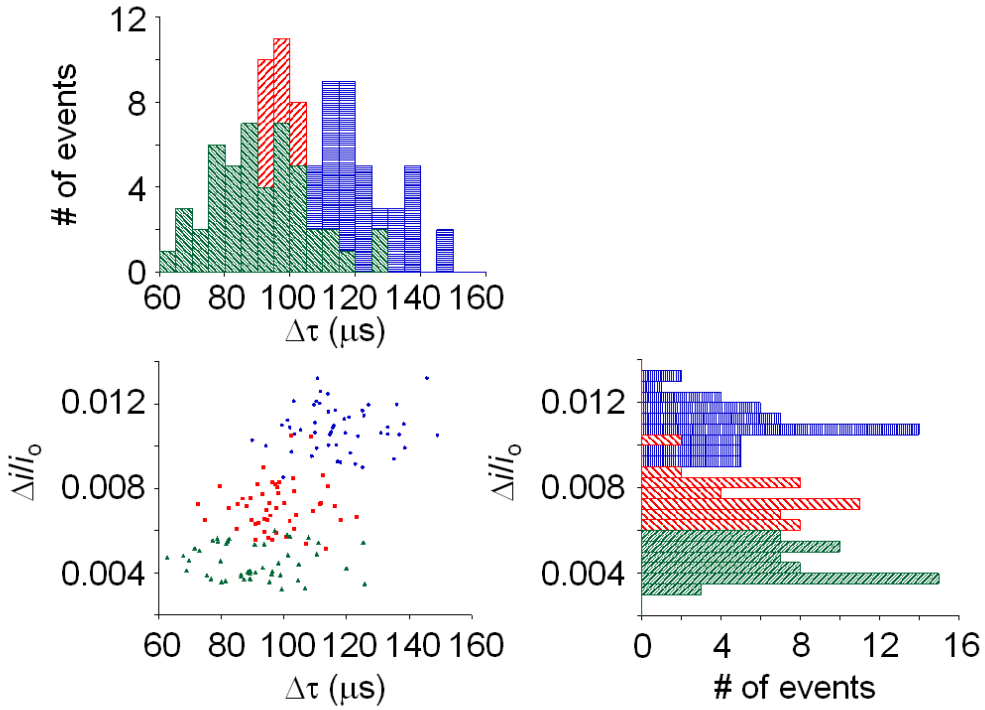

Figure 5.7. Distributions of translocation times, Δτ, and relative intensity changes, Δi/i for 570 nm microgel passage through 375 nm (blue), 509 nm (red), and 618 nm (green) pores. (N = 50 events for each measurement) Cluster plot represents individual events. Experiments have applied voltage of +0.1 V, and applied pressure of -50 mmHg, and were performed in buffered 10 mM KCl solutions with a 0.001 wt% microgel concentration.[1]

Up to now the particles have been studied at a single pressure, which correlates nicely to the experimental pressure in **Chapter 3** and the biological pressure differentials in the kidneys. It was found that at these pressures in the nanopore experiments, the particles were to pass through pores that were about 65% smaller than there dilute solution size as opposed to 10% of their size as observed in the experiments in **Chapter 3**. However, the charge repulsion between the glass nanopores and negatively charged microgel particles is a significant difference in the two experimental conditions. In the cases of the track etch membranes the pores were not charged. In the case of the kidneys

there is a slight negative charge, but the magnitude compared to the glass pore is unknown.

Now that RPA using glass nanopores and microgels has been performed at small pressure differentials, we wanted to observe what would happen if we varied the pressures. Similar experiments can be performed, only now when current blockages occur at small pressure differentials with smaller pores, they actually can pass if the pressure differential is increased. As shown in **Figure 5.8,** the same 570 nm microgels block a 302 nm glass pore as expected from the results above, however, if the pressure differential is increased from 50 to 150 mmHg the particles can now pass. Now similarly to before, the passage conditions for different pore radius to microgel radius ($R_{pore}/R_{\mu gel}$) can be measured only now the pressure was varied in order to determine the absolute limits of passage. **Figure 5.9** shows a representative plot of event rates vs. applied pressure differentials for 5 different pore to particle size ratios. As is expected from previous experiments for pores less than about 60% the size of the microgel it takes more pressure to force them through the pore. Similar to before, once particles start passing through pores, the event rate increases slower than would be expected based on the volumetric flow rate. This effect is probably due to the negatively charged particle having to squeeze through the smaller pore.

From these plots, a minimum pressure can be determined to pass the particles through a particular $R_{pore}/R_{\mu gel}$ (**Figure 5.10**). Here, passage events can be seen at pore radii down to approximately ~40% of the size of the pore under greater pressures. Then the slope of event rate vs. pressure differential are plotted vs. $R_{pore}/R_{\mu gel}$. It is shown that the slopes are considerably lower than the volumetric flow rate.

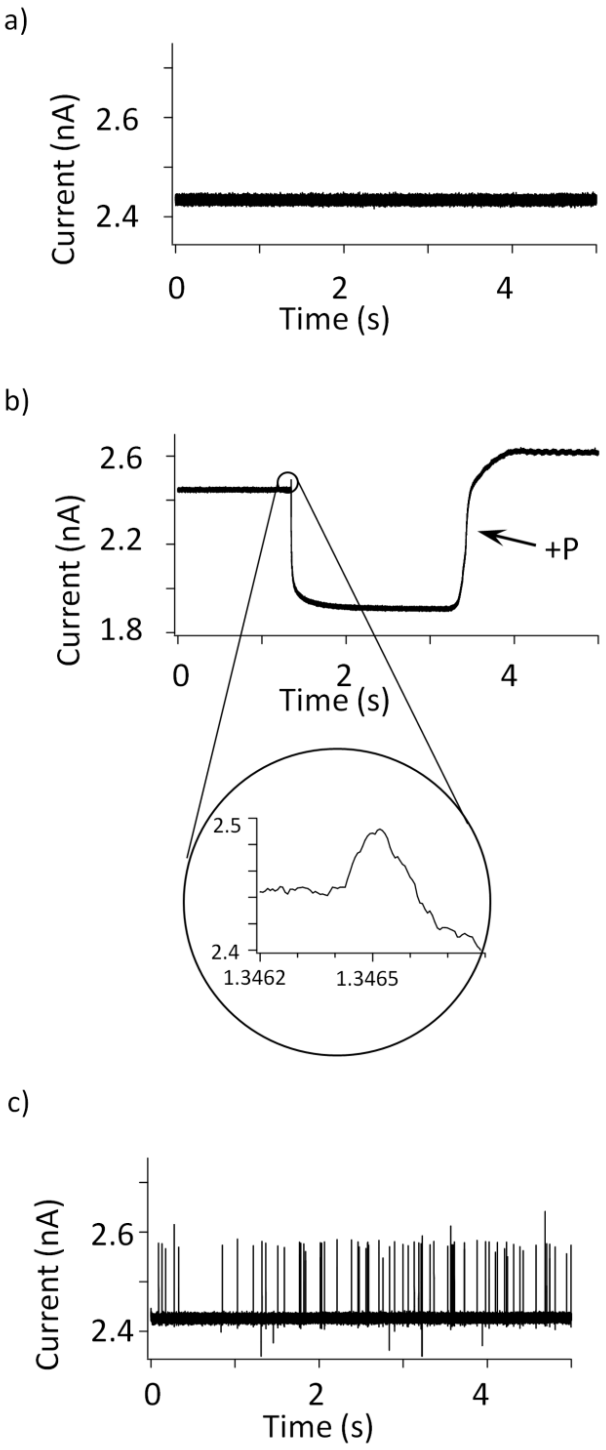

Figure 5.8. a) open pore current of a 302 nm radius pore b) blockage created by 570 nm microgels (0.00025 wt%) pushed through the pore under a -50 mmHg (inside vs. outside) pressure differential. Inset is the small typical current increase as the particle enters the pore just before the large decrease due to clogging the pore. c) Translocation events after increasing the pressure differential to -150 mmHg. All buffered 10 mM KCl solutions. All experiments have an applied voltage of +0.1 V (internal vs. external).[2]

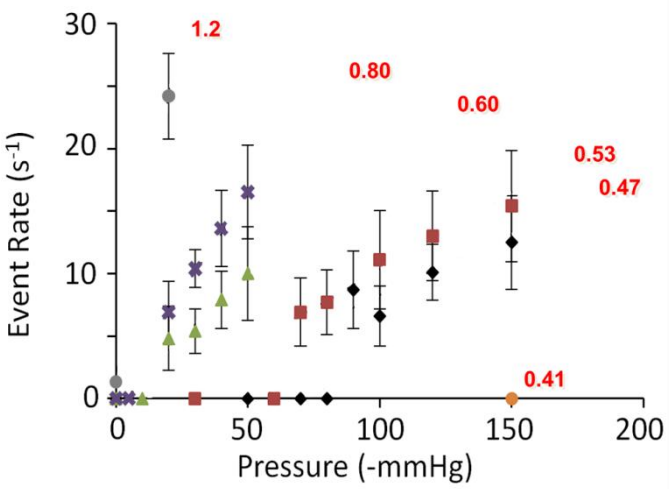

Figure 5.9. Event rates vs. pressure for passage experiments with 570 nm microgels at different pore radius to microgel radius ratios ($R_{pore}/R_{\mu gel}$) (●, 1.2); (x, 0.8); (▲, 0.6); (■ , 0.53); and (♦, 0.47). Applied voltage of +0.1 V. All experiments in buffered solutions of 10 mM KCl with 0.00025 wt% microgel.[2]

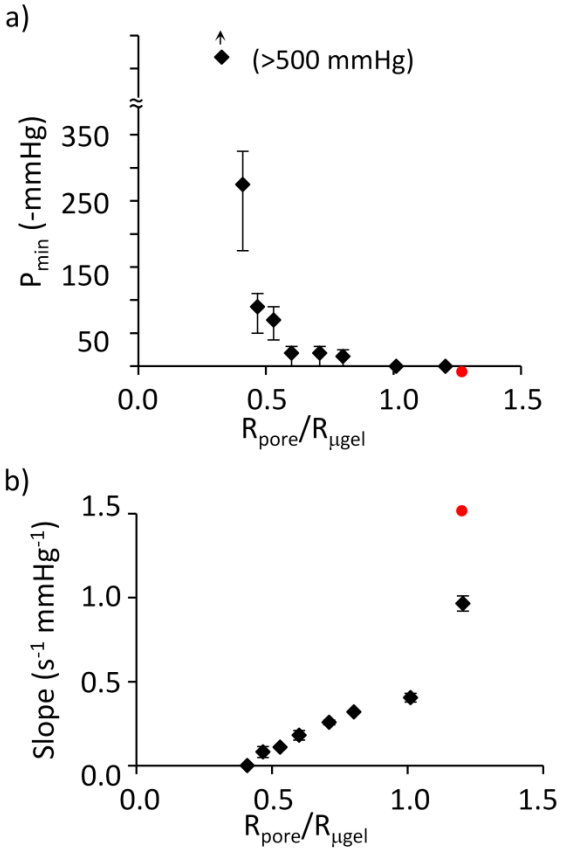

Figure 5.10. a) Minimum pressure, P_{min} to observe translocation for various $R_{pore}/R_{\mu gel}$. b) Slopes of the linear best fit lines to data in **Figure 5.9** vs. $R_{pore}/R_{\mu gel}$. Red dots in both a) and b) correspond to expected values for $R_{pore}/R_{\mu gel}$ = 1.2 based on volumetric flow rate.[2]

Another interesting aspect to these experiments with carefully controlled $R_{pore}/R_{\mu gel}$ and pressure is to inspect the transient shapes. As shown in **Figure 5.11**, the peak shapes for events occurring at certain $R_{pore}/R_{\mu gel}$ and pressures vary significantly. These shapes potentially give insight into the mechanism of particle passage. When the pressure is varied with the same solution salt concentration and pore size the peak shape goes from a narrow single increasing current peak at high pressure to a wide peak that increases and then decreases bellow baseline at smaller pressures. At high pressure, the particle deforms through the pore creating an increasing current at these low ionic strengths due to the ion content. As the pressure differential decreases, the particle no longer has the force to purely deform and pass through the pore elastically, but now must pass viscoelasticlly by draining some of the solvent and deswelling. This deswelling is evidenced by the decrease in current in the middle of the transient due to draining of ions and solvent. In the intermediate pressure cases, the particle then quickly re-swells giving the transient 2 maxima; however, when the pressure is sufficiently low the particle drains enough solvent and ions to dip below the baseline current and then as it passes it merely recovers to baseline current levels. A similar effect is observed if the pressure is kept constant and the size of the pores is changed. It should be noted that the deswelling kinetics suggest that the observed translocation times (< 2ms) are on the same order as the transient times seen here for the longer translocations.[55,56] Also, **Equation 5.5** published by Matsuo and Tanaka, defines the network relaxation time, $\boldsymbol{\tau}$.[57]

Equation 5.5. $$\boldsymbol{\tau} = \frac{R^2}{\pi^2 D_c}$$

Here, R^2 is the radius of the gel and D_c is the so-called collective diffusion coefficient as defined by Tanaka and Fillmore.[58] The collective diffusion coefficient is defined by the movement of the polymer network and the water in a gel. The approximate value of this diffusion is ~ 3 x 10^{-7} cm^2/s. Using this value and the radius of our gels (~570 nm), **τ** is ~1.1 ms and if a standard 10% polydispersity in radius is considered τ would vary between 0.9 ms and 1.3 ms. This approximate calculation supports the idea that in the shortest translocation times, deswelling is minimal, where as it is possible during the longer transients for much more deswelling.

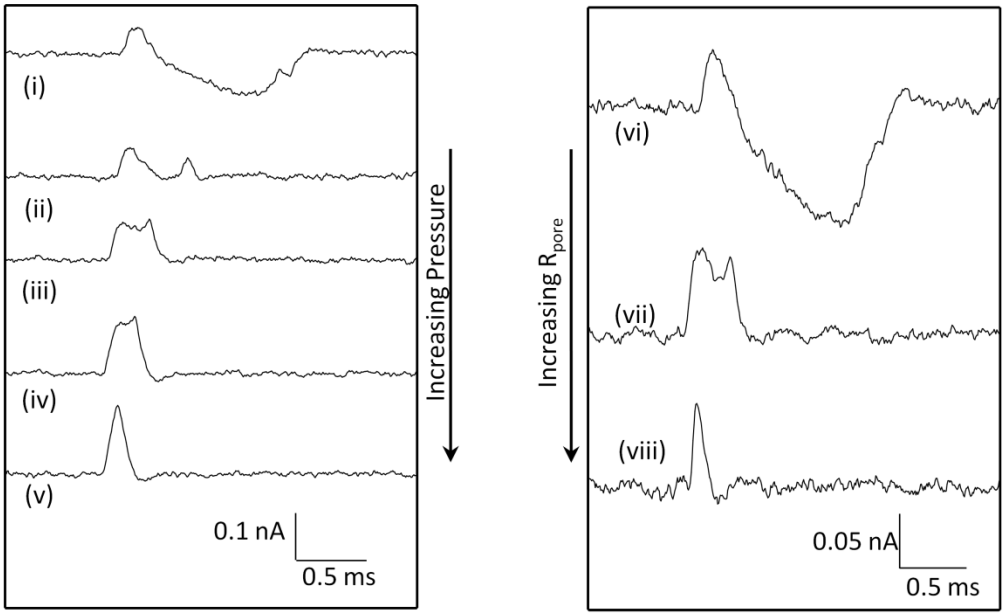

Figure 5.11. Transients of 570 nm microgel passage through 302 nm pores under pressure differentials of (i) -70, (ii) -80, (iii) -100, (iv) -120, and (v) -150 mmHg. As well as transients of 570 nm radius microgel passage through pores of (vi) 266, (vii) 302, and (viii) 405 nm radii under a -100 mmHg pressure differential. All buffered 10 mM KCl solutions.[2]

The White group has done finite element simulations of these pores as shown in **Figure 5.12**. Here, a 2-dementional cross-section of a 300 nm radius pore and the resulting field are presented under the same experimental conditions as in the above

experiments. These simulations show that the expected peak shape based on the shape of the pore is similar to the peak shape in cases where the pressure or the pore size is high enough or large enough to pass through, as we describe it, “elastically”. Here, due to the fact that the particle is entering a sharp increase in field at the opening of the pore a sharp increase is seen. Then, as the particle passes through the pore, the field decreases more gradually and so does the current. However, these other interesting shapes cannot purely be described based on the conical pore shape and are attributed to particle deswelling.

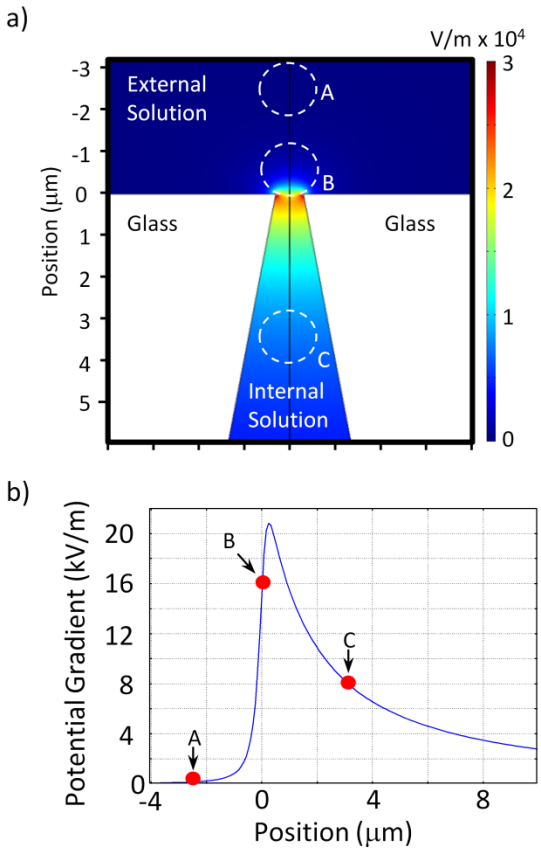

Figure 5.12. Finite element simulation of a 300 nm pore with a solution of 10 mM KCl and an applied voltage of +100 mV similar to the experiments. b) Shows the potential as a particle pass through the center of a pore. Positions A, B, and C are given for reference.[2]

5.4 Conclusions and Outlook

We have shown that the RPA technique can be extended to studying the mechanics of microgels. More specifically, the mechanics of a 570 nm NIPAm-AAc microgel passing through a conical glass nanopore has been studied. Here, the passage limits for a the charged microgel under 50 mmHg pressure were discovered to be a pore to particle ratio of 0.65, where as if the pressure was allowed to be increased to 500 mmHg passage, a ratio of 0.4 was observed. These passage parameters are likely dependent on the particle design as well as the pore charge. Therefore, this method could be extended to characterize many different microgel formulation passage parameters.

The effects of salt concentration on peak magnitude as well as sign have been investigated and may provide an interesting avenue to charge characterization in microgels. Lastly, the microgel passage mechanism has been studied by analyzing the transient shapes and time scales. These resistive pulse analysis methods could provide a valuable technique for studying the mechanics in the elastic and viscoelastic regions of microgels on the single particle level. This kind of information should provide important insights on the absolute design rules for soft, deformable microgel drug delivery vehicles and their ability to pass through small biological pores.

5.5 Implications of Softness

It is not difficult to understand where the role of microgel softness is present in the experiments described in the chapter. As mentioned in the introduction if microgel particles are going to be utilized in biotechnology it is important to understand the role that a soft, flexible nanoparticle could play in all aspects of their application. Much of the attention is given to the cargo real estate that these particles possess due to their low

density and solvent content. However, just as advantageous might be the ability to be cleared easily through the kidneys or to penetrate deep into a tumor. It might also be advantageous to use the fact that particles might have to deswell to pass under certain conditions as way to design a particle that would only release material when in tight junctions as in the kidneys or in tumor vasculature. After we published the data above, the White group extended these studies to liposomes. They found that, unless raised above the lipid bilayer transition temperature, the liposomes could not pass pores smaller than their size.[59]

Besides the insights to the design of a biomaterial that studying the softness in this way might provide, these techniques could provide fundamental "softness" information as well. I think that these experiments provide the ability to study softness in a way that is very difficult to do with any other technique. This experiment could perform single microparticle rheology. What has yet to be worked out is how one could relate these data to know rheological values. The differences in transient shapes and translocation times as the pressure is changed show the richness of the mechanics in these hydrogel microparticle systems. The softness is composed of both an elastic component as well as a viscoelastic component which is very hard to characterize on a single particle basis. Here, we might have a technique that could accomplish those measurements.

5.6 References

[1] Holden, D.A.; Hendrickson, G.; Lyon, L.A.; White, H.S. Resistive Pulse Analysis of Microgel Deformation During Nanopore Translocation. *Journal of Physical Chemistry C* **2011**, *115*, 2999-3004.

[2] Holden, D.A.; Hendrickson, G.R.; Lan, W.J.; Lyon, L.A.; White, H.S. Electrical Signature of the Deformation and Dehydration of Microgels During Translocation through Nanopores. *Soft Matter* **2011**, *7*, 8035-8040.

[3] Mitragotri, S.; Lahann, J. Physical Approaches to Biomaterial Design. *Nature Materials* **2009**, *8*, 15-23.

[4] Nel, A.E.; Madler, L.; Velegol, D.; Xia, T.; Hoek, E.M.V.; Somasundaran, P.; Klaessig, F.; Castranova, V.; Thompson, M. Understanding Biophysicochemical Interactions at the Nano-Bio Interface. *Nature Materials* **2009**, *8*, 543-557.

[5] Chen, C.S.; Mrksich, M.; Huang, S.; Whitesides, G.M.; Ingber, D.E. Geometric Control of Cell Life and Death. *Science* **1997**, *276*, 1425-1428.

[6] Engler, A.J.; Griffin, M.A.; Sen, S.; Bonnetnann, C.G.; Sweeney, H.L.; Discher, D.E. Myotubes Differentiate Optimally on Substrates with Tissue-Like Stiffness: Pathological Implications for Soft or Stiff Microenvironments. *Journal of Cell Biology* **2004**, *166*, 877-887.

[7] Engler, A.J.; Sen, S.; Sweeney, H.L.; Discher, D.E. Matrix Elasticity Directs Stem Cell Lineage Specification. *Cell* **2006**, *126*, 677-689.

[8] Ingber, D.E. Cellular Mechanotransduction: Putting All the Pieces Together Again. *Faseb Journal* **2006**, *20*, 811-827.

[9] Shen, H.; Tan, J.; Saltzman, W.M. Surface-Mediated Gene Transfer from Nanocomposites of Controlled Texture. *Nature Materials* **2004**, *3*, 569-574.

[10] Banquy, X.; Suarez, F.; Argaw, A.; Rabanel, J.-M.; Grutter, P.; Bouchard, J.-F.; Hildgen, P.; Giasson, S. Effect of Mechanical Properties of Hydrogel Nanoparticles on Macrophage Cell Uptake. *Soft Matter* **2009**, *5*, 3984-3991.

[11] Beningo, K.A.; Wang, Y.L. Fc-Receptor-Mediated Phagocytosis Is Regulated by Mechanical Properties of the Target. *J. Cell Sci.* **2002**, *115*, 849-856.

[12] Gao, H.J.; Shi, W.D.; Freund, L.B. Mechanics of Receptor-Mediated Endocytosis. *Proceedings of the National Academy of Sciences of the United States of America* **2005**, *102*, 9469-9474.

[13] Kohane, D.S. Microparticles and Nanoparticles for Drug Delivery. *Biotechnology and Bioengineering* **2007**, *96*, 203-209.

[14] Kumar, M. Nano and Microparticles as Controlled Drug Delivery Devices. *Journal of Pharmacy and Pharmaceutical Sciences* **2000**, *3*, 234-258.

[15] Singh, M.; Chakrapani, A.; O'Hagon, D. Nanoparticles and Microparticles as Vaccine-Delivery Systems. *Expert Review of Vaccines* **2007**, *6*, 797-808.

[16] Choi, H.S.; Liu, W.; Misra, P.; Tanaka, E.; Zimmer, J.P.; Ipe, B.I.; Bawendi, M.G.; Frangioni, J.V. Renal Clearance of Quantum Dots. *Nature Biotechnology* **2007**, *25*, 1165-1170.

[17] Hendrickson, G.R.; Lyon, L.A. Microgel Translocation through Pores under Confinement. *Angewandte Chemie-International Edition* **2010**, *49*, 2193-2197.

[18] Asgeirsson, D.; Venturoli, D.; Rippe, B.; Rippe, C. Increased Glomerular Permeability to Negatively Charged Ficoll Relative to Neutral Ficoll in Rats. *American Journal of Physiology-Renal Physiology* **2006**, *291*, F1083-F1089.

[19] Deen, W.M.; Lazzara, M.J.; Myers, B.D. Structural Determinants of Glomerular Permeability. *American Journal of Physiology-Renal Physiology* **2001**, *281*, F579-F596.

[20] Lau, C.; Sudbury, I.; Thomson, M.; Howard, P.L.; Magil, A.B.; Cupples, W.A. Salt-Resistant Blood Pressure and Salt-Sensitive Renal Autoregulation in Chronic Streptozotocin Diabetes. *American Journal of Physiology-Regulatory Integrative and Comparative Physiology* **2009**, *296*, R1761-R1770.

[21] Rippe, C.; Rippe, A.; Torffvit, O.; Rippe, B. Size and Charge Selectivity of the Glomerular Filter in Early Experimental Diabetes in Rats. *American Journal of Physiology-Renal Physiology* **2007**, *293*, F1533-F1538.

[22] Salmon, A.H.J.; Toma, I.; Sipos, A.; Muston, P.R.; Harper, S.J.; Bates, D.O.; Neal, C.R.; Peti-Peterdi, J. Evidence for Restriction of Fluid and Solute Movement across the Glomerular Capillary Wall by the Subpodocyte Space. *American Journal of Physiology-Renal Physiology* **2007**, *293*, F1777-F1786.

[23] Blackburn, W.H.; Dickerson, E.B.; Smith, M.H.; McDonald, J.F.; Lyon, L.A. Peptide-Functionalized Nanogels for Targeted Sirna Delivery. *Bioconjug. Chem.* **2009**, *20*, 960-968.

[24] Dickerson, E.B.; Blackburn, W.H.; Smith, M.H.; Kapa, L.B.; Lyon, L.A.; McDonald, J.F. Chemosensitization of Cancer Cells by Sirna Using Targeted Nanogel Delivery. *Bmc Cancer* **2010**, *10*.

[25] Smith, M.H.; Lyon, L.A. Multifunctional Nanogels for Sirna Delivery. *Accounts of Chemical Research* **2012**, *45*, 985-993.

[26] Coulter, W.H. Means for Counting Particles Suspended in Fluid. US2656508 **1953**.

[27] Bayley, H.; Martin, C.R. Resistive-Pulse Sensing - from Microbes to Molecules. *Chemical Reviews* **2000**, *100*, 2575-2594.

[28] Choi, Y.; Baker, L.A.; Hillebrenner, H.; Martin, C.R. Biosensing with Conically Shaped Nanopores and Nanotubes. *Physical Chemistry Chemical Physics* **2006**, *8*, 4976-4988.

[29] Harrell, C.C.; Choi, Y.; Horne, L.P.; Baker, L.A.; Siwy, Z.S.; Martin, C.R. Resistive-Pulse DNA Detection with a Conical Nanopore Sensor. *Langmuir* **2006**, *22*, 10837-10843.

[30] Henriquez, R.R.; Ito, T.; Sun, L.; Crooks, R.M. The Resurgence of Coulter Counting for Analyzing Nanoscale Objects. *Analyst* **2004**, *129*, 478-482.

[31] Ito, T.; Sun, L.; Bevan, M.A.; Crooks, R.M. Comparison of Nanoparticle Size and Electrophoretic Mobility Measurements Using a Carbon-Nanotube-Based Coulter Counter, Dynamic Light Scattering, Transmission Electron Microscopy, and Phase Analysis Light Scattering. *Langmuir* **2004**, *20*, 6940-6945.

[32] Ito, T.; Sun, L.; Henriquez, R.R.; Crooks, R.M. A Carbon Nanotube-Based Coulter Nanoparticle Counter. *Accounts of Chemical Research* **2004**, *37*, 937-945.

[33] Lan, W.-J.; Holden, D.A.; Zhang, B.; White, H.S. Nanoparticle Transport in Conical-Shaped Nanopores. *Anal. Chem.* **2011**, *83*, 3840-3847.

[34] Lee, S.; Zhang, Y.H.; White, H.S.; Harrell, C.C.; Martin, C.R. Electrophoretic Capture and Detection of Nanoparticles at the Opening of a Membrane Pore Using Scanning Electrochemical Microscopy. *Anal. Chem.* **2004**, *76*, 6108-6115.

[35] Petrossian, L.; Wilk, S.J.; Joshi, P.; Goodnick, S.M.; Thornton, T.J., in *International Symposium on Advanced Nanodevices and Nanotechnology*, *Vol. 109* (Eds.: S. M. Goodnick, D. K. Ferry), **2008**, pp. 12028-12028.

[36] Carbonaro, A.; Mohanty, S.K.; Huang, H.; Godley, L.A.; Sohn, L.L. Cell Characterization Using a Protein-Functionalized Pore. *Lab on a Chip* **2008**, *8*, 1478-1485.

[37] Wu, Y.; Benson, J.D.; Critser, J.K.; Almasri, M. Mems-Based Coulter Counter for Cell Counting and Sizing Using Multiple Electrodes. *Journal of Micromechanics and Microengineering* **2010**, *20*.

[38] Zhang, H.P.; Chon, C.H.; Pan, X.X.; Li, D.Q. Methods for Counting Particles in Microfluidic Applications. *Microfluidics and Nanofluidics* **2009**, *7*, 739-749.

[39] Deblois, R.W.; Mayyasi, S.A.; Schidlov.G; Wesley, R.; Wolff, J.S. Virus Counting and Analysis by Resistive Pulse (Coulter Counter) Technique. *Proceedings of the American Association for Cancer Research* **1974**, *15*, 104-104.

[40] Deblois, R.W.; Wesley, R.K.A. Sizes and Concentrations of Several Type-C Oncornaviruses and Bacteriophage-T2 by Resistive-Pulse Technique. *Journal of Virology* **1977**, *23*, 227-233.

[41] Harms, Z.D.; Mogensen, K.B.; Nunes, P.S.; Zhou, K.; Hildenbrand, B.W.; Mitra, I.; Tan, Z.; Zlotnick, A.; Kutter, J.P.; Jacobson, S.C. Nanofluidic Devices with Two Pores in Series for Resistive-Pulse Sensing of Single Virus Capsids. *Anal. Chem.* **2011**, *83*, 9573-9578.

[42] Vogel, R.; Willmott, G.; Kozak, D.; Roberts, G.S.; Anderson, W.; Groenewegen, L.; Glossop, B.; Barnett, A.; Turner, A.; Trau, M. Quantitative Sizing of Nano/Microparticles with a Tunable Elastomeric Pore Sensor. *Anal. Chem.* **2011**, *83*, 3499-3506.

[43] Wharton, J.E.; Jin, P.; Sexton, L.T.; Horne, L.P.; Sherrill, S.A.; Mino, W.K.; Martin, C.R. A Method for Reproducibly Preparing Synthetic Nanopores for Resistive-Pulse Biosensors. *Small* **2007**, *3*, 1424-1430.

[44] Bayley, H. Sequencing Single Molecules of DNA. *Current Opinion in Chemical Biology* **2006**, *10*, 628-637.

[45] Deamer, D.W.; Branton, D. Characterization of Nucleic Acids by Nanopore Analysis. *Accounts of Chemical Research* **2002**, *35*, 817-825.

[46] Fologea, D.; Gershow, M.; Ledden, B.; McNabb, D.S.; Golovchenko, J.A.; Li, J.L. Detecting Single Stranded DNA with a Solid State Nanopore. *Nano Letters* **2005**, *5*, 1905-1909.

[47] Gierhart, B.C.; Howitt, D.G.; Chen, S.J.; Zhu, Z.; Kotecki, D.E.; Smith, R.L.; Collins, S.D. Nanopore with Transverse Nanoelectrodes for Electrical Characterization and Sequencing of DNA. *Sensors and Actuators B: Chemical* **2008**, *132*, 593-600.

[48] Han, A.P.; Schurmann, G.; Mondin, G.; Bitterli, R.A.; Hegelbach, N.G.; de Rooij, N.F.; Staufer, U. Sensing Protein Molecules Using Nanofabricated Pores. *Applied Physics Letters* **2006**, *88*.

[49] Sexton, L.T.; Mukaibo, H.; Katira, P.; Hess, H.; Sherrill, S.A.; Horne, L.P.; Martin, C.R. An Adsorption-Based Model for Pulse Duration in Resistive-Pulse Protein Sensing. *Journal of the American Chemical Society* **2010**, *132*, 6755-6763.

[50] Ying, Y.-L.; Wang, H.-Y.; Sutherland, T.C.; Long, Y.-T. Monitoring of an Atp-Binding Aptamer and Its Conformational Changes Using an Alpha-Hemolysin Nanopore. *Small* **2011**, *7*, 87-94.

[51] Zhang, B.; Galusha, J.; Shiozawa, P.G.; Wang, G.L.; Bergren, A.J.; Jones, R.M.; White, R.J.; Ervin, E.N.; Cauley, C.C.; White, H.S. Bench-Top Method for Fabricating Glass-Sealed Nanodisk Electrodes, Glass Nanopore Electrodes, and Glass Nanopore Membranes of Controlled Size. *Anal. Chem.* **2007**, *79*, 4778-4787.

[52] Debord, J.D.; Lyon, L.A. Thermoresponsive Photonic Crystals. *Journal of Physical Chemistry B* **2000**, *104*, 6327-6331.

[53] Yi, Y.D.; Bae, Y.C. Volume-Phase Transition of Submicron-Sized N-Isopropylacrylamide/N-Tert-Butylacrylamide Particles by Photon Correlation Spectroscopy. *Journal of Applied Polymer Science* **1998**, *67*, 2087-2092.

[54] Davis, J.E.; Solsky, R.L.; Giering, L.; Malhotra, S. Clinical-Chemistry. *Anal. Chem.* **1983**, *55*, R202-R214.

[55] Kim, J.; Serpe, M.J.; Lyon, L.A. Photoswitchable Microlens Arrays. *Angewandte Chemie-International Edition* **2005**, *44*, 1333-1336.

[56] Suarez, I.J.; Fernandez-Nieves, A.; Marquez, M. Swelling Kinetics of Poly(N-Isopropylacrylamide) Minigels. *Journal of Physical Chemistry B* **2006**, *110*, 25729-25733.

[57] Matsuo, E.S.; Tanaka, T. Kinetics of Discontinuous Volume Phase-Transition of Gels. *Journal of Chemical Physics* **1988**, *89*, 1695-1703.

[58] Tanaka, T.; Fillmore, D.J. Kinetics of Swelling of Gels. *The Journal of Chemical Physics* **1979**, *70*, 1214-1218.

[59] Holden, D.A.; Watkins, J.J.; White, H.S. Resistive-Pulse Detection of Multilamellar Liposomes. *Langmuir* **2012**, *28*, 7572-7577.

CHAPTER 6

CONCLUSIONS, OUTLOOK, FUTURE DIRECTIONS

6.1 Microgels as Microlenses

Microgels adsorbed to surfaces asymmetrically deswell and create individual lenses (**Chapter 2**). These lenses have a soft, responsive structure that allows for changes in lens focus by changes in microgel refractive index and curvature. Lenses have been designed to respond to temperature, pH, light, and biomolecules. However, the optimum target density on the surface of a flexible, conformable polymer particle for the most sensitive sensor is difficult to define. In addition, not enough is known about the optimal topology or morphology of the microgel design to create the most sensitive lens. Different core/shell designs were synthesized and tested as sensors, but did not lead to an optimal structure. The size of the particles and conformational flexibility allow for an interesting sensing platform, but may not be optimal for sensing molecules with typical antibody binding constants. In the future, as more complex particle designs are developed or different sensing methodologies could allow for sensing of relevant concentrations of biomolecules by individual particles. However, the current transduction mechanism of optically observed changes in lensing does not seem to be the optimal. Instead maybe small changes in polymer density could be sensed using techniques that measure accurate size or mechanical properties.

6.2 Microgel Passage through Pores

Microgel passage through pores smaller than their dilute solution diameter was observed using two different techniques. In the first experiment, suspensions of microgel particles were forced at low pressure through track-etch membranes with pores 10 times smaller than the size of the particle (**Chapter 3**). These experiments were done at pressures similar to the pressures in the kidneys during renal filtration. Experiments were not only performed with 1000 nm particles traversing 100 nm pores, but also with 100 nm particles passing through 10 nm pores. In the case of the smaller particles, the size of the nanogels and pores were similar to the size of nanogels used by our group in siRNA delivery and the size of the pores in human kidneys, respectively.

In a very different experiment, individual microgels were detected using resistive pulse analysis (**Chapter 4**) as they passed through glass nanopores (**Chapter 5**). Particle passage in this case only occurred when the pore radius was at least 40% as large as that of the particle. These much more modest passage parameters are due to the repulsion between charged glass nanopore and the charged microgel. It was also observed that the passage rate and sign of the resistive pulse were dependent on solution ionic strength. The most important result is that the passage rate dependence on pore size and back pressure were not linear suggesting a change in passage mechanism different from purely elastic deformation. We have suggested that an observation of passage with and without particle deswelling. In other words, elastic and viscoelastic passage mechanisms were observed.

The range of possible characterization experiments that could be performed using this technique is large. Experiments using various microgels with different cross-linking

densities and charges could be used to determine the mechanical property dependence on passage. Also, a range of experiments could be performed to study the passage of a particle through a functionalized pore. Here the pore could be made neutral or opposite charge of the microgel. Lastly, passage could be monitored as the microgel releases a loaded drug, binds a soluble ligand, or binds a ligand on the pore surface. While the specific nanopores used in these experiments are not trivial to fabricate, similar experiments could be performed using a different resistive pulse technique.

6.3 Microgel Softness

The work presented here has described different techniques and various potential applications for microgels. The unifying theme of this dissertation is microgel softness. These chapters describe the use of the inherent microgel colloidal deformation which allows for creation of individual lensing elements and stabilization of emulsions (**Appendix A and B**). Secondly, the conformational polymer flexibility allows for responsive changes to environmental cues or presence of biomolecules. Lastly, we observed both the colloidal deformation and polymer conformational flexibility, allow microgel passage through small pores. Although, the softness of microgels and the effects of this softness in some applications are well known they still remain difficult to characterize.

APPENDIX A

CO-STABILIZED EMULSIONS: PROTEINS AND MICROGELS

A.1 Introduction

Emulsions have been studied in a wide range of industries and applications including food,[1-7] cosmetics,[8,9] pharmaceuticals,[10,11] synthetic chemistry,[12-16] and separations.[17,18] Emulsions are colloids which are formed from relatively high energy mixing of immiscible liquids creating small droplets of the dispersed phase in the continuous phase.[19,20] Some of the most familiar emulsions are formed with oil and water in food products. Some examples of oil-in-water (O/W) emulsions include milk, ice cream, dressings, and mayonnaise. Conversely, some water-in-oil (W/O) emulsions include butter and margarine. In either case, the immiscible phases have a high interfacial surface energy; therefore, since the interfacial surface area between the continuous phase and the dispersed phase are increased during emulsion formation or homogenization, emulsions are inherently thermodynamically unstable. However, additives called emulsifiers can make the emulsion more kinetically stable. The emulsifier keeps the droplets of the dispersed phase from undergoing one of five types of destabilization processes; creaming, sedimentation, flocculation, coalescence, or Ostwald ripening. Creaming or sedimentation occurs when the dispersed phase has a lower or higher density, respectively, than the continuous phase and the droplets undergo gravitational separation. The droplets rise in the case of creaming and fall to the bottom in the case of sedimentation. Either of these processes can be aided by the other three instability mechanisms. Flocculation is when droplets aggregate together but do not combine.

Coalescence is when two or more droplets merge. Ostwald ripening occurs when larger droplets grow through transport of the dispersed phase through the continuous phase from smaller drops. The choice of the emulsifier, dispersed phase, and continuous phase can help reduce all of these instabilities. There are many different formation strategies[21-23] and types of emulsions that have been developed.[24] Specifically, the emulsifier identity can vary from proteins to particles and will be discussed below.

A.1.1 Protein Stabilized Emulsions

Probably the most famous protein stabilized emulsion is milk. Here, the main emulsifiers are proteins called caseins, which stabilize the fat in milk in droplets that are large enough to scatter visible light giving milk its white appearance.[25] Proteins are good candidates for emulsifiers because they are amphiphilic which allows for interactions with both a polar and non-polar phase. Most common protein emulsions are found in food, however, there are examples of other proteins used as emulsifiers such as human serum albumin (HSA), bovine serum albumin (BSA), lysozyme, β-lactoglobulin, and fibrinogen.[26-30] Many of these protein emulsifiers have been made as a fundamental study of protein stabilized emulsions, but a particularly interesting case is a fibrinogen emulsion made to carry docetaxel, an anti-cancer drug.[28]

A.1.2 Pickering Emulsions

Pickering emulsions are particle stabilized emulsions first observed and published by Pickering in 1907.[31] Where as with most surfactants the most important parameter for emulsion stabilization is the amphiphilicity, for particles it is thought to be one of three factors: the three phase contact angle, capillary forces formed between two emulsions trying to merge, or long range electrostatic repulsion between droplets.[32,33] Many

different particle types have been shown to be effective emulsifiers including barium sulfate, calcium carbonate, silica, polystyrene, and polytetrafluoroethylene particles.[34] One of the most interesting factors of Pickering emulsions is their incredible stability. In fact, the desorption energy for these particles can be thousands of k_BT, whereas normal surfactants have a desorption energy around k_BT.[35] To calculate these values, the size of the particle, interfacial tension between the continuous and dispersive phases, and the contact angle between the particle and the two phases are used. Interestingly there have also been Pickering emulsions formed from protein particulates like ferritin and zein.[36,37] It can be argued that most protein emulsions might have a Pickering effect, due to different protein micelles or aggregates that might aid in stabilization. However, in most cases, the still soluble protein is thought to have a major role in stability, which is not the case for the intentional protein particulates. Lastly, one very interesting structure that was formed by first forming a Pickering emulsion is a colloidosome.[38] Colloidosomes are often made by forming a Pickering emulsion, connecting the particles together (e.g. chemical cross-linking), and removing the inner liquid, so that the inner solution and outer solution are the same liquid. The name comes from liposomes only instead of lipids they are formed of colloids.

A.1.3 Microgel Stabilized Emulsions

Of the many different particles that have been used to form Pickering emulsions, microgel particles are an interesting class.[39] These emulsions can be made to be responsive by choosing a responsive microgel. It has been shown that thermoresponsive poly(N-isopropylacrylamide) microgels used as emulsifiers create thermoresponsive emulsions, where the emulsion breaks at high temperature above the volume phase

transition temperature (VPTT) of the microgels.[40-44] Also, if acid moieties are incorporated into the microgel network creating a pH-responsive microgel, then the emulsions can be destabilized by lowering the pH of the solution.[40-43] These studies suggest that charge and water content somehow affect emulsion stability. However, it has been shown in at least two studies that the charge alone does not cause emulsion stability. In the first study, emulsions stabilized by microgels with a positive charge and a negative charge were mixed and coalescence was not observed.[45] The second study utilized core/shell microgels were in one set of particles the shell contained acid groups and in the other the core contained acid groups.[46] Here, it was shown that emulsions stabilized by both particles were pH dependent even though the surface charge of the core localized acid particles was very low. This led the authors to the conclusion that surface charge was not the sole reason for stability of the microgel stabilized emulsions. Similarly, it was observed that microgels with lower crosslinking densities were better emulsifiers.[47] All of these observations, as well as the fact that the microgels have been shown to deform quite substantially at the oil water interface (**Scheme A.1**), have led to the thought that the deformability of the microgels is the reason for the stability.[46,48,49] This hypothesis agrees with all the experiments showing that lower cross-linked, fully swollen microgels form stable emulsions, while deswollen particles destabilize the emulsion.

Using these soft deformable stabilizers, groups have created microgel based colloidosomes,[50] performed biocatalysis,[51] and made rupturing microgel capsules.[52] To our knowledge, co-stabilization of emulsions has not been performed using both a protein and a microgel. Observations of co-stabilized emulsions were made with pNIPAm

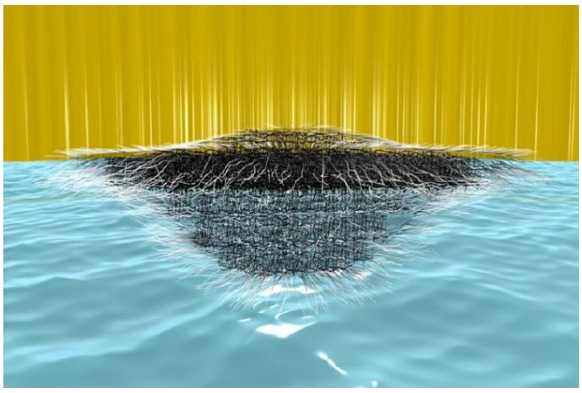

Scheme A.1 Cartoon demonstration the deformation of a microgel at the interface of oil (yellow) and water (blue) based on experiments by Prof. Walter Richtering and co-workers.[49]

microgels (1 % BIS cross-linked) and bovine serum albumin (BSA) or fibrinogen. In these experiments, crude typical emulsion formation methods were used such as homogenizing, vortexing, or stirring. Then, after 24 hrs, protein was added and the solution was imaged. In our work, microgel emulsions were then formed using a more controlled microfluidic approach and incubated with protein to test the hypothesis that the protein is gradually replacing the microgels as the main stabilizer. Not only would these observations lead to some interesting conclusions about the effectiveness of microgels as emulsifiers vs. proteins, but, if well understood, these co-stabilized emulsions could introduce an interesting class of hybrid emulsions.

A.2 Experimental

A.2.1 Materials

Monomer *N*-isopropylacrylamide (NIPAm; Aldrich) was recrystallized from hexanes (Fisher Scientific) before microgel synthesis. Cross-linker *N,N'*-methylenebis(acrylamide) (BIS; Aldrich), ammonium persulfate (APS; Aldrich), acrylic acid (AAc; Fluka), rhodamine cadaverine conjugate (Invitrogen), bovine serum albumin (BSA; Sigma), and bovine serum albumin Alexfluor 488 conjugate (Invitrogen) were all

used as received. The pH 7 buffer was a 10 mM (IS = 100 mM) phosphate buffer. The pH 3 buffer was a 10 mM (IS = 100 mM) formate buffer. The pH 5 buffer was a 10 mM (IS = 100 mM) MES buffer. All buffers were ionic strength adjusted using NaCl. All water used in the experiments was purified to 18 mΩ (Barnstead E-pure system). Materials for fabrication of microfluidic devices included square capillaries (1,0 mm ID, 1.4 mm OD; VitroCom), round capillaries (1.0 mm OD, 0.58 mm ID; Sutter Instruments) and epoxy (5 minute; Devcon).

A.2.2 Microgel Synthesis

Large microgels were synthesized by precipitation polymerization of NIPAm, BIS (1 mol % or 0 mol %), and AAc (10 mol%) with a total monomer concentration of 100 mM in 1000 mL. All components were dissolved in distilled, deionized water and stirred under a nitrogen purge while heating to 68 °C. Then APS (0.01 mM) was added to initiate the reaction. The reaction was allowed to stir under nitrogen at 68 °C overnight. All particle solutions were filtered through glass wool and purified via dialysis for 10 days (10,000 MWCO dialysis tubing vs. nanopure water). The samples were then freeze-dried for storage and then re-dispersed into desired concentrations.

The microgels were then conjugated with 6-carboxytetramethylrhodamine cadaverine via carbodiimide coupling to the acid groups on the microgel particles. Both the ULC particles the 1 % cross-linked microgels were dispersed in pH 5.5 MES buffer at 5 mg/mL. Then solutions EDC (1-ethyl-3-(3-dimethylaminopropyl) carbodiimide hydrochloride), N-hydroxysulfosuccinimide (Sulfo-NHS), and the rhodamine conjugate were added to the particles and the solution shook at room temperature overnight. Then the particles were purified by centrifugation and concentrated to stock solutions of 10 mg/mL.

A.2.3 Microgel Characterizations

Dynamic light scattering (DLS) was used to determine the hydrodynamic radius (R_h) under different pH conditions as described earlier.[53,54] This was done with a Wyatt Technologies DynaPro plate reader DLS using a laser wavelength of 830 nm. Scattering intensity fluctuations were detected for 10 s per reading by an avalanche photodiode at and angle of 158° (back scattering) from the incident laser. Dynamics software (Wyatt Technologies Corp.) was used to calculate and fit an autocorrelation function plotted from the random fluctuations in scattering intensity. These fits of the autocorrelation functions were used to calculate the diffusion coefficients and then through the Stokes-Einstein equation, the R_h. The plate reader DLS provided the opportunity to use small volumes (50 μL) of particle solution and to run different aliquots in series without further sample preparation. These measurements were performed in both pH 7 and pH 3 buffers.

These particles were also imaged after depositing them on glass coverslips. Glass coverslips were cleaned by sonication in an Alconox solution, DI water, acetone, isopropyl alcohol, and ethanol. Then, the coverslips were incubated in a 1 % solution of 4-aminopropylsilane in absolute ethanol for 2 hrs and then rinsed and stored in ethanol. Next, the particles were deposited using a centrifuging technique published previously.[55] The functionalized coverslips were placed in solutions of particles in a 6-well plate and spun to the surface using a plate rotor centrifuge for 10 min at 2250*g*. Then, the coverslips were allowed to shake overnight in DI water, rinsed, and dried under N_2 before imaging with atomic force microscopy.

A.2.4 Emulsion Formation

Emulsion formation was performed using a microfluidic co-flow device similar to those published previously.[23,56,57] Briefly, the devices, as shown in **Figure A.1**, were fabricated on top of microscope slides. A square capillary of 1.0 mm inner-diameter (ID)

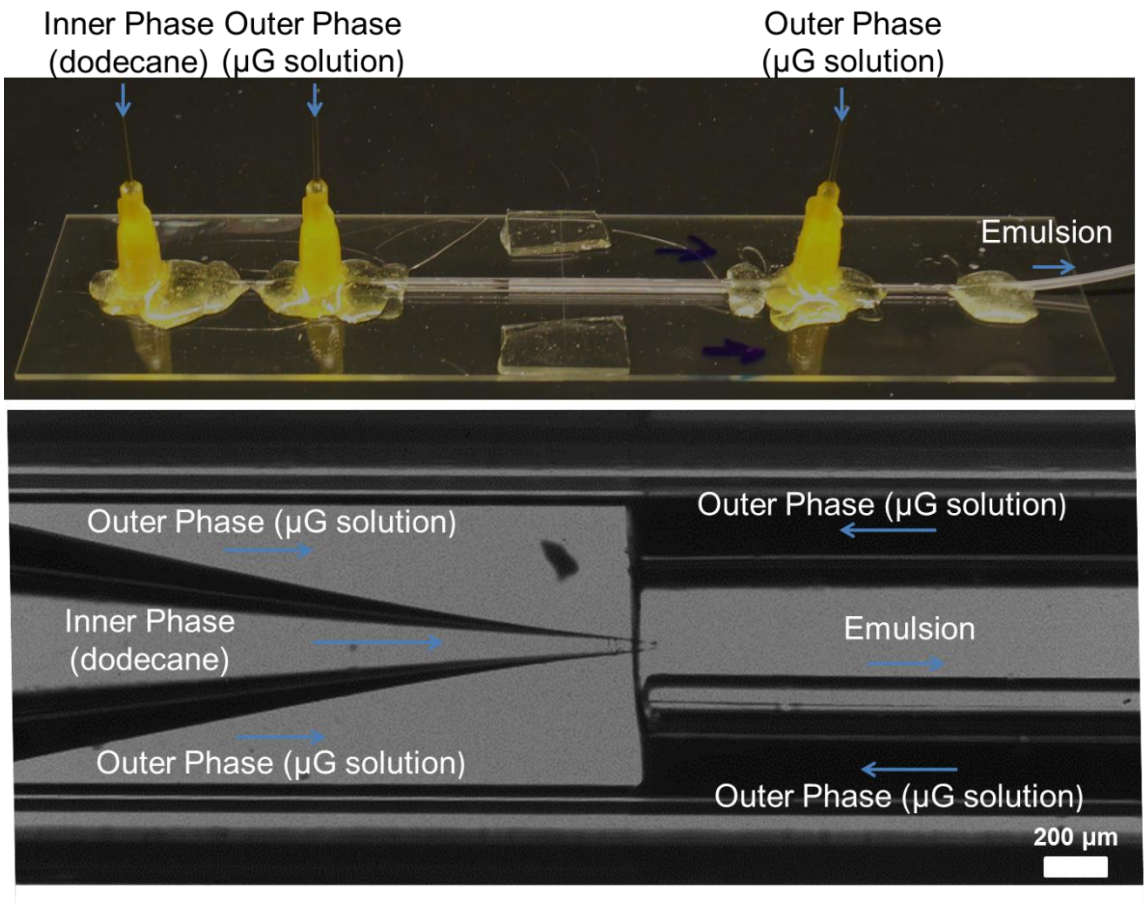

Figure A.1. Digital camera (top) image of the complete emulsion formation device and an optical microscopy image of the area where the emulsions are formed with flows of materials indicated.

is mounted using an epoxy to a large microscope slide formed by joining two separate slides, epoxy, and small pieces of glass. Then, two round capillaries of outer-diameter (OD) 1 mm and ID of 0.58 mm are chosen that just fit into the square capillary. One of the round capillaries is then pulled to using a Sutter Instruments pipette puller. Next, the pulled capillary and the round capillary are cut to length and rinsed with acetone. Then, the pulled capillary is inserted into one end of the mounted square capillary. Tubing is placed on one end of the other round capillary and then inserted into the square capillary opposite of the pulled capillary. The capillaries are aligned as shown in **Figure A.1** and secured with epoxy. Next, plastic short syringe tips are modified to slide over the capillaries at 3 different locations; the end of the pulled capillary, where the pulled

capillary and square meet, and where the un-pulled capillary and the square meet. These syringe tips are attached over these openings to allow for liquid introduction with epoxy. First, a small amount of epoxy is used to attach them to the glass surface over the openings of the capillaries being careful not to clog the capillaries. Second, a small amount of epoxy is used to seal around the base of the syringe base. Lastly, a liberal amount of epoxy is used to seal all the way around the base and up the outside of the plastic syringe. After 24 hours of drying, the device is tested for leaks by attaching tubing to all three outlets and pushing deionized water through the previous attached tubing. If leaks are seen then they are dried and resealed with epoxy.

This device is used to form emulsions by flowing the inner and outer phase in the same direction with a small back flow coming through the other end of the square capillary. The inner liquid flow is stabilized by the flow of the outer liquid and the small back flow allows for focusing of the stream into the collection capillary. In this case, the inner liquid is dodecane and the outer liquids are suspensions of microgels. The microgels stabilize the droplets as they break off of the liquid jet formed as the liquids are introduced using syringe pumps. The microgel suspensions are between 1-3 mg/mL concentration and the outer flow, inner flow, and back flow are 8-12 mL/min, 5-10 mL/hr, and 5 mL/hr, respectively. These experiments can be observed using a microscope and camera.

A.2.5 Protein Introduction Experiments

After emulsion formation, the solution was allowed to sit for 24 hrs in order for emulsion equilibration. Then 1 mL aliquots of the emulsion were placed in small vials. Next, a BSA/BSA-Alexafluor 488 (100/1) of 100 mg/mL was diluted into the emulsion suspensions at final concentrations of 0.1, 1, 5, and 10 mg/mL. Small 40 μL aliquots of these solutions were removed 1 hr, 24 hrs, and 48 hrs, placed into small Coverwell profusion chambers placed on glass coverslips, and imaged using confocal microscopy at

20x (0.8 NA) and 63x (1.40 NA). In another experiment a 127 μL aliquot of the original emulsion was added to a larger gasket/coverslip sample chamber and while visualizing the emulsion a 20 μL of the 100 mg/mL BSA solution was added and imaged for 1 hr.

A.3 Results and Discussion

Microgels were used to stabilize oil-in-water (O/W) emulsions. The microgels used were prepared by precipitation polymerization with monomers of NIPAm and AAc and a BIS cross-linker. Preparation of the emulsions was performed by re-suspending freeze dried fluorescently conjugated microgels into pH 7 PBS buffer, adding either extra virgin olive oil or heptane, and vortexing or stirring to create the emulsion. Then protein, either BSA or fibrinogen, was added to create a microgel emulsion with adsorbed protein. These solutions contained a wide variety of emulsions as shown in **Figure A.2**. Some of the emulsions had little to no protein adsorption, while some had mostly protein and only a few particles. Probably the most interesting case is when the protein was adsorbed in between the particles on the surface of the emulsion. The range of different protein and microgel adsorption states led to the hypothesis that the protein was slowly displacing the microgels from the surface of the emulsion droplet. However, since emulsions created with the crude techniques above create very concentrated and heterogeneous emulsions, a different method for emulsion formation was used to test this hypothesis.

The microgels used for this study were made in a 1 litter synthesis due to the high particle consumption of the co-flow emulsion formation method using microfluidics. These particles had an R_h of 482 nm with a polydispersity of 11 % and 305 nm with a polydispersity of 9 % at pH 7 and pH 3, respectively. The deswelling at lower pH is due to the protonation of the incorporated acid groups and release of counter ions and their

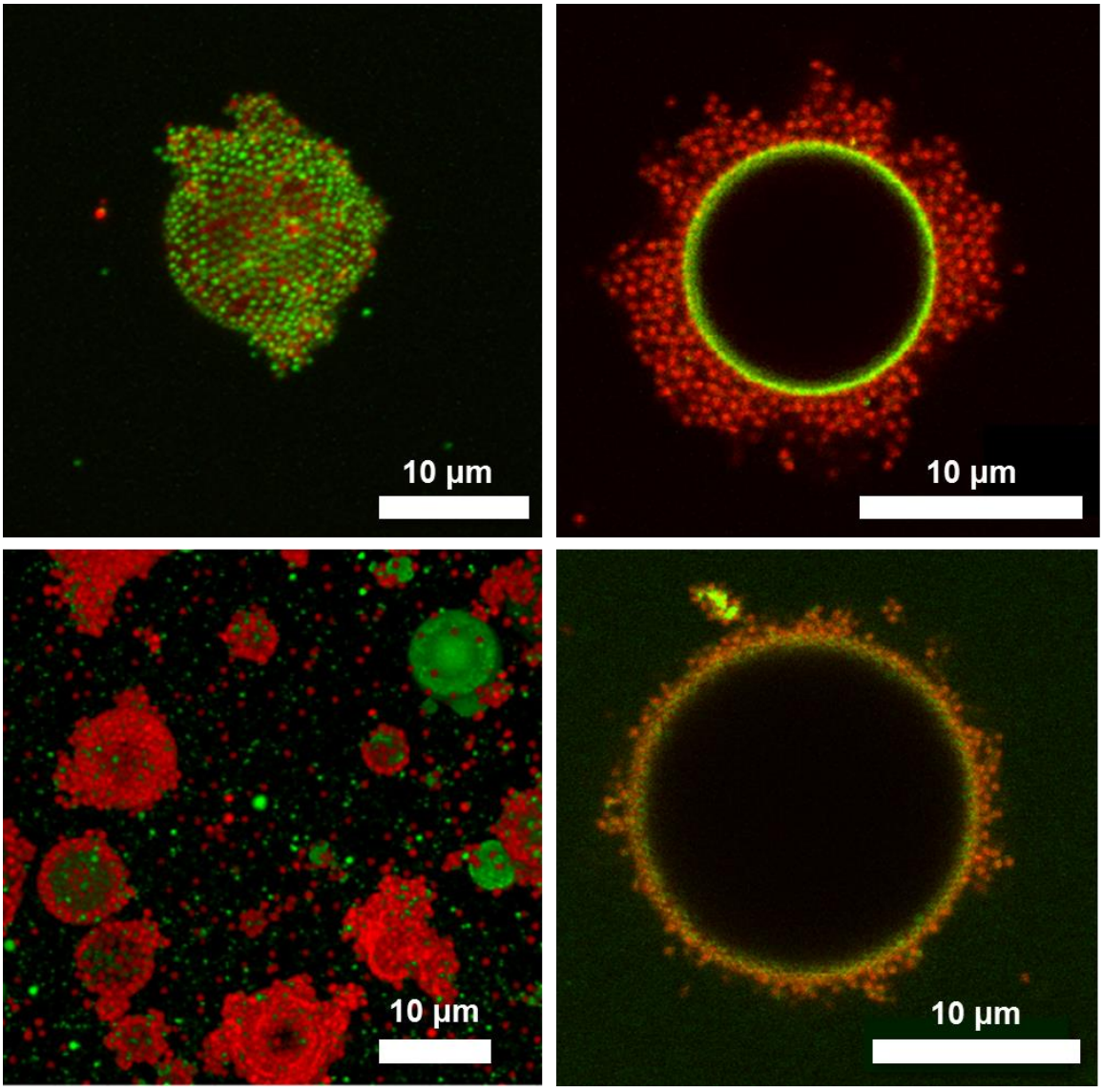

Figure A.2. Confocal microscopy images of different emulsions with proteins adsorbed. Top left is a microgel (green) with fibrinogen (red) stabilized extra virgin olive oil emulsion. Top right, bottom right, and bottom left are a microgel (red) heptane-in-water emulsions with BSA adsorbed (red).

associated water. After synthesis, these particles were functionalized with a rhodamine conjugate using carbodiimide coupling and then purified and imaged with AFM and confocal microscopy (**Figure A.3**). Solutions of these particles at 2 mg/mL in pH 7 buffer were used for emulsion formation by microfluidics. The devices used are shown in **Figure A.1**. Here, the 2 mg/mL microgel outer solution flowed at 12 mL/min, while the

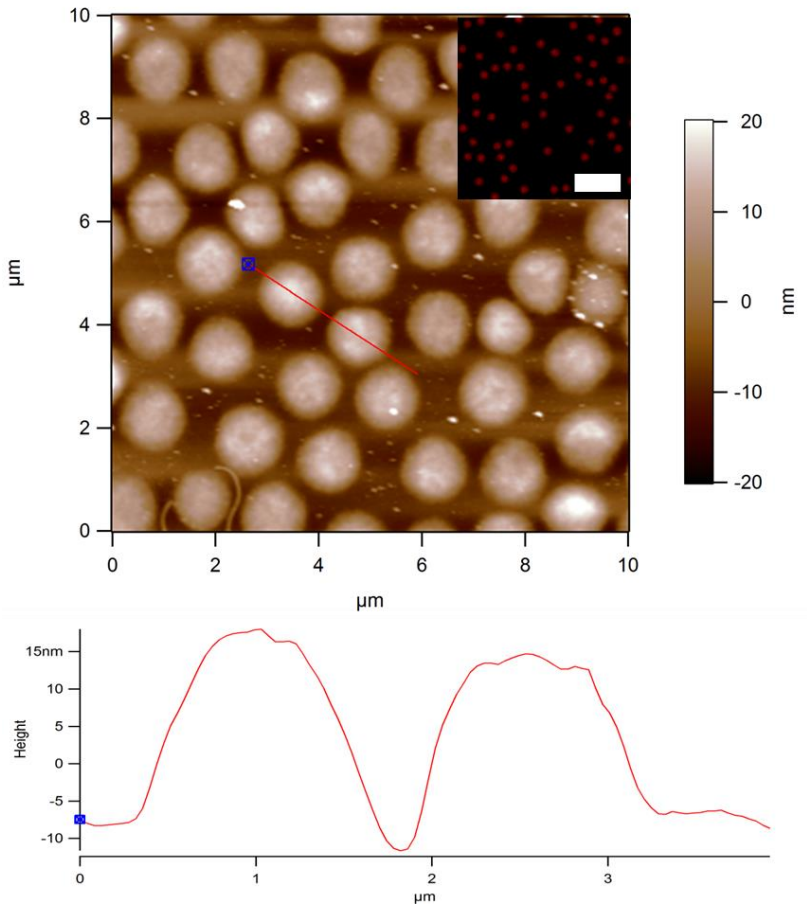

Figure A.3. AFM image of the 1% cross-linked microgels adsorbed on an amino-silane functionalize glass surface with a line trace showing the height of the particles. (Inset) confocal image of microgels adsorbed to a glass surface. Scale bar = 5 µm.

inner solution of dodecane was flowed at a rate of 8 mL/min. These two flows constitute a co-flow device which creates a jet of dodecane and the stabilized emulsions break off of the jet. The backward flow of the outer solution was the same concentration as the co-flow microgel solution but was run at only 5 mL/hr. This flow helps focus the oil jet into the collection capillary (on the right in the picture). This technique created emulsions of ~4 ± 1 µm (average of 29 emulsions by confocal image analysis) in diameter and fairly dilute due to the high outer flow rate. A confocal microscopy 3D reconstruction of an emulsion is shown in **Figure A.4**.

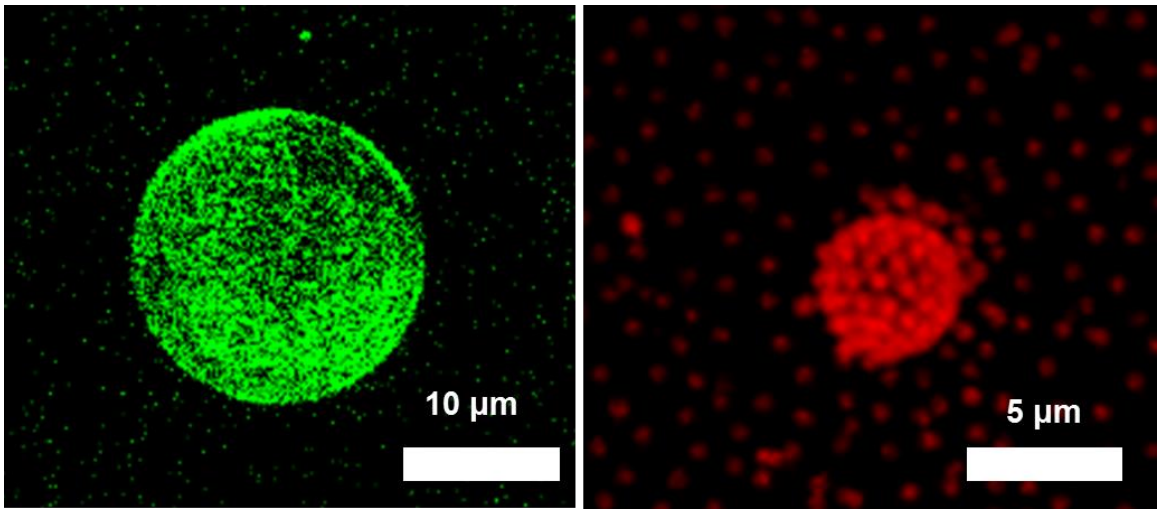

Figure A.4. 3D construction of confocal images of emulsions made with BSA (left) by vortexing and made with microgels (right) by microfluidics.

To test the adsorption of protein to these emulsions, 5-1 mL aliquots of the emulsion were placed in small vials and allowed to sit for 48 hrs. to stabilize. Then, different amounts of a 100 mg/mL solution of BSA/BSA-Alexafluor 488 (100:1) were added to each aliquot to make solutions of 0, 0.1, 1, 5, and 10 mg/mL of BSA/BSA-Alexafluor 488. Small amounts of the emulsion and protein solutions were imaged with confocal microscopy at 1, 24, and 48 hr after protein addition. Examples of the emulsions at these time points and different protein concentrations are shown in **Figure A.5**. These images show that no protein preferentially adsorbed to these emulsions no matter the concentration of protein or incubation time. Next, a sample of the emulsion without protein was placed on the confocal microscope and a small drop of 100 mg/mL BSA/BSA-Alexafluor 488 was added. This single emulsion was imaged for 1 hr to observe protein adsorption. This experiment allowed for imaging of a single emulsion

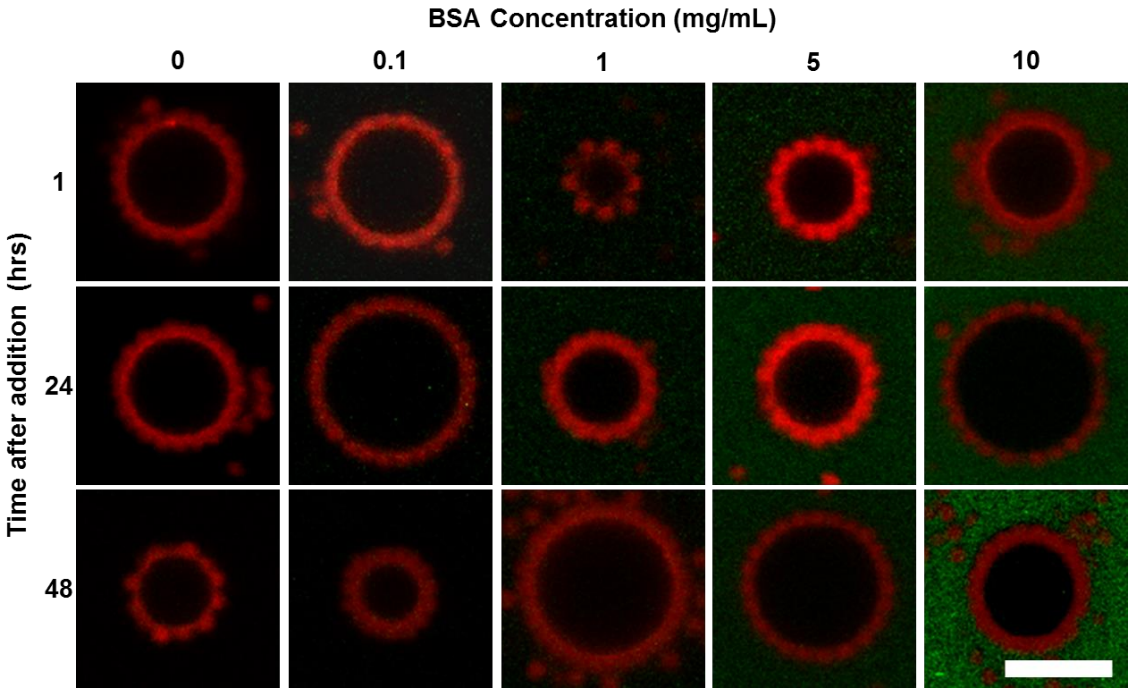

Figure A.5. Confocal images of microgel (red) stabilized emulsions at different incubation times with different BSA (green) concentrations. Scale bar = 5 μm

while being immersed in protein solution. While observing this emulsion it lost a little brightness due to photobleaching but no protein adsorption was observed (**Figure A.6**). These results suggest that the hypothesis of protein displacement of microgels at an emulsion surface is not the mechanism for the creation of the emulsions as in **Figure A.2**. Therefore, these co-stabilized emulsions must be made by a different mechanism which could be dependent on the choice of inner phase or emulsion formation strategy.

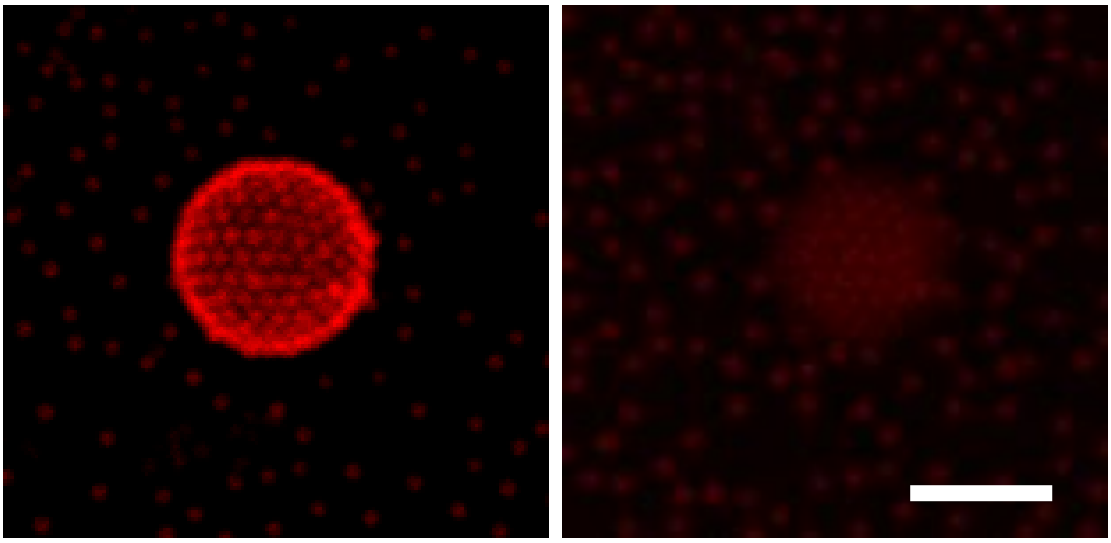

Figure A.6. 3D confocal reconstruction of a microgel (red) stabilized emulsion before (left) and after (right) incubation with 13 mg/mL BSA/BSA-Alexafluor 488 (green). Scale bar = 5 μm.

A.4 Conclusions and Outlook

We have tested the hypothesis that microgels are being replaced by proteins when used to stabilize emulsions. By forming microgel stabilized emulsions with a method which produces a more monodisperse, dilute emulsion, we were able to ensure homogeneous mixing of the emulsions with the protein and a more consistent result. Our results indicated that at the very least this phenomenon is not general to all microgel stabilized emulsions and more likely that our interesting observation was due to a completely different mechanism. However, these results suggest that when making observations of emulsion behavior, care needs to be taken to consider the concentration, homogeneity, and stability of the emulsion when different observations are made and mechanisms are proposed.

A.5 Implications of "Softness"

The stability of microgel emulsions is owed to their softness and deformability as discussed in the introduction. The conformational flexibility of microgels allows for amazing stability at the surface of these emulsions even when proteins, which have long

been established as good emulsifiers, are present. The more rigid proteins cannot displace the microgels even at the edge of particle. This is encouraging for the stability of microgel emulsions in protein-rich solutions such as in biomedical applications.

A.6 References

[1] Barham, P.; Skibsted, L.H.; Bredie, W.L.P.; Frost, M.B.; Moller, P.; Risbo, J.; Snitkjaer, P.; Mortensen, L.M. Molecular Gastronomy: A New Emerging Scientific Discipline. *Chemical Reviews* **2010**, *110*, 2313-2365.

[2] Goff, H.D. Colloidal Aspects of Ice Cream - a Review. *International Dairy Journal* **1997**, *7*, 363-373.

[3] Guichard, E. Interactions between Flavor Compounds and Food Ingredients and Their Influence on Flavor Perception. *Food Reviews International* **2002**, *18*, 49-70.

[4] Madene, A.; Jacquot, M.; Scher, J.; Desobry, S. Flavour Encapsulation and Controlled Release - a Review. *International Journal of Food Science and Technology* **2006**, *41*, 1-21.

[5] Mezzenga, R.; Schurtenberger, P.; Burbidge, A.; Michel, M. Understanding Foods as Soft Materials. *Nature Materials* **2005**, *4*, 729-740.

[6] Santana, R.C.; Perrechil, F.A.; Cunha, R.L. High- and Low-Energy Emulsifications for Food Applications: A Focus on Process Parameters. *Food Engineering Reviews* **2013**, *5*, 107-122.

[7] Syrbe, A.; Bauer, W.J.; Klostermeyer, N. Polymer Science Concepts in Dairy Systems - an Overview of Milk Protein and Food Hydrocolloid Interaction. *International Dairy Journal* **1998**, *8*, 179-193.

[8] Gutierrez, J.M.; Gonzalez, C.; Maestro, A.; Sole, I.; Pey, C.M.; Nolla, J. Nano-Emulsions: New Applications and Optimization of Their Preparation. *Current Opinion in Colloid & Interface Science* **2008**, *13*, 245-251.

[9] Rosenberg, E.; Ron, E.Z. Bioemulsans: Microbial Polymeric Emulsifiers. *Current Opinion in Biotechnology* **1997**, *8*, 313-316.

[10] Badiee, A.; Shargh, V.H.; Khamesipour, A.; Jaafari, M.R. Micro/Nanoparticle Adjuvants for Antileishmanial Vaccines: Present and Future Trends. *Vaccine* **2013**, *31*, 735-749.

[11] Benita, S.; Levy, M.Y. Submicron Emulsions as Colloidal Drug Carriers for Intravenous Administration - Comprehensive Physicochemical Characterization. *Journal of Pharmaceutical Sciences* **1993**, *82*, 1069-1079.

[12] Antonietti, M.; Landfester, K. Polyreactions in Miniemulsions. *Progress in Polymer Science* **2002**, *27*, 689-757.

[13] Landfester, K. Miniemulsion Polymerization and the Structure of Polymer and Hybrid Nanoparticles. *Angewandte Chemie-International Edition* **2009**, *48*, 4488-4507.

[14] Landfester, K.; Mailander, V. Nanocapsules with Specific Targeting and Release Properties Using Miniemulsion Polymerization. *Expert Opinion on Drug Delivery* **2013**, *10*, 593-609.

[15] Qiu, J.; Charleux, B.; Matyjaszewski, K. Controlled/Living Radical Polymerization in Aqueous Media: Homogeneous and Heterogeneous Systems. *Progress in Polymer Science* **2001**, *26*, 2083-2134.

[16] Song, H.; Chen, D.L.; Ismagilov, R.F. Reactions in Droplets in Microflulidic Channels. *Angewandte Chemie-International Edition* **2006**, *45*, 7336-7356.

[17] Schwuger, M.J.; Stickdorn, K.; Schomacker, R. Microemulsions in Technical Processes. *Chemical Reviews* **1995**, *95*, 849-864.

[18] Watarai, H. Microemulsions in Separation Sciences. *Journal of Chromatography A* **1997**, *780*, 93-102.

[19] Maali, A.; Mosavian, M.T.H. Preparation and Application of Nanoemulsions in the Last Decade (2000-2010). *Journal of Dispersion Science and Technology* **2013**, *34*, 92-105.

[20] McClements, D.J. Critical Review of Techniques and Methodologies for Characterization of Emulsion Stability. *Critical Reviews in Food Science and Nutrition* **2007**, *47*, 611-649.

[21] Chu, L.Y.; Utada, A.S.; Shah, R.K.; Kim, J.W.; Weitz, D.A. Controllable Monodisperse Multiple Emulsions. *Angewandte Chemie-International Edition* **2007**, *46*, 8970-8974.

[22] Fryd, M.M.; Mason, T.G., in *Annual Review of Physical Chemistry, Vol 63, Vol. 63* (Eds.: M. A. Johnson, T. J. Martinez), **2012**, pp. 493-518.

[23] Shah, R.K.; Shum, H.C.; Rowat, A.C.; Lee, D.; Agresti, J.J.; Utada, A.S.; Chu, L.Y.; Kim, J.W.; Fernandez-Nieves, A.; Martinez, C.J.; Weitz, D.A. Designer Emulsions Using Microfluidics. *Materials Today* **2008**, *11*, 18-27.

[24] McClements, D.J. Advances in Fabrication of Emulsions with Enhanced Functionality Using Structural Design Principles. *Current Opinion in Colloid & Interface Science* **2012**, *17*, 235-245.

[25] Dickinson, E. Proteins at Interfaces and in Emulsions - Stability, Rheology and Interactions. *Journal of the Chemical Society-Faraday Transactions* **1998**, *94*, 1657-1669.

[26] Yampolskaya, G.; Platikanov, D. Proteins at Fluid Interfaces: Adsorption Layers and Thin Liquid Films. *Advances in Colloid and Interface Science* **2006**, *128*, 159-183.

[27] Tcholakova, S.; Denkov, N.D.; Ivanov, I.B.; Campbell, B. Coalescence in Beta-Lactoglobulin-Stabilized Emulsions: Effects of Protein Adsorption and Drop Size. *Langmuir* **2002**, *18*, 8960-8971.

[28] Jakate, A.S.; Einhaus, C.M.; DeAnglis, A.P.; Retzinger, G.S.; Desai, P.B. Preparation, Characterization, and Preliminary Application of Fibrinogen-Coated Olive Oil Droplets for the Targeted Delivery of Docetaxel to Solid Malignancies. *Cancer Research* **2003**, *63*, 7314-7320.

[29] van Rijn, P.; Wang, H.H.; Boker, A. Ultra-Sound Assisted Formation of Biodegradable Double Emulsion Capsules from Hen Egg White. *Soft Matter* **2011**, *7*, 5274-5280.

[30] Jutz, G.; Boker, A. Bio-Inorganic Microcapsules from Templating Protein- and Bionanoparticle-Stabilized Pickering Emulsions. *Journal of Materials Chemistry* **2010**, *20*, 4299-4304.

[31] Pickering, S.U. Emulsions. *Journal of the Chemical Society* **1907**, *91*, 2001-2021.

[32] Binks, B.P. Particles as Surfactants - Similarities and Differences. *Current Opinion in Colloid & Interface Science* **2002**, *7*, 21-41.

[33] Tcholakova, S.; Denkov, N.D.; Lips, A. Comparison of Solid Particles, Globular Proteins and Surfactants as Emulsifiers. *Physical Chemistry Chemical Physics* **2008**, *10*, 1608-1627.

[34] Aveyard, R.; Binks, B.P.; Clint, J.H. Emulsions Stabilised Solely by Colloidal Particles. *Advances in Colloid and Interface Science* **2003**, *100*, 503-546.

[35] Leal-Calderon, F.; Schmitt, V. Solid-Stabilized Emulsions. *Current Opinion in Colloid & Interface Science* **2008**, *13*, 217-227.

[36] Fujii, S.; Aichi, A.; Muraoka, M.; Kishimoto, N.; Iwahori, K.; Nakamura, Y.; Yamashita, I. Ferritin as a Bionano-Particulate Emulsifier. *Journal of Colloid and Interface Science* **2009**, *338*, 222-228.

[37] de Folter, J.W.J.; van Ruijven, M.W.M.; Velikov, K.P. Oil-in-Water Pickering Emulsions Stabilized by Colloidal Particles from the Water-Insoluble Protein Zein. *Soft Matter* **2012**, *8*, 6807-6815.

[38] Dinsmore, A.D.; Hsu, M.F.; Nikolaides, M.G.; Marquez, M.; Bausch, A.R.; Weitz, D.A. Colloidosomes: Selectively Permeable Capsules Composed of Colloidal Particles. *Science* **2002**, *298*, 1006-1009.

[39] Li, Z.F.; Ngai, T. Microgel Particles at the Fluid-Fluid Interfaces. *Nanoscale* **2013**, *5*, 1399-1410.

[40] Brugger, B.; Richtering, W. Emulsions Stabilized by Stimuli-Sensitive Poly(N-Isopropylacrylamide)-Co-Methacrylic Acid Polymers: Microgels Versus Low Molecular Weight Polymers. *Langmuir* **2008**, *24*, 7769-7777.

[41] Brugger, B.; Rosen, B.A.; Richtering, W. Microgels as Stimuli-Responsive Stabilizers for Emulsions. *Langmuir* **2008**, *24*, 12202-12208.

[42] Ngai, T.; Auweter, H.; Behrens, S.H. Environmental Responsiveness of Microgel Particles and Particle-Stabilized Emulsions. *Macromolecules* **2006**, *39*, 8171-8177.

[43] Ngai, T.; Behrens, S.H.; Auweter, H. Novel Emulsions Stabilized by Ph and Temperature Sensitive Microgels. *Chemical Communications* **2005**, 331-333.

[44] Tsuji, S.; Kawaguchi, H. Thermosensitive Pickering Emulsion Stabilized by Poly(N-Isopropylacrylamide)-Carrying Particles. *Langmuir* **2008**, *24*, 3300-3305.

[45] Liu, T.T.; Seiffert, S.; Thiele, J.; Abate, A.R.; Weitz, D.A.; Richtering, W. Non-Coalescence of Oppositely Charged Droplets in Ph-Sensitive Emulsions. *Proceedings of the National Academy of Sciences of the United States of America* **2012**, *109*, 384-389.

[46] Schmidt, S.; Liu, T.T.; Rutten, S.; Phan, K.H.; Moller, M.; Richtering, W. Influence of Microgel Architecture and Oil Polarity on Stabilization of Emulsions by Stimuli-Sensitive Core-Shell Poly(N-Isopropylacrylamide-Co-Methacrylic Acid) Microgels: Mickering Versus Pickering Behavior? *Langmuir* **2011**, *27*, 9801-9806.

[47] Destribats, M.; Lapeyre, V.; Wolfs, M.; Sellier, E.; Leal-Calderon, F.; Ravaine, V.; Schmitt, V. Soft Microgels as Pickering Emulsion Stabilisers: Role of Particle Deformability. *Soft Matter* **2011**, *7*, 7689-7698.

[48] Geisel, K.; Isa, L.; Richtering, W. Unraveling the 3d Localization and Deformation of Responsive Microgels at Oil/Water Interfaces: A Step Forward in Understanding Soft Emulsion Stabilizers. *Langmuir* **2012**, *28*, 15770-15776.

[49] Richtering, W. Responsive Emulsions Stabilized by Stimuli-Sensitive Microgels: Emulsions with Special Non-Pickering Properties. *Langmuir* **2012**, *28*, 17218-17229.

[50] Shah, R.K.; Kim, J.W.; Weitz, D.A. Monodisperse Stimuli-Responsive Colloidosomes by Self-Assembly of Microgels in Droplets. *Langmuir* **2010**, *26*, 1561-1565.

[51] Wiese, S.; Spiess, A.C.; Richtering, W. Microgel-Stabilized Smart Emulsions for Biocatalysis. *Angewandte Chemie-International Edition* **2013**, *52*, 576-579.

[52] Croll, L.M.; Stover, H.D.H. Mechanism of Self-Assembly and Rupture of Cross-Linked Microspheres and Microgels at the Oil-Water Interface. *Langmuir* **2003**, *19*, 10077-10080.

[53] Debord, J.D.; Lyon, L.A. Thermoresponsive Photonic Crystals. *Journal of Physical Chemistry B* **2000**, *104*, 6327-6331.

[54] Yi, Y.D.; Bae, Y.C. Volume-Phase Transition of Submicron-Sized N-Isopropylacrylamide/N-Tert-Butylacrylamide Particles by Photon Correlation Spectroscopy. *Journal of Applied Polymer Science* **1998**, *67*, 2087-2092.

[55] South, A.B.; Whitmire, R.E.; Garcia, A.J.; Lyon, L.A. Centrifugal Deposition of Microgels for the Rapid Assembly of Nonfouling Thin Films. *Acs Applied Materials & Interfaces* **2009**, *1*, 2747-2754.

[56] Utada, A.S.; Fernandez-Nieves, A.; Gordillo, J.M.; Weitz, D.A. Absolute Instability of a Liquid Jet in a Coflowing Stream. *Physical Review Letters* **2008**, *100*.

[57] Utada, A.S.; Fernandez-Nieves, A.; Stone, H.A.; Weitz, D.A. Dripping to Jetting Transitions in Coflowing Liquid Streams. *Physical Review Letters* **2007**, *99*.

APPENDIX B

PLATELET CONTRACTION INDUCED DRUG RELEASE

B.1 Introduction

Many different drug release mechanisms have been proposed from numerous biomaterials.[1,2] Most commonly diffusion from an implanted material "depot" is used, perhaps with gating by ionic strength, pH, temperature, dilution, or erosion of the device. Here, it is proposed to use a mechanically-induced rupture of the device to cause drug release. The mechanical stress is provided by platelets which contract naturally in the presence of chemical cues during the clotting cascade.[3] The type of device that might be advantageous for mechanical destruction and release might be an emulsion, since the surface adsorbed emulsifier is critical for stability of the colloid. These emulsions are designed to bind platelets such that when the platelet contracts it disrupts the emulsion releasing the payload. Various emulsion formulations have been employed to induce binding of platelets and rupture. Applications of such a construct could be used to deliver drugs that reduce the formation of blood clots *in vivo* or in blood circulating medical devices as shown in **Scheme B.1**. The design targets locations of high concentrations of platelet activating factors such as areas of thrombosis.

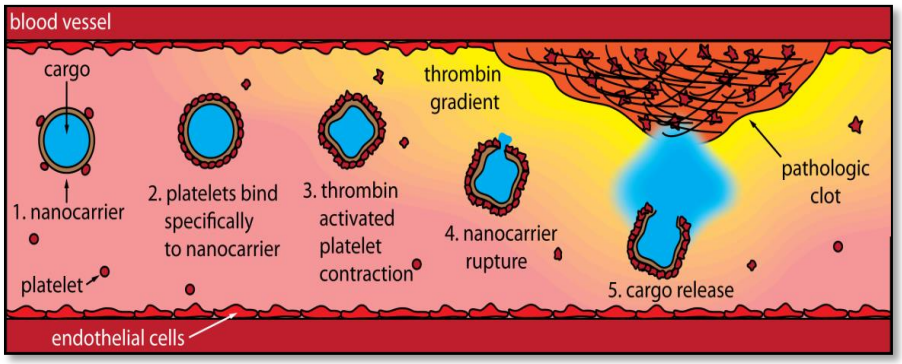

Scheme B.1. Scheme of proposed drug release mechanism. Scheme made by Dr. Wilbur Lam.

B.2 Experimental

B.2.1 Materials

Monomer *N*-isopropylacrylamide (NIPAm; Aldrich) was recrystallized from hexanes (Fisher Scientific) before microgel synthesis. Cross-linker *N,N'*-methylenebis(acrylamide) (BIS; Aldrich), ammonium persulfate (APS; Aldrich), acrylic acid (AAc; Fluka), rhodamine cadaverine conjugate (Invitrogen), Alexafluor 488 cadaverine (Invitrogen), bovine serum albumin (BSA; Sigma), bovine serum albumin Alexfluor 488 conjugate (Invitrogen), bovine serum albumin Alexfluor 555 conjugate (Invitrogen), fibrinogen, and Alexafluor 488 (Invitrogen) were all used as received. The pH 7 buffer was a 10 mM (IS = 100 mM) phosphate buffer. The pH 5 buffer was a 10 mM (IS = 100 mM) MES buffer. All buffers were ionic strength adjusted using NaCl. All water used in the experiments was purified to 18 mΩ (Barnstead E-pure system).

B.2.2 Microgel Synthesis

Large microgels were synthesized by precipitation polymerization of NIPAm, BIS (1 or 3 mol %), and AAc (10 mol%) with a total monomer concentration of 100 mM in 100 mL. All components were dissolved in distilled, deionized water and stirred under a nitrogen purge while heating to 68 °C. Then APS (0.01 mM) was added to initiate the

reaction. The reaction was allowed to stir under nitrogen at 68 °C overnight. All particle solutions were filtered through glass wool and purified via centrifugation. The samples were then freeze-dried for storage and then re-dispersed into desired concentrations.

The microgels were either conjugated with conjugated with **6-carboxytetramethylrhodamine** cadaverine or Alexafluor 488 cadavverine via carbodiimide coupling to the acid groups on the microgel particles. The 3 % cross-linked microgels were dispeserd in pH 5.5 MES buffer at 5 mg/mL. Then solutions EDC (1-ethyl-3-(3-dimethylaminopropyl) carbodiimide hydrochloride), N-hydroxysulfosuccinimide (Sulfo-NHS), and the fluorescent conjugate were added to the particles and the solution shook at room temperature overnight. Then, the particles were purified by centrifugation and concentrated to stock solutions of 10 mg/mL.

B.2.3 Microgel Characterizations

Dynamic light scattering (DLS) was used to determine the hydrodynamic radius (R_h) under different pH conditions as described earlier.[4,5] This was done with a Wyatt Technologies DynaPro plate reader DLS using a laser wavelength of 830 nm. Scattering intensity fluctuations were detected for 10 s per reading by an avalanche photodiode at an angle of 158° (back scattering) from the incident laser. Dynamics software (Wyatt Technologies Corp.) was used to calculate and fit an autocorrelation function plotted from the random fluctuations in scattering intensity. These fits of the autocorrelation functions were used to calculate the diffusion coefficients and then through the Stokes-Einstein equation, the R_h. The plate reader DLS provided the opportunity to use small volumes (50 μL) of particle solution and to run different aliquots in series without further sample preparation. These measurements were performed in both pH 7 and pH 3 buffers.

B.2.4 Emulsion Formulations and Formation Methods

Emulsion Formulation	Emulsion Formation
Microgels and Fibrinogen/evoo	Vortexing Stirring
Microgels with targeting peptides/evoo	Vortexing
Fibrinogen/evoo	Vortexing
Fibrinogen cross-linked emulsions/evoo	Vortexing
Fibrinogen and BSA Co-Stabilized Emulsions/evoo	Vortexing
Fibrinogen/dodecane	Vortexing Homogenizing Microfluidics

Table B.1. Table of formulations and formation methods for drug delivery emulsions (evoo = extra virgin olive oil)

Table B.1 above lists the emulsion formulations and emulsification methods used thus far for interaction with platelets. Emulsions were formed with 4 different methods and they include vortexing for 1-2 min., stirring for 30 sec to 10 min., homogenizing for 30 sec to 2 min, and finally using the microfluidic device described below. The microfluidic approach was performed using a microfluidic co-flow device similar to those published previously.[6-8] The microfluidic device fabrication is described in detail in **Appendix A**.

B.3 Preliminary Results

A variety of delivery vehicles were fabricated for use in delivery of theraputics to thrombotic regions in the body. The targeting mechnism is the concentration of factors involved in the clotting cascade which would only be high in the regions close to thombosis. When these factors are present in high enough concnetration, the platelets that are assosiated with the delivery vehicle would contract releaseing the contents of the carrier. In this case, the drug delivery vehicle is an emulsion. The emulsion should get disrupted by binding to the surface and then contaction of the platelets. The difficultes are forming an emulsion which will interact with platelets and then visualizing the effect

when thrombin, a critical factor in the clotting cascade that signals platelet contraction, is introduced.

The first experiments were performed with microgel stabalized emulsions and two stratagies were employed for platelet adhesion. The first was adsorption of fibrinogen to the microgel emulsion, and the second was to conjugate a platelet binding peptide to the microgel and then form the microgel emulsion. Fibrinogen is a blood circulating protien which, upon exposure to thrombin, areas of fibrinogen are cleaved allowing for its self-assosiation into a fibrinogen polymer which is called fibrin. Fibrin is the biopolymer that makes up the majority of a clot. Platelets do not bind to blood circulating fibrinogen but will bind to surface adsorbed fibrinogen. Therfore, it might bind fibrinogen that is deposted on the surface of the emulsions. **Figure B.1** shows an image of the microgel emulsion after incubation with fibrinogen. A platelet binding peptide that had been grafted to surfaces that then bound platelets was used.[9,10] A cystine-terminated peptide was conjugated through malimide-polyethylene glycol-amine (MAL-PEG-NH_2) to the acid groups on the microgel particle. When either construct was incubated with platelets, the platelets seemed largely uninterested in the emulsions. Shown in **Figure B.2** is an example of one microgel and fibrinogen emulsion that has some platelets near it, but this seemed to be the exception. It was hypothesized that the particles which seem to stick out further than the fibrinogen might prevent the platelets for getting to the fibrinogen. The peptides were unsuccessful, however, concentrations of the peptide on the surface of the particles might need to be adjusted.

Since contact with the fibrinogen surface seemed like it might be inhibited by the microgels, emulsions purely stabalized by fibrinogen were formed. A few different formulations were attempted; mixed BSA and fibrinogen stabalized emulsions, fibrinogen emulsions formed and then cross-linked via gluteraldehyde cross-linking of amines, and fibrinogen emulsions with different hydrophobic phases. The mixed BSA

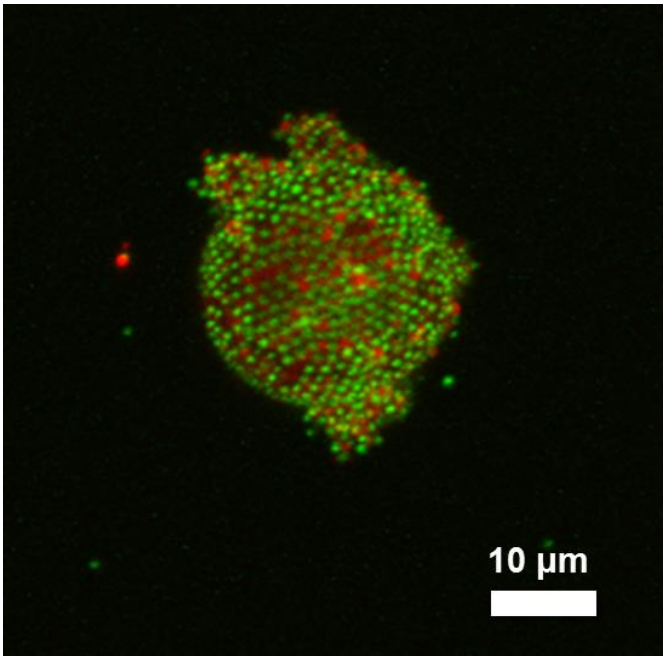

Figure B.1. 3D confocal reconstruction of microgel (green) stabilized emulsion after incubation with fibrinogen (red).

and fibrinogen emulsions were formed to reduced the amount of fibrinogen on the surface of the emulsion, since it has been observed that too much firbinogen does not allow for platelet adhesion.[11] However, these proteins did not form very uniform BSA-fibrinogen emulsions. Most of the emulsions were one protien or the other one. Cross-linked fribrinogen was used based on unpublished results in the Lyon lab that suggest that cells do not adhere well to mobile multilayer substates. Therfore, if the fibrinogen is locked in place, the platelets might bind more easily. Although,a large number of experiments were not attempted, the cross-linked fibrinogen emulsions also did not bind platelets. Lastly, all previous emulsions were made using extra virgin olive oil (evoo); however, it was noticed that olive oil in buffer made an emulsion that was quite stable, so the oil was changed to dodecane to simplify the system, since it readily separates with buffer without the pressence of an emulsifier.

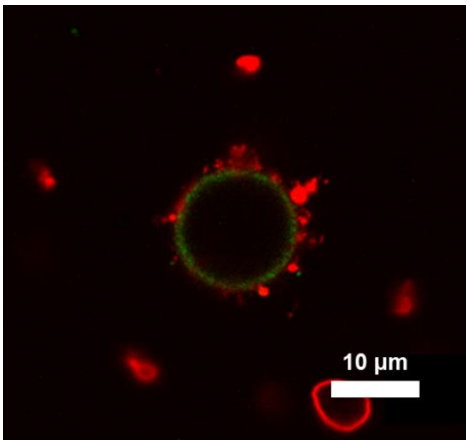

Figure B.2. Confocal image of microgel (green) stabalized emulsion after incubation with fibrinogen and addition of platelets (red).

As platelet experiments were on-going, attempts to produce more stable and monodisperse fibrinogen emulsions were made. Vortexing and stirring with different speeds, concentrations, and times were attempted and although there was some variability in the formed emulsion, they were all very similar. They were very polydisperse in size and only stable for a few hours to creaming. Creaming was the most common instability observed which can be a result of a few different instabilities. Aggregation, coelecence, and Ostwald rippening can lead to creaming which can be enhanced by solvent density differences, emulsion size dispersity, and emulsion size. Therefore, microfluidic devices as describe above have been used to atempt to form more monodisperse, stable emulsions. Fabrication of the co-flow devices has lead to formation of emulsions of 50-80 µm in diameter and fairly monodisperse. However, these emulsions, made with dodecane and fibrinogen, creamed fairly quickly, and this method uses a large amount of protien. A few different statagies, that will be discussed later, can be used to decrease the emulsion size which should help increase stability as well as decrease the material demands.

After emulsions were formed, experiments were performed to observe interactions between platelets and the emulsions. In most cases, experiments were

performed by mixing either washed platelets (WP) or platelet-rich plasma (PRP) with emulsions, and then activating the platelets with a thrombin and Ca^{2+} while observing with confocal microscopy. The platelets are labled with a near or far red fluorophore and the microgels and/or fibrinogen are labled with a rhodamine or Alexafluor 488 conjugate. Confocal setups have included either a 20x (0.8 NA) or a 63x (1.40 NA) objective and in most cases a gasket placed on a coverslip was used to hold the samples. **Figure B.3** shows an example of a few cases where platelets were attached to the emulsions; however, release or contraction was not observed. These cases were also rare potentialy due to the instability of the emulsion to creaming, and the emulsions floating out of viewing area, while the platelets spread on the bottom of the sample chamber (**Figure B.3**).

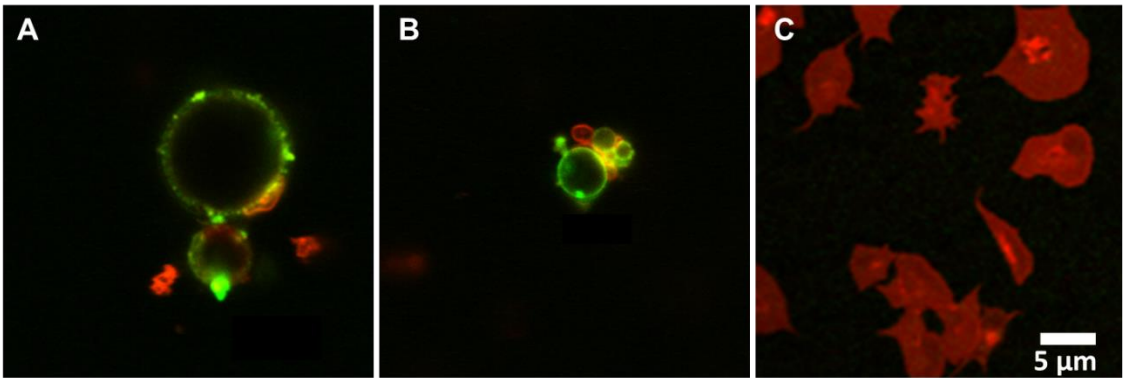

Figure B.3. (A) and (B) confocal images of fibrinogen (green) stabalized emulsions with platelets (red) attached. (C) Confocal image of platelets (red) spread on glass.

In addition to adapting the emulsion formation to make smaller emulsions, attempts have been made to use microfluidics to introduce the nanoemulsions, platelets, and platelet activators. These type of experiments should allow for better anticipation of the location of binding events as well as for detailed high numerical appeture imaging. An example of one of these experiments is shown in **Figure B.4**. Here, the microfluidic is a Y-shaped 50 µm x 50 µm channel where the thrombin and Ca^{2+} solution is introduced on one side with emulsions and platelets in the other channel. Due to laminer flow in

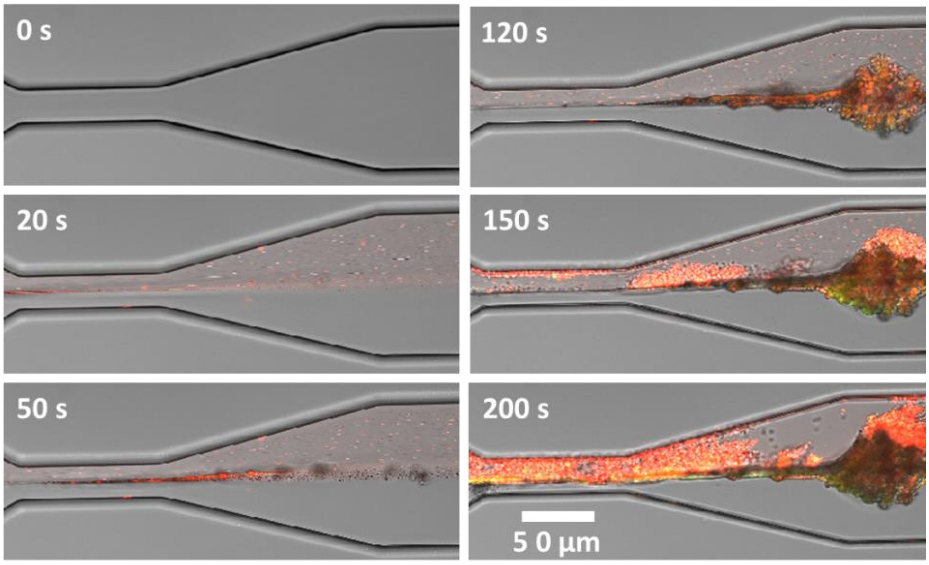

Figure B.4. Confocal images over time of the opening of Y-shaped PDMS microfluidic device with fibrinogen (green) emulsions mixed with platelets (red) coming in the top and a solution of thrombin and Ca^{2+} in the bottom. A fibrin clot with mixed in platelets forms at the junction of the two liquids.

these channels, diffusion of thrombin across the interface between the two liquids is fairly slow and the formation of fibrin starts at the interface, as shown in **Figure B.4**. Platelets (red) start attaching to the fibrin (green) network. Unforunately, emulsion droplets did not make it into the channel due to there larger size, which adds to the efforts to make smaller more stable emulsions.

With some results suggesting platelet binding, some macroscopic experiments were performed with a large amount of platelets and emulsions in vials. **Figure B.5** shows and example of these experiments. Here, PRP was mixed with fibrinogen, fibrinogen stabalized emulsions, microgel stabalized emulsions, buffer, and fibrinogen stabalized emulsions in ratios of 1:10,1:10,1:10,1:10, and 1:1, respectively. The platelet number was held constant. In these experiments, the solutions were mixed and then the activatior solution was added which induces fibrin formation (clot formation) and activates platelets to become contractile. Over time a clot is formed and then the platelets attach to the fibrin network and contract the network. All cases look similar except for the

case where a high concentration of emulsions were added. Here, it looks as if the emulsions might prevent further shrinkage of the clot. However, it is unclear if this broke the emulsion or if the emulsion is still intact.

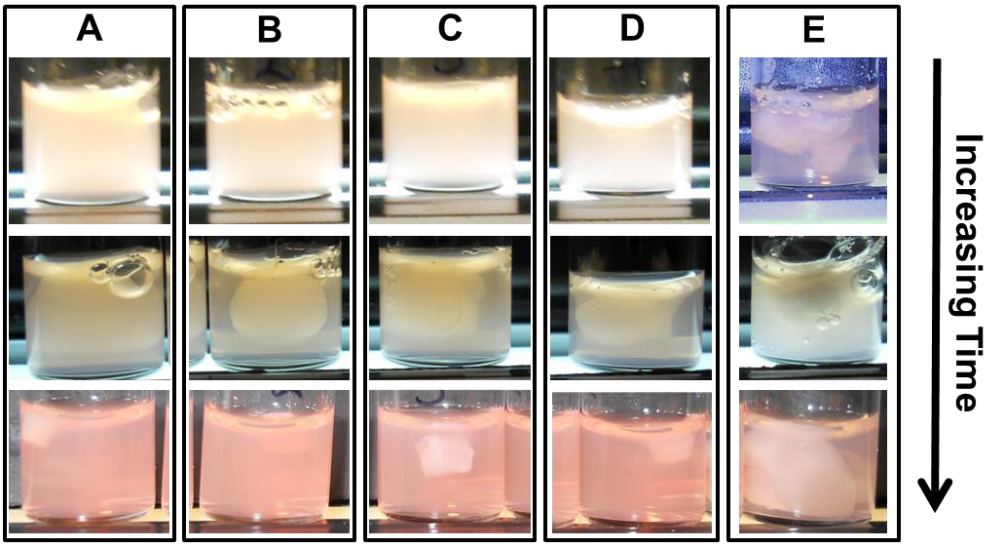

Figure B.5. Digital camera images of vials of (A) 1:10 v/v ratio of fibrinogen and PRP, (B) 1:10 v/v fibrinogen emulsions (FE) and PRP, (C) 1:10 v/v microgel emulsions and PRP, (D) 1:10 v/v buffer and PRP, and (E) 1:1 v/v FE and PRP 5 min (top), 20 min (middle), and 15 hrs (bottom) after addition of thrombin and Ca^{2+} .

Lastly, an observation that was made without platelet addition is that the fibrinogen emulsions can grow fibrin off of their surfaces (**Figure B.6**). Here, fibrinogen emulsions were incubated with thrombin and imaged via confocal. Fibrin fibers are seen growning off of these emulsions. The question remains will this help stabilize the emulsions in a clot making it hard to rupture the emulsion or will the incorportation of the emulsion into the clot actually destabalize it emough to release its contents.

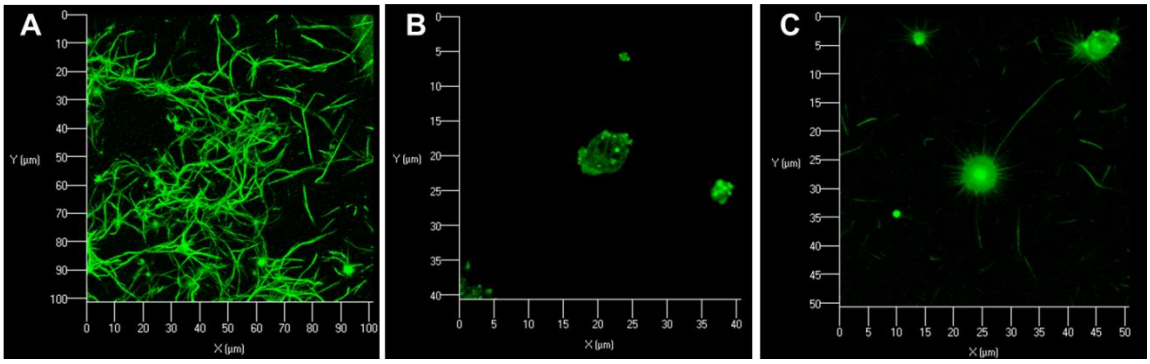

Figure B.6. 3D reconstructions of confocal images of (A) fibrinogen with thrombin added, (B) fibrinogen stabalized emulsion, and (C) fibrinogen stabalized emulsion with thrombin.

B.4 Outlook

The preliminary results here have encouraged further investigation into platelet induced release and emulsion incorporation into clots. The formation of stable small emulsions will continue with modifications to flow focusing and co-flow devices with help from Prof. Alberto Fernandez-Nieves and Dr. Josef Guerrero. More specifically, the modifications will use less material and make smaller emulsions. The first new device includes a co-flow device similar to what has been used in these experiments only with a size-limiting collection aperture. The second is a flow focusing device in which emulsions are also collected through and aperture. Another technique that will be attempted is extrusion similar to the way that liposomes have been formed. Here, an emulsion is formed by a conventional crude method (stirring, vortexing, homogenizing), and then the size is determined and distribution is narrowed by forcing the emulsion through a certain pore size. Smaller and more stable emulsions should increase the platelet experimental reproducibility. Overall, we have established and interesting project in both platelet induced contraction and formation of fibrinogen stabilized emulsions. This project was performed in collaboration with Dr. Wilbur Lam's lab with Yumiko Sakurai and much of the work will be continued by Caroline Hansen in Prof. Andrew Lyon's lab.

B.5 References

[1] Soppimath, K.S.; Aminabhavi, T.M.; Kulkarni, A.R.; Rudzinski, W.E. Biodegradable Polymeric Nanoparticles as Drug Delivery Devices. *Journal of Controlled Release* **2001**, *70*, 1-20.

[2] Uhrich, K.E.; Cannizzaro, S.M.; Langer, R.S.; Shakesheff, K.M. Polymeric Systems for Controlled Drug Release. *Chemical Reviews* **1999**, *99*, 3181-3198.

[3] Lam, W.A.; Chaudhuri, O.; Crow, A.; Webster, K.D.; Li, T.D.; Kita, A.; Huang, J.; Fletcher, D.A. Mechanics and Contraction Dynamics of Single Platelets and Implications for Clot Stiffening. *Nature Materials* **2011**, *10*, 61-66.

[4] Debord, J.D.; Lyon, L.A. Thermoresponsive Photonic Crystals. *Journal of Physical Chemistry B* **2000**, *104*, 6327-6331.

[5] Yi, Y.D.; Bae, Y.C. Volume-Phase Transition of Submicron-Sized N-Isopropylacrylamide/N-Tert-Butylacrylamide Particles by Photon Correlation Spectroscopy. *Journal of Applied Polymer Science* **1998**, *67*, 2087-2092.

[6] Shah, R.K.; Shum, H.C.; Rowat, A.C.; Lee, D.; Agresti, J.J.; Utada, A.S.; Chu, L.Y.; Kim, J.W.; Fernandez-Nieves, A.; Martinez, C.J.; Weitz, D.A. Designer Emulsions Using Microfluidics. *Materials Today* **2008**, *11*, 18-27.

[7] Utada, A.S.; Fernandez-Nieves, A.; Gordillo, J.M.; Weitz, D.A. Absolute Instability of a Liquid Jet in a Coflowing Stream. *Physical Review Letters* **2008**, *100*.

[8] Utada, A.S.; Fernandez-Nieves, A.; Stone, H.A.; Weitz, D.A. Dripping to Jetting Transitions in Coflowing Liquid Streams. *Physical Review Letters* **2007**, *99*.

[9] Holmback, K.; Danton, M.J.S.; Suh, T.T.; Daugherty, C.C.; Degen, J.L. Impaired Platelet Aggregation and Sustained Bleeding in Mice Lacking the Fibrinogen Motif Bound by Integrin Alpha(Iib)Beta(3). *Embo Journal* **1996**, *15*, 5760-5771.

[10] Sanchez-Cortes, J.; Mrksich, M. The Platelet Integrin Alpha Iib Beta 3 Binds to the Rgd and Agd Motifs in Fibrinogen. *Chemistry & Biology* **2009**, *16*, 990-1000.

[11] Podolnikova, N.P.; Yermolenko, I.S.; Fuhrmann, A.; Lishko, V.K.; Magonov, S.; Bowen, B.; Enderlein, J.; Podolnikov, A.V.; Ros, R.; Ugarova, T.P. Control of Integrin Alpha(Iib)Beta(3) Outside-in Signaling and Platelet Adhesion by Sensing the Physical Properties of Fibrin(Ogen) Substrates. *Biochemistry* **2010**, *49*, 68-77.

VITA

GRANT ROBERT HENDRICKSON

Grant was born in Greenville, South Carolina and grew up in Greer, South Carolina. He attended Christ Church Episcopal School for elementary, middle, and high school. Grant graduated with distinction from Furman University with a Bachelor of Science degree in Chemistry in 2005 and continued his education at Furman earning a Master of Science in Chemistry. During his studies at Furman, Grant did research with Prof. Lon B. Knight before moving on to start his doctoral work with Prof. L. Andrew Lyon at the Georgia Institute of Technology. Grant's interests in his spare time include working out, woodworking, golf, watching or playing almost any sporting event and spending time with his wife and best friend, Lee.